Drug Metabolism in Early Stage Drug Discovery and Drug Development

BY
NAN ZHANG
B.S., China Pharmaceutical University, China, 2006

THESIS
Submitted as partial fulfillment of the requirements
for the degree of Doctor of Philosophy in Medicinal Chemistry
in the Graduate College of the
University of Illinois at Chicago, 2014

Chicago, Illinois

Defense Committee:

Scott Franzblau, Chair and Advisor
HyunYoung Jeong, Co-advisor, Pharmacy Practice
Larry Klein
Richard van Breemen
Larry Danziger, Pharmacy Practice

This dissertation is dedicated to my parents and my friends for their consistent support for my studies.

ACKNOWLEDGMENTS

I first and foremost would like to thank my advisor, Dr Scott G. Franzblau and Dr Hyunyoung Jeong for being wonderful mentors. Dr Franzblau has mentored and inspired me throughout my entire graduate studies and has led me in my research directions and specific experiments. Dr Jeong is always there coaching and polishing my skills on DMPK studies and other scientific skills, such as writing and presentation. I would also like to acknowledge my committee members Dr Larry Klein, Dr Richard van Breemen, and Dr Larry Danziger for all the kind advices during my graduate studies and writing the dissertation. Special thanks to Dr Larry Klein for taking care of me since my first day in ITR. Special thanks to Dr Yang Song and Dr Kuan-wei Peng for helping in all aspects of my experiments. They have been a great help during the difficult times no matter it is about work or life.

I would also like to acknowledge all the present and past members of Institute for Tuberculosis Research for providing an incredibly fun environment. Inparticular, I am grateful to Dr Sang Cho, for being always available and patient in discussing experiments. Also, I would like to thank Dr Yuehong Wang and Baojie Wan who have been caring about me like their child and whom I shared “joys and griefs” during the entire graduate school; Dr Changhua Hwang, Valentina Petukhova, Geping Cai, Wei Gao, Dr Hiten Gutka, for making the lab work a wonderful experience, for being always available in helping out with experiments.

This work was funded by grant NIH-1R21AI095795-01A1.

Chapter 1 in this work has been published previously in *Drug Metabolism and Disposition* as an article with the title *Characterization of Inhibition Kinetics of (S)-Warfarin Hydroxylation by Noscapine: Implications in Warfarin Therapy*.

NZ

TABLE OF CONTENTS

TABLE OF CONTENTS (continued)

TABLE OF CONTENTS (continued)

TABLE OF CONTENTS (continued)

LIST OF TABLES

LIST OF FIGURES

FIGURE PAGE

LIST OF FIGURES (continued)

FIGURE PAGE

LIST OF FIGURES (continued)

FIGURE PAGE

LIST OF FIGURES (continued)

FIGURE PAGE

LIST OF FIGURES (continued)

FIGURE PAGE

LIST OF ABBREVIATIONS

$[I]_{in\ vivo}$	inhibitor concentration at the enzyme active site
4-MU	4-methylumbelliferone
4-MUG	4-methylumbelliferone-β-D-glucuronide
ABT	1-aminobenzotriazole
AUC	area under the plasma drug concentration versus time curve
AUC_i/AUC	ratio of the area under the curve with and without inhibitor
cDNA	complementary DNA
CL_{int}	Intrinsic clearance, the intrinsic ability of hepatic enzymes to metabolize the drug
C_{max}	maximal plasma concentration
$C_{max,u}$	unbound maximal plasma concentration
CLA	clarithromycin
CYP450s	cytochrome P450 enzymes
D	dose
DDIs	drug-drug interactions
DMPK	drug metabolism and pharmacokinetics
F_a	fraction absorbed from the gut into the portal vein
F_A	fraction of CYP2C9 activity resulting from the combination of mutated alleles
FCS	fetal calf serum
f_m	fraction of the substrate metabolized by the inhibited enzyme
$f_{m(CYP2C9)}$	the extent of CYP2C9-mediated metabolism in overall (S)-warfarin elimination

LIST OF ABBREVIATIONS (continued)

f_u	unfound fraction
G-6-P	glucose-6-phosphate
HLMs	human liver microsomes
HPLC	high-performance liquid chromatography
HS9	human liver S9 fractions
I_{av}	average systemic plasma concentration
IC_{25}	25% of maximum reversible inhibition
IC_{50}	half maximal inhibitory concentration
I_{in}	maximum hepatic input concentration
$I_{in,u}$	maximum unbound hepatic input concentration
I_{max}	maximum systemic plasma concentration
$I_{max,u}$	maximum unbound systemic plasma concentration
INR	international normalized ratio
IVIVE	in vitro-in vivo extrapolation
k	elimination rate constant
k_a	absorption rate constant
$k_{deg(CYP2C9)}$	first-order rate constant of in vivo degradation of CYP2C9
K_i	enzyme-inhibitor constant
K_I	inactivator concentration required for half the maximal inactivation rate
$K_{i,u}$	reversible inhibition constant adjusted by the free fraction of noscapine in pooled HLMs
$K_{I,u}$	unbound K_I adjusted by the free fraction of noscapine in pooled HLMs
k_{inact}	maximal inactivation rate

LIST OF ABBREVIATIONS (continued)

K_m, S_{50}	substrate concentration that yields a half-maximal velocity
k_{obs}	observed rate of inactivation
LC-MS/MS	liquid chromatography-tandem mass spectrometry
LORA	low oxygen recovery assay
LTBI	latent TB infection
MABA	microplate Alamar Blue assay
MBI	mechanism-based inactivation
MDR-TB	Multidrug-resistant TB
MGS	metabolite generation system
MLM	mouse liver microsomes
MS	mass spectrometer
PM, IM, EM	poor, intermediate, extensive metabolizer, respectively
Q_h	hepatic blood flow rate
RFU	relative fluorescence units
RLU	relative luminescence units
RS9	Rat Liver S9 Fractions
S, I	concentrations of substrate and inhibitor, respectively
TAMA	TB-active metabolite assay
TB	tuberculosis
TDI	time-dependent inhibition
TFP	trifluoperazine
TFPG	trifluoperazine glucuronide
TKIs	tyrosine kinase inhibitors

TPMT	thiopurine S-methyltransferase
UDPGA	uridine 5-diphosphoglucuronic acid trisodium salt
UGT	UDP-glucuronosyltransferase;
v, V_{max}	velocity and maximal velocity of the enzymatic reaction, respectively
VTE	venous thromboembolism
XDR-TB	drug-resistant TB
τ	dosing interval of inhibitors

Summary

Drug metabolism (and pharmacokinetics) plays a delicate and important role in interfacing with the various disciplines, including medicinal chemistry, pharmacology, preclinical development, safety assessment, clinical development and regulatory affairs in the complex and multidisciplinary process of drug discovery and development. With the increasing efforts of applying DMPK principles for drug candidate optimization, selection and characterization during the drug discovery and development process, the frequency of clinical trial failures due to undesirable DMPK properties have decreased in the last several years.

However, the current methodologies of this discipline are neither practical nor adequate for predicting and solving all the problems encountered in the process of drug discovery and development. In contemporary drug discovery algorithms, drug discovery efforts often begin with the screening of focused or diverse compound libraries against either molecular targets or whole cells and hits are subsequently identified. Compounds that are inactive in such screens but which might be converted to active metabolites in vivo by liver enzymes go undetected. (Such prodrugs are occasionally designed later in the drug discovery scheme only when a clinical candidate requires chemical modification to improve ADME properties). Selected hits that emerge from initial screens will be subjected to a number of in vitro filters in the hit-to-lead phase prior to choosing a smaller number for scale up synthesis and evaluation of pharmacokinetics and/or efficacy in animal models. Library hits or synthesized analogs with poor stability in the presence of liver enzymes (as determined by LC-MS) are typically not progressed to in vivo evaluation of pharmacokinetics or efficacy. In our own experience, liver microsome instability is the most commonly encountered deficit among selectively anti-TB hits

and their subsequently synthesized analogs. In cases where the compound is deemed to be of sufficient interest, identification of the major metabolite(s) is determined in order to guide analog synthesis toward more stable compounds. To assess whether such metabolites might possess activity equal to or greater than that of the parent compound, the metabolite need not only to be identified but to be synthesized as well. Because of the amount of effort involved, this is usually part of the more downstream lead optimization process and only performed on compounds which already have some degree of metabolic stability.

The consequence of relying only upon chemical measurements of metabolic stability is that hits or synthesized analogs that are rapidly metabolized to equally or more active compounds by liver enzymes will be missed in the hit-to-lead phase of drug discovery. This is especially disconcerting considering that such metabolites often make better drugs than their respective parent compounds. As the product of metabolism and detoxification, active metabolites usually have lower drug-drug interactions and improved physicochemical (e.g. solubility), pharmacokinetic and overall safety profiles than the parent drug. Examples of clinical drugs in the market that were developed from active metabolites include sulfanilamide (parent drug: prontosil), acetaminophen (parent drug: phenacetin), digoxin (parent drug: parent drug: β-methyldigoxin), fexofenadine (parent drug: terfenadine), mesoridazine (parent drug: thioridazine) and morphine (parent drug: codeine), et al. Some existing and experimental anti-tuberculosis drugs also have known or suspected active liver enzyme-generated metabolites. For example, the experimental compounds SQ-109 and LL3858 are reported to be active in vivo, but are not stable in the presence of liver microsomes. These findings highlight the need to develop early-stage methods for evaluating parent compounds and their metabolites.

The overall goal in Chapters 2 was to develop TB-Active Metabolite Assays (TAMA) by combining a metabolite generation system (MGS) with a rapid anti-TB assay in 96-well format. Both enzymatic and cellular MGS were evaluated with the goal of using the former in a one pot TAMA for HTS. The TAMA has the potential to significantly increase the chance of identifying active metabolites in early drug discovery including prodrugs. The use of MGS in general should effectively expand the chemical diversity of compound libraries. It should also greatly impact early go/no go decisions in other infectious and non-infectious disease drug discovery.

In this work, two compounds and their corresponding enzyme derived metabolites were selected as the positive control for type-3 (active parent, active metabolite) and type-4 prodrug (inactive parent, active metabolite) compounds, which are clarithromycin/14-(R)-OH clarithromycin (CLA/14-(R)-OH CLA) and amidoxime/amidine, respectively. In order to obtain the expected metabolite of these two positive controls, various MGS were examined, including human liver microsomes (HLM), mouse liver microsomes (MLM), rat liver S9 fractions (RS9) and human liver S9 fractions (HS9), with NADPH, NADH and NAD+ as the cofactor, respectively, and HepaRG cells. This initial comparison suggested that MLM with NADH was the most efficient MGS in metabolizing the amidoxime and producing the corresponding amidine, while it was not detected in the HepaRG cell-based MGS. Generation of the amidine was subsequently found to be optimal using a combination of 0.1 mg/ml MLM, 0.5% rat S9 and 1.0 mM NAD+ in PBS at pH 6.0 resulting in the production of 8 μM of the amidine from 15.4 μM of the amidoxime.

An additional, unanticipated problem was the loss of biological activity of the MGS-generated metabolite due to protein binding, an issue that had not been originally anticipated. A series of extraction methods including sonication, centrifugation, ultrafiltration and precipitation with organic solvent – acetonitrile (ACN), were explored, among which, only the latter yielded a sufficient yield of biologically active amidine. Although preliminary experiments had suggested that bioassay of the MGS/parent/product(s) mixture could be performed directly by inoculation with M. tuberculosis without significant inhibition, further studies demonstrated that the blank control (only MGS with incubation) and negative control (MGS plus amidoxime prodrug without incubation) of type 4 positive control also inhibit the growth of M. tuberculosis H37Rv lux ABCDE, although there was certain differentiation at higher fold dilutions of the controls in the antibacterial assay. It was later found that the organic solvent (ACN) used in the extraction step was responsible for inhibition of the blank and negative controls. When methanol was used instead, this inhibition was not detected in blank and negative controls.

The activity of amidine produced from amidoxime in this MGS was confirmed with an MIC of 1.5 μM against M. tuberculosis H37Rv lux ABCDE by measuring the quantity of the amidine with LC/MS/MS, while that of the organic synthetic amidine was 0.1μM ~ 0.5 μM.

The MGS was also investigated for the formation of 14-(R)-OH CLA from CLA. This exploration ceased due to several reasons. First, the inhibitory activity of 14-(R)-OH CLA against replicating M. tuberculosis H37Rv luxABCDE is quite moderate compared to that of the parent CLA, with a MIC of 35 μM versus 1.8 μM. This was unexpected considering that this metabolite is known to

have potency comparable to the parent compound against other bacteria. According to a previous study of CLA metabolism in HLM (Rodrigues et al., 1997), besides the formation of 14-(R)-OH CLA, there are several other metabolites, including N-desmethyl CLA and 14-(S)-OH CLA. The formation of N-desmethyl-CLA and 14-(R)-OH CLA both contribute greatly to the clearance of CLA with a V max/KM of 3.3 ± 0.53 µl/min/mg protein and 4.2 ± 0.21 µl/min/mg protein, which means that the percentage of 14-(R)-OH CLA formed from CLA in humans is only around 56% at most. If so, in order to achieve a concentration above 70 µM of 14-(R)-OH CLA from CLA in MGS, the parent concentration should be at least 125 µM. Even if the yield of 14-(R)-OH CLA is 100%, the concentration of CLA in MGS would still need to be as high as 70 µM in order to realize a 90% inhibition in the antibacterial assay with a metabolite concentration of 14-(R)-OH CLA at 35 µM. However, in this case, the negative control, containing 35 µM CLA, would be too inhibitory to come up with a data analysis method to correlate bioassay-generated data with type-3 positive control inhibition profile. Secondly, with 25 mM NADP+ as the optimal concentration to generate the active metabolite of CLA, the background inhibition from the MGS will be as high as 45%, which is not acceptable for the assay control. HLM at the optimal concentration of 0.5 mg/ml could still be an inhibition factor even if solvent extraction could remove most of it.

HepaRG cells were utilized as the cell-based, liver metabolic enzyme source to generate metabolites. The specific cell culture method is critical to ensure the expression of the metabolizing enzymes and transporters. For the type 3 positive control CLA/14-(R)-OH CLA, in the in-house customized medium, the formation of metabolite 14-(R)-OH CLA was higher than that in the commercial medium. However, the yield of the metabolite of CLA in the optimized

assay was still too low to inhibit M. tuberculosis even when this yield was improved by raising the ratio of cell numbers versus the parent molecules. In addition, the MIC of 14-(R)-OH CLA for M. tuberculosis H37Rv lux ABCDE is much higher than that of the parent (35 μM vs 0.9 μM), an unexpected result which makes CLA unsuitable for use as a positive control for type 3 compounds.

The liver microsome-based MGS optimized for type 4 positive control was tested with ten marketed drugs with known metabolism by different CYP450s by measuring the disappearance of parent compounds. The challenge is its low efficiency in metabolism, which leads to a low yield of metabolites, especially when the parent compounds are incubated at a high concentration, such as 50 μM. A prolonged incubation facilitates metabolite accumulation which is suitable for compounds such as the amidine which don't appear to be further metabolized (to inactive products).

Besides the methodology development of in vitro drug metabolism to expedite the process of drug discovery, studies of drug metabolism in the presence of inhibitors were also performed with marketed drugs.

To achieve the desired therapeutic plasma or tissue concentration and maintain it for a certain period of time, a balance must be reached between the amount of administered drug and the rate of drug clearance. Since hepatic metabolism is the major clearance pathway for small molecule drug substances, the inhibition of these enzymes by co-administered drug(s) can

cause overexposure to the victim drugs and thus increased toxicities, i.e., leading to drug-drug interactions (DDIs). Both phase I and phase II enzymes can be inhibited by drugs. Pharmacokinetic DDIs have been observed with the inhibitor drugs, which require caution when they are co-administered with the victim drugs. For example, clarithromycin inhibits CYP3A4 through a mechanism-based inactivation, and the co-administration of clarithromycin incurred significant AUC increases of midazolam (a CYP3A4 substrate) following i.v. and oral dosing by 3.2-fold and 8.0-fold, respectively.

The drug-drug interactions associated to tyrosine kinase inhibitors (TKIs) recently received considerable attention due to their clinical relevance. In the first part of chapter 3 the effects of four TKIs, axitinib, imatinib, lapatinib and vandetanib, on UDP-glucuronosyltransferase (UGT) activities were investigated and compared to quantitatively evaluate their DDI potential due to UGT inhibition. Lapatinib exhibited potent competitive inhibition against UGT1A1 activity with a Ki of 0.5 µM. Imatinib was found to exhibit broad inhibition of several UGTs, with particularly potent competitive inhibition against UGT2B17 with a Ki of 0.39 µM. All four TKIs also exerted intermediate inhibition against several UGTs, including UGT1A7 by lapatinib, UGT1A1 by imatinib, UGT1A4, 1A7 and 1A9 by axitinib, as well as UGT1A9 by vandetanib. Further "quantitative prediction of DDI risk indicated that the [*co-administration of lapatinib or imatinib*] at clinical doses could result in a significant increase of AUC of drugs primarily cleared by UGT1A1" or UGT2B17, suggesting that lapatinib and imatinib could induce clinically significant DDI with co-administered UGT1A1 or 2B17 substrates.

Besides the evaluation of the inhibition of drug metabolism for potential DDIs, an exploration of the inhibition mechanism of drug metabolism with observed adverse reactions was performed. Since the metabolizing enzyme inhibited is polymorphic, it is likely that this inhibition is also different among its genetic variant proteins.

“Noscapine is an antitussive and potential anticancer drug. Clinically significant interactions between warfarin and noscapine have been previously reported. In order to provide a basis for warfarin dosage adjustment, the inhibition kinetics of noscapine” against warfarin metabolism was characterized. The enzyme kinetics data obtained from human liver microsomes and recombinant CYP2C9 proteins indicate that noscapine is a competitive inhibitor of the (S)-warfarin 7-hydroxylation reaction by CYP2C9. Interestingly, noscapine also inhibited (S)-warfarin metabolism in a NADPH- and time-dependent manner, and removal of unbound noscapine and its metabolites by ultrafiltration did not reverse inhibition of (S)-warfarin metabolism by noscapine, suggesting mechanism-based inhibition of CYP2C9 by noscapine. Spectral scanning of the reaction between CYP2C9 and noscapine revealed the formation of an absorption spectrum at 458 nm indicating the formation of a metabolite-intermediate complex. Surprisingly, noscapine is a 2- to 3-fold more efficient inactivator of CYP2C9.2 and CYP2C9.3 variants than it is of the wild-type, by unknown mechanisms. Based on the inhibitory kinetic data, (S)-warfarin exposure is predicted to increase up to 7-fold (depending on CYP2C9 genotypes) upon noscapine coadministration, mainly due to mechanism-based inactivation of CYP2C9 by noscapine. Together, these results indicate that mechanism-based inhibition of CYP2C9 by noscapine may dramatically alter pharmacokinetics of warfarin and provide a basis for warfarin dosage adjustment when noscapine is co-administered.

In summary, this dissertation has covered the studies about drug metabolism in different stages of drug discovery and development, including early stage screening assay development and the evaluation of DDI potential of drug co-administration and drug dose adjustment due to DDIs in clinical practice. The work in chapter 2 elaborates the importance of the methodology development of drug metabolism in drug discovery. Although this work has yet to result in the development of a practical HTS assay, it has provided the proof of concept. The two studies in chapter 3 utilized the theories and approaches of DDIs to exemplify the applications and significance of the emphasis of drug metabolism in drug discovery and development, which is essential to avoid drug attrition.

Chapter 1
Introduction to Drug Metabolism in Drug Discovery and Development

1.1 Introduction to Drug Metabolism

In the early 19th century, the first mammalian drug metabolite hippuric acid was identified and isolated in the urine of diabetic human (Liberg, 1829; Lehmann, 1835; Ure, 1841). The discipline of drug metabolism was not fully established until it was demonstrated that 4-dimethylaminoazobenzene could form 4-monomethylaminoazobenzene and 4-aminoazobenzene in rat liver homogenates (Mueller and Miller, 1948; Mueller and Miller, 1949; Mueller and Miller, 1953). The investigators found that this *in vitro* system was functional only when nicotinamide adenine dinucleotide phosphate ($NADP^+$), O_2, and both the microsomal and soluble fractions from liver homogenates were present, and that the microsomal fraction functioned as an oxidase (Brodie et al., 1955; Mason, 1957). Later this microsomal fraction was found to exhibit strong UV-VIS absorption maxima at the wavelength of 450 nm when it was reduced upon exposure to CO. Based on the above characteristics, these microsomal proteins were named cytochrome P450s (CYP450s) (Garfinkel, 1958; Klingenberg, 1958).

In 1982, the amino acid sequences of two CYP450 enzymes were determined for the first time in history. The sequences of CYP101 of *Pseudomonas putida* (Haniu et al., 1982) and phenobarbital-inducible form P450b (i.e., CYP2B1) of rat were deduced from the cloned cDNA (Fujii-Kuriyama et al., 1982). Since then, numerous CYP450s have been discovered. CYP450s are found in practically all living organisms and have been retained and adapted through evolution (Urlacher, 2012). The analysis of human genome indicates that approximately sixty CYP450s are present in *Homo sapiens* (Lewis, 2004). Based on the homology of amino acid sequence, the CYP450 superfamily is divided into several subfamilies, and the drug

metabolizing CYP450s belong to subfamilies 1, 2, 3, and 4. These subfamilies are further divided into isoforms, the majority of which are involved in the metabolism of xenobiotics in humans, such as CYP1A2, CYP2C9, CYP2C19, CYP2D6 and CYP3A4 (Nelson et al., 1993). The CYP450s not in the other superfamily are responsible for synthesizing endogenous structural and signaling molecules. For example, CYP51 and CYP19A synthesize cholesterol and estrogen, respectively (Lephart, 1996; Rozman et al., 1996; Lewis and Ito, 2009).

The metabolism of xenobiotics in humans includes a range of metabolic reactions that are broadly divided into phase I and phase II reactions. Phase I metabolism involves the functionalization reactions whereby a polar functional group is introduced onto the molecule. Examples include hydroxylation of an aliphatic or aromatic carbon or epoxidation of an aromatic or olefinic double bond, such as 7- and 6- hydroxylation of (*S*)-warfarin (Kaminsky and Zhang, 1997; Patki et al., 2003). CYP450s are the major enzymes involved in phase I reactions. Phase I metabolites are excreted as such or undergo phase II metabolism prior to elimination. Phase II metabolism is mediated by a group of conjugation enzymes. Phase II enzymes include UDP-glucuronosyltransferase (UGT), sulfotransferase and glutathione *S*-transferase, among others. These enzymes catalyze the transfer of small polar endogenous molecules, such as glucuronic acid, sulfate and amino acids, to parent molecules or its phase I metabolites. Through phase I and/or phase II metabolism, parent molecules are transformed into water-soluble metabolites and readily excreted into the urine or bile.

1.2 Drug Metabolism in Drug Discovery and Development

The process of drug discovery and development is inherently multidisciplinary, involving medicinal chemistry, pharmacology, preclinical development, safety assessment, clinical

development and regulatory affairs (Yengi et al., 2007). Drug metabolism and pharmacokinetics (DMPK) plays a delicate and important role in interfacing with these various disciplines (Figure 1.1). Pharmaceutical industry expends significant effort in applying DMPK principles for drug candidate optimization, selection and characterization during the drug discovery and development process. "In fact, in 1990 it was estimated that approximately 40% of drug attrition was due to undesirable DMPK properties. In 2000, this number was reduced to 10%" based on the incorporation of DMPK knowledge in early stages of drug development (Yengi et al., 2007). (Figure 1.2 a, b, c and d). During the years between 2008 and 2010, based on a report of phase II and phase III trials, the undesirable properties of pharmacokinetics and bioavailability (PKBA) are only responsible for 1% failures in phase II trials, while in phase III trials, there were no failures due to DMPK (Arrowsmith and Miller, 2013). Between 2011 and 2012, none of the failures in phase II and III trials was caused by undesired DMPK properties (Arrowsmith and Miller, 2013). All these indicates that incorporating DMPK in early drug development process helps increase the success rate of drug development and reduce the average cost.

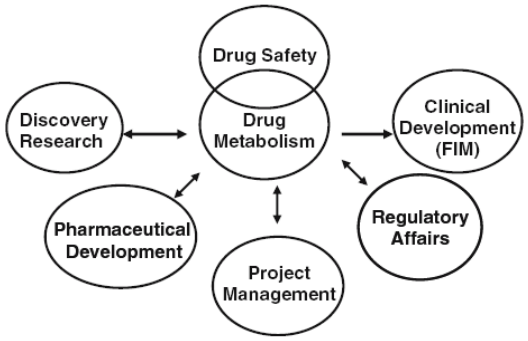

Figure 1.1 A central role of drug metabolism (and drug safety) in pharmaceutical research

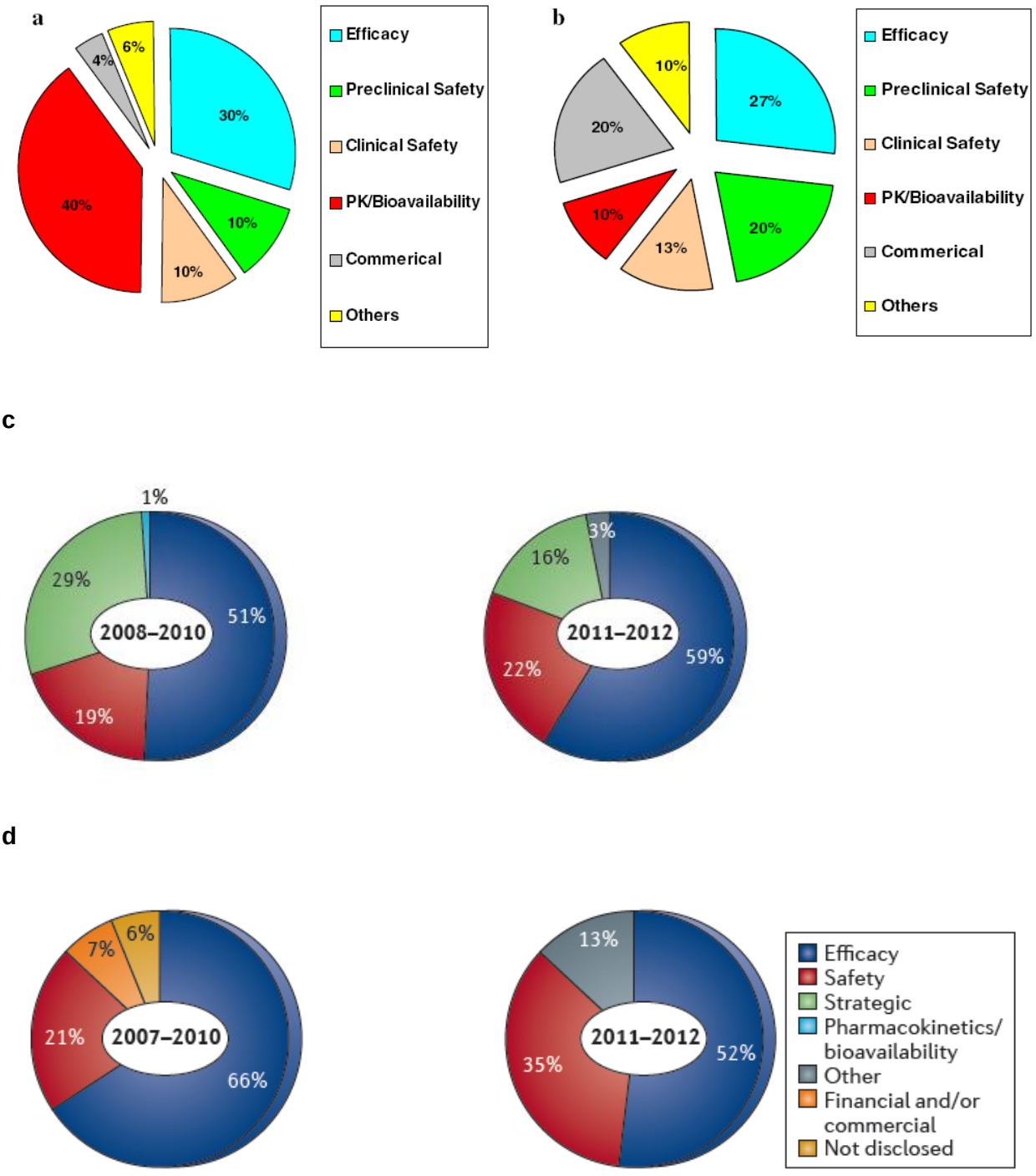

Figure 1.2 Factors causing attrition in drug development in 1990 (a) and 2000 (b); factors for drug failures in phase II trials between 2008 and 2012 (c); and drug failures in phase III trials and submission between 2007 and 2012 (d)

1.2.1 Identification of Lead Compounds

1.2.1.1 Metabolic Stability of Lead Compounds

At the early discovery stage, results from metabolic stability studies provide a basis for choosing the lead compounds. Intrinsic clearance (CL_{int}, the intrinsic ability of hepatic enzymes to metabolize the drug) estimated from using liver tissue fractions have been one of the most important determinants of its pharmacokinetic parameters, and are critical in predicting the hepatic clearance of the candidate compound *in vivo*. Briefly, *in vitro* systems of liver homogenates or cryopreserved hepatocytes are used to determine of CL_{int} of the compound, and then *in vivo* hepatic clearance values can be estimated through *in vitro-in vivo* extrapolation (IVIVE) approaches (Wilkinson and Shand, 1975; Pang and Rowland, 1977; Obach, 1999; Poulin, 2013). The *in vivo* clearance values estimated through IVIVE were shown to be in good agreement with the observed *in vivo* hepatic clearance values in different species, as demonstrated for indinavir (Lin et al., 1996).

For human risk assessment, not only the systemic exposure of an unchanged drug is required by regulatory agencies, but also that of its major metabolites and the relative contribution of the corresponding metabolic pathways to the overall elimination of the drug. In addition, the structural identification of the metabolites could facilitate rational modifications of drug candidates during the optimization process aimed at blocking the relevant metabolic soft spots.

1.2.1.2 Identification of Active Metabolites

For the host system, the metabolism of the xenobiotics is a detoxifying process accomplished by increasing its hydrophilic properties to facilitate elimination it through excretion in urine or bile. In drug discovery, this metabolism usually leads to the inactivation of the pharmacologically

active parent drug and therefore reduces the portion of the parent drug responsible for its efficacy *in vivo*. However, there is increasing evidence that the metabolites of some drugs are pharmacologically active, and therefore, this process of drug metabolism is utilized to improve the DMPK properties of the drug candidate by synthesizing a prodrug. Such an example can be found in pafuramidine, an orally available inactive prodrug of DB75 for the treatment of malaria, which was developed to overcome the poor bioavailability of DB75 due to rapid reduction of amidine bond (Figure 1.3). Also, pharmacologically active metabolites have been used as a source of new drug candidates. For example, acetaminophen is an *O*-deethylated metabolite of phenacetin, and when compared with phenacetin, acetaminophen shows superior analgesic activity but lacks the adverse effects, including methemoglobinemia and hemolytic anemia resulting from the formation of *N*-hydroxyphenatidine, a metabolite of phenacetin (Figure 1.4) (Jensen and Jollow, 1991).

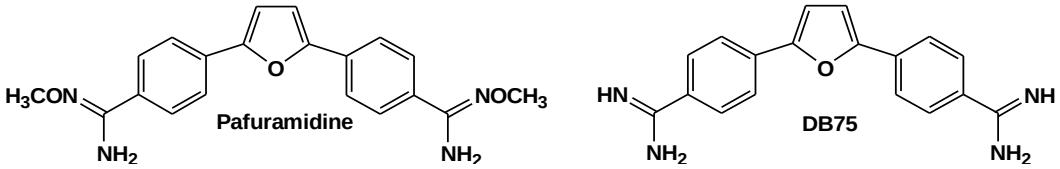

Figure 1.3 The structure of the prodrug pafuramidine and its active metabolite DB75

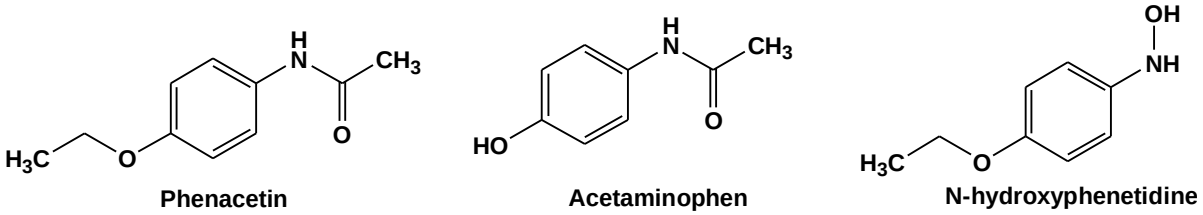

Figure 1.4 The structure of phenacetin, its active metabolite acetaminophen and its toxic metabolite N-hydroxyphenetidine

1.2.2 Prediction of Drug-drug Interactions

For the metabolically unstable drug candidate, the identification of the specific drug-metabolizing enzymes is important for determining its involvement in drug-drug interactions (DDIs). Metabolic DDIs occur when one therapeutic agent alters the concentration of another agent by either increasing or decreasing its metabolic clearance through the induction or inhibition of the metabolizing enzymes (Lemke, 2012). In drug discovery and development, the drug candidate may be subject to DDI as a victim whose metabolism is affected by another drug or drugs or a precipitant drug (the drug that affects the efficacy of the targeted drug) or a precipitant affecting metabolism of interacting drugs.

"Metabolism of drugs is often very complex, involving several pathways and various enzyme systems. In some cases, all the metabolic reactions of a drug are catalyzed by a single enzyme, whereas, in other cases, a single metabolic reaction may involve multiple enzymes". If the enzyme identified in the phenotyping assay is responsible for 25% or more of the systemic clearance of the drug candidate, the potential a drug-drug interaction should be studied (USFDA, 2012b).

If this drug candidate is metabolically stable, it is still likely that it interferes the metabolizing enzymes with other drugs as the substrates. Therefore, an *in vitro* investigation of this drug candidate as an interacting drug of an enzyme (precipitant) with most sensitive substrates will be done in terms of its inhibition and induction potential (USFDA, 2012b). *In vivo* studies with other substrates selected based on likely co-administration and/or narrow therapeutic range will be conducted when significant interactions are observed *in vitro*.

Metabolic DDIs may occur via two mechanisms: inhibition and induction of DME activity. To assess the potential for metabolic DDIs through enzyme inhibition, it is routinely tested whether a drug candidate as the precipitant reversibly inhibits CYP450 activity. Also, mechanism-based inactivation (MBI) of CYP450s by compounds harboring functional groups such as methylenedioxyphenyls, acetylenes, furans, thiophenes, secondary or tertiary amines are increasingly being recognized as a source of inhibitory DDIs (Yengi et al., 2007). Understanding the mechanisms of MBI allows the determination of potential structure-inhibition relationships, and the possibility to modify the structure of the drug candidates without the features responsible for bio-activation and inhibition. Enzyme induction is the other mechanism leading to DDIs. Induction of hepatic drug metabolism was recognized in animals as early as 1956 that 3-methylcholanthrene increased the ability to metabolize methylated aminoazo dyes (Lin and Lu, 1997). Induction of drug-metabolizing enzymes may lead to either a decrease in toxicity through an elevated detoxification, or an increase in toxicity due to an enhanced reactive metabolite formation. Overall, induction can lead to a beneficial or harmful outcome depending on the balance between detoxification and activation.

1.3 Drug Metabolism in Clinical Practice

The concomitant administration of multiple drugs is common especially for elderly people and hospitalized patients (Lin and Lu, 1997). The risk of clinical consequences from DDIs is higher with drugs with narrow therapeutic index. Therefore, metabolic DDIs have become an important aspect to ensure the safety and efficacy of drugs used in combination. For example, it was found that the AUC of atorvastatin was increased by 494% due to its inhibition of CYP3A4 (Jacobson, 2004). Besides, significant increases the AUC had also been observed with the coadministered drugs including digoxin, midazolam, trizolam etc. With the inhibition of more than 26 marketed drugs in humans, mibefradil has been withdrawn from market since 1998 (Po and Zhang, 1998). Another example, it was observed during a clinical trial that a combination of dextromethorphan (a substrate of CYP2D6) and quinidine (a CYP2D6 inhibitor), each drug at a dose of 30 mg twice daily, enhanced the plasma AUC of paroxetine (20 mg daily) by 30%. For dextromethorphan and quinidine, the AUC exposure increased by 50% and 40%, respectively, which indicated that patients should be monitored for adverse reactions, and dosage adjustment should be considered when combining these agents (Schoedel et al., 2012).

1.4 Pharmacogenetics of Drug Metabolism

Pharmacogenetics is a study of genetic differences in metabolic pathways which can affect individual responses to drugs, both in terms of therapeutic effect as well as adverse effects (Klotz, 2007). This “concept that inheritance can have an important role in individual variation in drug response originally grew out of clinical observations of large differences among patients in their response to doses of a drug” and plasma concentrations or other pharmacokinetic parameters are highly heritable for some drugs (Weinshilboum and Wang, 2004). Drug metabolism is one of the major determinants of the pharmacokinetics characteristics involved in the majority of 'classic' pharmacogenetic traits. Mutations in the gene for a drug-metabolizing enzyme, due to environmental or evolutionary factors, can result in enzyme variants with higher, lower, or no activity. Sometimes, such mutations may lead to gene deletion (Lin and Lu, 1997). This genetic variability can cause interindividual variation in the rate and extent of drug metabolism. For example, CYP2C9*2 and CYP2C9*3 allele carriers have a reduced *S*-warfarin clearance by 35% (Hirota et al., 2013). Patients carrying CYP2C9.2 and CYP2C9.3 experience more toxicity (Wang et al., 2009), indicating that individuals who inherit an impaired ability to catalyze enzymatic reactions may be at an increased risk of concentration-related adverse effects and toxicity.

The thiopurine S-methyltransferase (TPMT) genetic polymorphism is one of the most studied examples in pharmacogenetics. TPMT is responsible for various activation and deactivation steps of thiopurine drugs, which are used for the treatment of acute lymphoblastic leukaemia of childhood, inflammatory bowel disease and organ transplant recipients. However, thiopurine drugs have a narrow therapeutic index with the potential for life-threatening drug-induced toxicity, primarily myelosuppression. It was found that inherited decrease in the level of red blood cell TPMT activity makes more drug available for the multistep pathway that leads to the

formation of active metabolites, 6-thioguanine nucleotides, resulting in drug-induced myelosuppression. Therefore, genetic polymorphisms of TPMT has become one of the causes that lead to decreased methylation and decreased inactivation of the drugs. The most common variant allele for TPMT in Caucasians is TPMT*3A, that has a frequency of approximately 5% in Caucasian populations, but is rarely, if ever, observed in East Asian populations. For the homozygous carriers of TPMT*3A, they are at greatly increased risk for life-threatening myelosuppression when treated with standard doses of thiopurine drugs, and approximately 90% reduction of the standard dose with careful monitoring has to be made for their treatment (Weinshilboum and Wang, 2004; Wang and Weinshilboum, 2006).

These advances and insights have affected drug metabolism studies in terms of the design and conduct of and interpretation of results in the drug discovery and development process (Yengi et al., 2007). For example, a strong CYP2D6 inhibitor, such as fluoxetine will increase the plasma concentrations of atomoxetine, a CYP2D6 substrate, in extensive metabolizers (EMs) of CYP2D6, but will have negligible effect in poor metabolizers (PMs) of CYP2D6, since PMs do not have active enzyme to inhibit. However, it should be noted that CYP2D6 PMs will have significantly increased plasma levels of atomoxetine if they are given usual doses (USFDA, 2012b). Taken these together, the consideration of pharmacogenetics in drug metabolism studies, especially DDIs have proven to be of significant value in the success drug discovery and development.

1.5 Rationale and Overview of Proposed Research

Although the last two decades have witnessed significant progress in the development and application of the theories and methodologies of drug metabolism, much remains to be explored and applied. The goal of this dissertation is to utilize the knowledge and methodology of drug metabolism to solve specific problems that are encountered from early drug discovery to clinical pharmacy practice.

Aim 1. Develop an *in vitro* assay to detect liver enzymes derived active metabolites against *M. tuberculosis*.

A direct *in vitro* system will be developed to incubate compounds with and without a liver enzyme metabolite generation system (MGS) prior to incubation with *M. tuberculosis*. Both particle/enzymatic and cellular MGS will be evaluated using control compounds. The substrate concentration, incubation time and organic solvent concentrations will be optimized. A data analysis method will be established to correlate bioassay-generated data with mass spectrometry data to identify active metabolite(s). In the end, this TB-active metabolite assay (TAMA) will be applied in anti-tuberculosis drug discovery.

Aim 2. Identify the *in vitro* inhibitory activities of tyrosine kinase inhibitors against UGT isoforms and predict the *in vivo* impact on AUC of the substrate drug

A series of tyrosine kinase inhibitors toward the inhibition of the glucuronidation of the non-selective substrate will be screened across a panel of UGT isoforms to establish their inhibitory profiles. The selectivity and potency of each TKI in terms of inhibiting glucuronidation among these UGT isoforms will be investigated *in vitro*. With the characterized inhibition kinetics of these TKIs, a prediction of AUC change for the non-selective UGT substrates and victim drug (the drug that is affected due to the existence of another drug or drugs in DDIs) will be made.

Aim 3. Investigate the mechanism of DDIs between noscapine and warfarin, and its clinical implications

An adverse reaction of warfarin with an elevated international normalized ratio, which indicates a higher risk of bleeding, had been observed in clinical practice due to the suspected drug-drug interactions with noscapine. The mechanism of this DDI will be explored through a series of experiments and predictions. This DDI will also be investigated in CYP2C9 variants in order to recommend a dose adjustment based on the inhibition of noscapine and the clearance of different genotype carriers.

Chapter 2
Drug Metabolism in Early Stage anti-TB Drug Discovery

2.1 Introduction

2.1.1 Introduction to Tuberculosis

Tuberculosis (TB) is an infectious disease caused by members of the *Mycobacterium tuberculosis* complex, which includes *Mycobacterium tuberculosis*, *M. africanum*, *M. bovis*, *M. caprae*, *M. microti*, *M. pinnipedii* and *M. canettii (Zumla et al., 2013)*. TB is transmitted through droplet aerosolization by an individual with active pulmonary disease (Sia and Wieland, 2011). TB can affect any organ system, though typically targets the lungs. TB infection begins when the mycobacteria reach the pulmonary alveoli, where they invade and replicate within endosomes of alveolar macrophages (Ahmad, 2011). The ensuing immune response arrests further growth of bacteria. The pathogen is completely eradicated in ~10% of those infected, while in the remaining ~90%, the immune response only succeeds in containment of the infection. Some bacilli are able to escape killing by blunting the microbicidal mechanisms of immune cells and subsequently remain in a non-replicating state in old lesions. About 10% of immunocompetent persons with latent TB infection (LTBI) will develop active TB over their lifetime, half of these occurring during the first 2 years post-infection (Sia and Wieland, 2011). For those with active TB, symptoms present insidiously, most commonly with fever, cough, weight loss, fatigue, and night sweats. Less common symptoms include chest pain, dyspnea, and hemoptysis. TB remains the eighth leading cause of death in the world.

An estimated one-third of the world's population is infected with *M. tuberculosis*. According to a World Health Organization report on the worldwide incidence of TB, "in 2011 there were 8.7 million new cases and 1.4 million deaths from TB, including 350,000 deaths associated with co-

infection with HIV" (Zumla et al., 2013). "Sub-Saharan Africa has the highest rates per capita of TB, which is driven primarily by the HIV epidemic in that region. India, China, South Africa and the Russian Federation have almost 60% of the world's TB cases". Multidrug-resistant TB (MDR-TB), which is a TB resistant to at least isoniazid and rifampin, is now ubiquitous with an estimated half million cases reported in 2011. The more critical one, extensively drug-resistant TB (XDR-TB), which is resistant to isoniazid and rifampin, plus any fluoroquinolone and at least one of three injectable second-line drugs, has been reported in 84 countries (Zumla et al., 2013).

2.1.2 Current TB Regimens

The first antibiotic used for TB, streptomycin (STD), was purified from Streptomyces griseus, and showed some promise in curing TB patients (Zumla et al., 2013). However, drug resistance rapidly developed since it was used as monotherapy. "In the 1950s, several additional TB drugs with different mechanisms of action were discovered and developed, including para-amino salicylic acid, isoniazid, pyrazinamide, cycloserine and kanamycin", which led to a combination therapy of 18-months duration or longer. The current therapeutic regimen of isoniazid, rifampicin, pyrazinamide and ethambutol, developed in the 1960s, shortened the treatment duration to 6 months. Besides the above four first-line TB drugs, there are three groups of second-line TB drugs which are the reserved therapy for TB resistant to the first-line drugs. Third-line TB drugs include one group and have "unclear efficacy or undefined roles" (Table I).

First-line anti-TB drugs	Oral: isoniazid, rifampicin/rifampin, pyrazinamide, ethambutol, rifapentine or rifabutin.
Second-line anti-TB drugs	**Group 1.** Injectable aminoglycosides: streptomycin, kanamycin , amikacin. Injectable polypeptides: capreomycin, viomycin.
	Group 2. Oral and injectable fluoroquinolones: ciprofloxacin, levofloxacin, moxifloxacin , ofloxacin, gatifloxacin.
	Group 3. Oral: para-aminosalicylic acid, cycloserine, terizidone, ethionamide, prothionamide , thioacetazone, linezolid .
Third-line anti-TB drugs	Clofazimine, linezolid, amoxicillin plus clavulanate, imipenem plus cilastatin, clarithromycin .

Table I. CLASSIFICATION OF DRUGS USED TO TREAT DRUG-SUSCEPTIBLE AND DRUG-RESISTANT TUBERCULOSIS (Zumla et al., 2013). This table is adapted from

At the end of 2012, the U.S. Food and Drug Administration approved bedaquiline (aka TMC-207; Sirturo®) as part of a combination therapy to treat adults with MDR-TB as a third-line drug (Gras, 2013). Bedaquiline possesses potent and selective *in vitro* mycobactericidal activity by inhibiting ATP synthesis under both aerobic and anaerobic conditions and it is active in *in vivo* murine models of TB. It is mechanistically and structurally unrelated to all existing TB drugs.

2.1.3 Global Urgencies of Discovering New Drugs for TB Treatment

The current TB regimen drugs were developed 40 years ago. The 6-month treatment duration results in poor patient compliance, and the current TB drugs are not sufficiently effective in treating MDR-TB, XDR-TB nor totally drug-resistant TB (TDR−TB) (Zumla et al., 2013). Effective treatment of HIV/TB co-infections requires the concurrent use of HIV and TB drugs, therefore

pharmacokinetic drug-drug interactions are another concern for the current TB regimen. Several TB drugs, including rifampin, are notorious for inducing liver CYP450s (Franzblau et al., 2012). Often, the intolerance and toxicities of current TB drugs results in treatment interruptions and changes to the regimen. With all the above shortcomings of the current TB treatment regimens, the primary goals of new drug development includes shortening and simplifying treatment of active TB, providing safer and more efficacious treatments for drug-resistant TB, eliminating drug-drug interactions for TB/HIV co-infections, and improving treatment for LTBI.

2.1.4 Traditional Methodologies in TB Drug Discovery

2.1.4.1 The Platform of TB Drug Discovery and its Deficiencies

Contemporary TB drug discovery efforts often start with screening focused or diverse compound libraries, and mostly utilize cellular assays. The classical whole cell screening assays, conducted for decades on solid media or in tube-based liquid media, were adapted to microplate format in the late 1990s for actively replicating cultures initially using the microplate Alamar Blue assay (MABA) (Collins and Franzblau, 1997) and later for use with non-replicating cultures, eventually with a colony forming unit (CFU)-independent readout using the low oxygen recovery assay (LORA) (Collins and Franzblau, 1997; Cho et al., 2007). The hits that showed inhibitory activities against replicating and/or non-replicating bacteria are selected from the initial screens and subjected to a number of *in vitro* filters, such as cytotoxicity against VERO cells (isolated from African green monkey kidney), bactericidal activities and anti-tuberculosis activity in the J774A.1 mouse macrophage-like cell line. The metabolic stability to mouse and human liver enzymes is another criterion in the hit-to-lead phase. As xenobiotics, such compounds typically undergo various metabolic reactions catalyzed by phase I and/or phase II liver enzymes, such as CYP450s and UGTs. Compounds with half-lives of less than 30 min due to liver metabolism are considered to be metabolically unstable and less likely to be prioritized for

scale up synthesis or pharmacokinetic and/or efficacy evaluation in animal models (Thompson, 2001; Di et al., 2003).

With this TB drug discovery platform, there are several shortcomings. It is possible that compounds that are inactive in the *in vitro* antibacterial assays might still be converted to active metabolites *in vivo* by liver enzymes. Also library hits or synthesized, active analogs, which are poorly stable in the presence of liver enzymes, are typically not further progressed to *in vivo* pharmacokinetics or efficacy evaluation although structural instability may not necessarily result in loss of anti-TB activity. Our own experience concludes that liver microsome instability is the most common deficit among selectively toxic anti-TB hits and their subsequently synthesized analogs. For example, 27 of 34 prioritized hit classes from 3 libraries screened in our lab had half-lives of less than 30 min in liver microsomes. For compounds with potential of becoming a lead for *in vivo* testing, identification of the soft-spots and the major metabolite(s) are critical to guide analog synthesis toward more stable compounds, while maintaining the antibacterial activities. The process of determining whether such metabolites might possess equal or greater activity than that of the parent compound is time- and resource-consuming, requiring synthesis of the metabolites. Such an effort is part of the more downstream lead optimization process.

2.1.4.2 Anti-tuberculosis Assays in TB Drug Discovery

The radiometric BACTEC 460 system, based on the detection of $^{14}CO_2$ generated from the metabolism of 1-^{14}C-palmitic acid by replicating mycobacteria, had been used as the clinical drug susceptibility system of choice two decades ago (Heifets, 1991; Murray et al., 1995) due to its speed and reduced labor requirement relative to the counting/detection of *M. tuberculosis* colonies. However, due to its high cost, high culture volume, lack of high-throughput format, and

the requirement for radioisotope disposal, it was difficult to apply it in massive antimycobacterial drug screening. Collins and Franzblau developed MABA which detects the fluorescence produced from the reduction of Alamar Blue or resazurin by the reducing power of the live bacteria (Collins and Franzblau, 1997). The Alamar Blue (resazurin) is a general indicator of cellular growth and/or viability; the blue, non-fluorescent, oxidized form becomes pink and fluorescent upon reduction. Concentrations of established anti-TB agents effecting a reduction in fluorescence intensity (measured in a microplate fluorometer) of 90% relative to untreated control cultures correlated well with those effecting a reduction of 99% in $^{14}CO_2$ generation in the BACTEC 460 (which in turn had been correlated with reductions of 99% in CFU by classical methods); therefore such (interpolated) concentrations defined the minimum inhibitory concentration (MIC) in the MABA.

With MABA, the screening for antimycobacterial drugs can be performed rapidly and efficiently at relatively low cost. However, it is widely accepted that a physiological state of non-replicating persistence is responsible for antimicrobial tolerance in many bacterial infections. Cho et al. developed another assay LORA for rapidly screening compounds against non-replicating mycobacteria (Cho et al., 2007). A *M. tuberculosis* H37Rv luxAB strain expressing luciferase was adapted to low oxygen conditions by extended culture in a fermentor, and was subsequently incubated in microplate cultures maintained under anaerobic conditions for 10 days with test compounds before enabling metabolic recovery under ambient oxygen for another 28 hr. A luminescent signal was measured to calculate the MIC.

Since *M. tuberculosis* can replicate within endosomes of alveolar macrophages, macrophage assays to assess intracellular activity have been developed with a wide variety of cell sources

such as rat cell lines, bone-marrow derived macrophages, J774 and THP-1 cells (Franzblau et al., 2012). Mycobacteria are phagocytized by the macrophages and these cultures exposed to test compounds for varying periods of time and finally the viability of the *M. tuberculosis* assessed by CFU or metabolic/imaging readouts.

2.1.5 Significance of *in vitro* Detection of anti-TB Liver Metabolites in Early Drug Discovery

This traditional hit-to-lead process often neglects those metabolically unstable hits or synthesized analogs, which might be rapidly metabolized to equally or more active compounds by liver enzymes. As the product of liver metabolism and detoxification, active metabolites usually have lower drug-drug interactions and improved physicochemical (e.g. solubility), pharmacokinetic and overall safety profiles than the parent drug, which make them often better drugs than their respective parent compounds. For examples, ulfanilamide, acetaminophen, digoxin, fexofenadine, mesoridazine and morphine as the active metabolites, were developed from the parent drugs prontosil, phenacetin, β-methyldigoxin, terfenadine, thioridazine and codeine, respectively.

Some existing and experimental anti-tuberculosis drugs also have known or suspected liver enzyme-generated active metabolites (Table II). There are a total of 24 marketed drugs and 4 compounds (PA824, OPC67683, SQ109 and LL3858) at various stages of clinical trials for the treatment of TB. Out of these 24 anti-TB drugs approved, only 9 were found to form active metabolites. Eight of the 28 were studied for metabolite toxicity (Daniel et al., 2000; Jia et al., 2006; Matsumoto et al., 2006; Preziosi, 2007; 2008a; Budha et al., 2008; Henderson et al., 2008;

Diacon et al., 2009), of which 7 were found to have toxic metabolites. These findings highlight the need to develop early-stage methods for evaluating parent compounds and their metabolites.

Drug	Active metabolite	Toxic metabolite	Ref.	Drug	Active metabolite	Toxic metabolite	Ref.
Rifampin	25-deacetyl rifampicin (esterase)	NA*		p-Aminosalicylic acid	NA	N-acetylated PAS(NAT1)	(Yamada et al., 1991)
Isoniazid	NA	AcHZ, Hydrazine (MFO, CYP2E1)	(Preziosi, 2007)	Ethionamide	S-oxide Ethionamide (FMO)	S-oxide Ethionamide (FMO)	(Henderson et al., 2008)
Pyrazinamide	Pyrazinoic acid (xanthine oxidase)	PA, 5-OH-PA	(2008a; Budha et al., 2008)	Prothionamide	sulfoxide metabolite	NA	(Peters et al., 1983)
Ethambutol	NA	NA	(Shih et al., 2013)	Linezolid	Inactive metabolites (aminoethoxy-acetic and hydroxyethyl glycine derivatives)	NA	FDA label;(Barry and O'Connor, 2007)
Rifapentine	25-desacetyl-rifapentine	NA	(Rastogi et al., 2000)	Clofazimine	No major metabolite identified	No major metabolite identified	
Streptomycin	No major metabolite identified	No major metabolite identified		Imipenem	No major metabolite identified	No major metabolite identified	
Kanamycin	No major metabolite identified	No major metabolite identified		Clarithromycin (CLA)	14-(*R*)-OH CLA (CYP3A4)	NA	(2008a; Budha et al., 2008)
Amikacin	No major metabolite identified	No major metabolite identified		Thioridazine	Mesoridazine, sulforidazine (CYP2D6)	Thioridazine 5-sulphoxide	(Daniel et al., 2000; Wen and Zhou, 2009)
Capreomycin	NA	NA		Metronidazole	HO- metronidazole	HO-metronidazole	(Menéndez et al., 2002)
Ciprofloxacin	Four metabolites	NA	FDA label	PA824	NA	NA	

Ofloxacin/ levofloxacin	No major metabolite identified	No major metabolite identified		OPC67683	No major metabolite identified	No major metabolite identified	(Matsumoto et al., 2006)
Moxifloxacin	Inactive metabolites (glucuronide and sulphate moxifloxacin)	Inactive metabolites (glucuronide and sulphate moxifloxacin)	(2008a; Budha et al., 2008)	TMC207	N-monodesmethyl metabolite (CYP3A4)	N-monodesmethyl metabolite (CYP3A4)	(Rustomjee et al., 2008; Diacon et al., 2009; USFDA, 2012a; Dooley, Mar 3rd, 2013)
Gatifloxacin	No major metabolite identified	No major metabolite identified		SQ109	NA	NA	(Jia et al., 2006; Meng et al., 2009)
Cycloserine	No major metabolite identified	No major metabolite identified		LL3858	NA	NA	(2008b)

Table II. ESTABLISHED ANTI-TB DRUGS WITH ACTIVE OR TOXIC METABOLITES. THE ACTIVE OR TOXIC METABOLITE IS DEFINED TO BE THE METABOLITE WITH A MIC OR IC_{50} AT MICROMOLAR LEVEL DETERMINED BY *IN VITRO* ANTIBACTERIAL OR CYTOTOXICITY ASSAYS, RESPECTIVELY. NA: NO DATA AVAILABLE

2.1.6 Objective and Overall Research Strategies

At present, the platforms for anti-TB drug discovery, especially HTS-based anti-TB drug discovery, fail to account for the possibilities of active metabolites early in the drug discovery process. In this chapter, *in vitro* assays will be established to rapidly detect the anti-TB activity of liver enzyme-derived metabolites. These TB-active metabolite assays (TAMA) should obviate the need for metabolite ID and synthesis to confirm the presence or absence of an active metabolite. A novel method to evaluate metabolite activity will be developed by combining a liver enzyme MGS with an anti-TB assay. For detection of prodrugs (anti-TB inactive parent compound with liver enzyme-generated anti-TB active metabolites), an HTS-compatible assay will be established, which will also serve to increase compound library chemical diversity. To distinguish liver enzyme-derived anti-TB active metabolites of anti-TB active parent compounds (type 3 compounds) from anti-TB active parent compounds that are relatively stable to liver enzymes (type 1 compounds), concurrent LC/MS/MS analysis of parent compound stability is required along with optimized data analysis. The ability to detect liver enzyme-generated anti-TB active metabolites by this method early in the drug discovery process will allow for the further progression of some active (type 3) compounds with poor metabolic stability to liver enzymes that otherwise would be deprioritized using only LC/MS/MS based stability assays on the assumption that they were type 2 compounds, which are active anti-TB parent compound but generate inactive metabolites. The above methodology will be developed using established and modified control compounds and then applied to a HTS for proof of concept.

Aim 1. Develop and validate a direct *in vitro* system to measure the anti-TB activity of liver enzyme mediated metabolites.

Compounds are incubated with and without a liver enzyme MGS prior to incubation with *M. tuberculosis*. Both particle/enzymatic and cellular MGSs will be evaluated using control

compounds. The substrate concentration, incubation time and organic solvent concentrations will be optimized.

Aim1a. Evaluate enzymatic and cellular MGS with respect to metabolite formation and compatibility for coupling with a *M. tuberculosis* growth inhibition assay.

Aim1b. Validation of the assay with control compounds

Aim1c. Development of a HTS format assay

Aim 2. Establish a data analysis method to correlate bioassay-generated data with mass spectrometry data to identify active metabolite(s)

Aim 3. Application of a TB-active metabolite assay (TAMA) in anti-tuberculosis drug discovery.

A 100,000 compound library will be screened against *M. tuberculosis* with and without MGS using one of the systems developed in Aim 1. All active compounds (including Type 4 prodrugs) will be assessed for metabolic stability by LC/MS/MS and the reactions re-tested vs. TB in 2-fold dilution. Active metabolites will be identified and selected metabolites confirmed by synthesis and bioassay as proof of concept.

2.2 Assay Development to Detect Liver Microsomes Derived Active Metabolites against *M. tuberculosis*

2.2.1 Introduction

Our lab has been conducting anti-TB drug assay development and HTS-based anti-TB drug discovery for more than a decade. Our own screening efforts demonstrate that a large proportion of library compounds are not active, while among the active hits and synthesized analogs, a high percentage are metabolically unstable compounds/classes (Table III). Twenty-seven of thirty-four prioritized hit classes from 3 libraries and nearly half of the synthesized analogs had half-lives less than 30 minutes in liver microsomes. For compounds that are inactive in such screens but might be converted to active metabolites *in vivo* by liver enzymes, there is no way using our current approaches to detect the latter. Meanwhile, such unstable compounds tend to be deprioritized without knowing whether they are metabolized to equally or more active compounds by liver enzymes. For compounds deemed to be of sufficient interest, a significant effort must be made to determine the metabolic soft spots and to identify the structures of the corresponding metabolites, in order to guide analog synthesis toward more stable compounds.

Based on the anti-TB activity and stability to liver enzymes, we categorize compounds into four types (Table IV & Figure 2.1). An example of a type 1 compound (active and metabolically stable), is clofazimine which is active against replicating *M. tuberculosis* H37Rv *luxABC* with a MIC <0.2 µM, and in humans, its half-life is as long as 70 days. An example of a type 2 compound (active parent; inactive metabolite), is a mefloquine-isoxazole carboxylic acid ester (the subject of a previous unsuccessful lead optimization effort) with MICs of 0.6 µM and 3.0 µM against replicating and non-replicating *M. tuberculosis*, respectively. As the positive control for

type 4 compounds (prodrug: inactive parent; active metabolite) -- the amidoxime analog (LLK2-161) has an MIC against replicating *M. tuberculosis* H37Rv *luxABCDE* that is much higher than that of its active metabolite-amidine analog (LLK2-150), 28 µM vs. 0.2 µM, respectively. CLA, as the positive control for type 3 compounds (active parent; active metabolite) inhibits replicating *M. tuberculosis* H37Rv *luxABCDE* with a MIC of 1.8 µM. However, the known active metabolite (vs. gram-positive bacteria) of CLA (14-(*R*)-OH CLA) is not as active vs. *M. tuberculosis* H37Rv *luxABCDE* as expected, with an MIC as high as 35 µM.

Subcellular fractions, such as liver microsomes and S9 fractions, have been great *in vitro* tools for investigating the metabolism of compounds, including intrinsic clearance, metabolite identification and drug-drug interactions since they contain many of the phase I and phase II drug metabolizing enzymes found in the liver. Liver microsomes and S9 fractions are easy to prepare from the liver tissue “and can be stored for long periods of time. They are easily adaptable to high throughput screens which enable large numbers of compounds to be screened rapidly and inexpensively”.

Library	Total Cmpd No.	Screening Conc./μM	Hits (chemical series)					Active analogs			Inactive analogs		
			No.	%	Evaluated for microsome stability								
					No.	$t_{1/2}$ < 30 min.		No.	$t_{1/2}$ < 30 min.		No.	$t_{1/2}$ < 30 min.	
						No.	%		No.	%		No.	%
Axinex	53620	3	76	0.14	21(12)	14 (9)	67	ND	ND	ND	ND	ND	ND
Analyticon	6000	3	13	0.22	8 (5)	8 (5)	100	ND	ND	ND	ND	ND	ND
Chembridge 2	102634	3	1105	1	5 (5)	5 (5)	100	7	5	71	16	8	50
Chembridge NovaCore	50000	10	60	0.12	ND	ND	ND	31	11	35	11	7	64
Actino extr	65000	10 ul/ml	312	0.48	ND	ND	ND	ND	ND	ND	ND	ND	ND

Table III. A SUMMARY OF THE COMPOUNDS SCREENED IN HOUSE WITH METABOLIC STABILITIES (ND, Not Determined)

	Type 1	Type 2	Type 3	Type 4 Prodrug
Parent	active	active	active	inactive
Stability	high	low	low	low
Metabolite	NA	inactive	active	active
Example	Clofazimine	Mefloquine-Isoxazole Carboxylic Acid Ester	CLA	In-house amidoxime analog

Table IV. DEFINITIONS OF 4 TYPES OF COMPOUNDS IN ANTI-TB SCREEN ASSAYS AND EXAMPLES AS THE CONTROLS

A

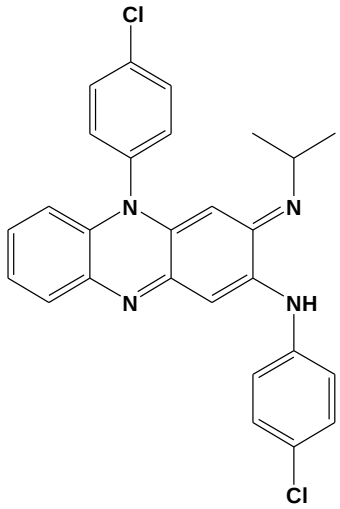

B

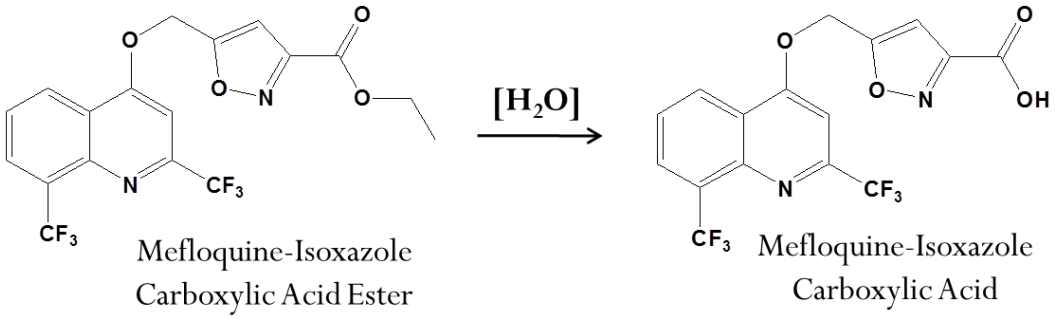
[H2O]
Mefloquine-Isoxazole Carboxylic Acid Ester
Mefloquine-Isoxazole Carboxylic Acid

C

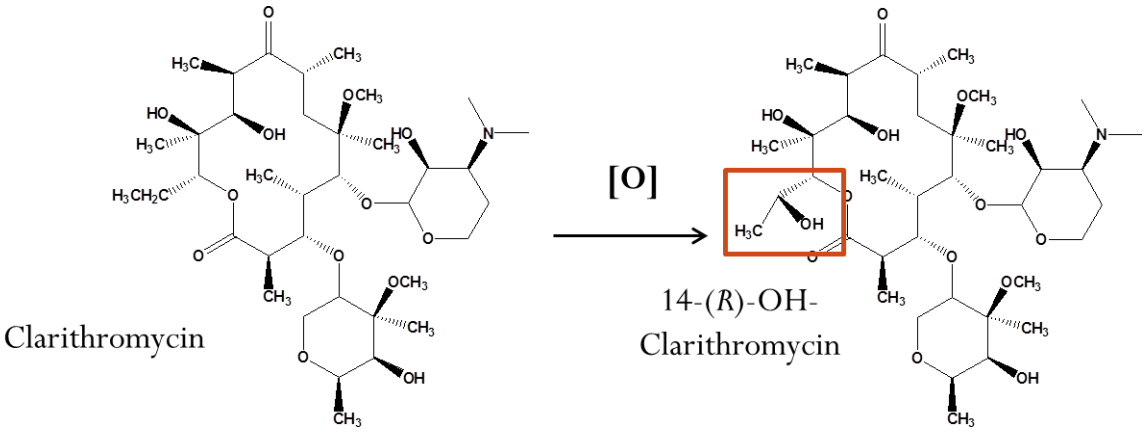
[O]
Clarithromycin
14-(R)-OH-Clarithromycin

D

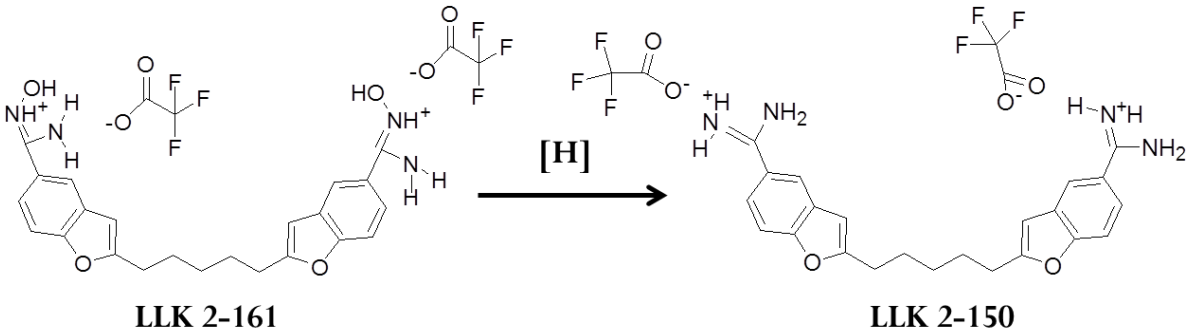

Figure 2.1 Structures of 4 type example compounds as the controls and their metabolism by liver enzymes (A. clofazimine; B. mefloquine-isoxazole carboxylic acid ester and its major metabolite mefloquine-isoxazole carboxylic acid by hydroxysis; C. CLA and its oxidative active metabolite 14-(*R*)-OH CLA; D. amidoxime prodrug-LLK2-161 and its reductive active amidine metabolite LLK2-150).

2.2.2 Materials and methods

2.2.2.1 Materials

Pooled mouse liver microsomes (MLM) and human liver microsomes (HLM) were purchased from XenoTech (Lenexa, KS). Rat Liver S9 Fractions (RS9) was purchased from Moltox (Boone, NC). All chemicals were purchased from Sigma Aldrich (St. Louis, MO). All solvents were HPLC grade and purchased from Fisher Scientific (Hanover Park, IL). Phosphate Buffered Saline (10X solution) was purchased from Fisher BioReagents.

2.2.2.2 Interference of NADPH, HLM and RS9 in Fluorometric Readout

NADPH, HLM and RS9, at final highest concentrations of 2 mM, 2 mg/ml and 2 mg/ml, respectively, were dissolved or suspended and serially diluted 2-fold in 7H12 medium before adding 20 µl 10x Alamar Blue dye and 12.5 µl 20% Tween-80 into the wells. After 20 hr incubation at 37°C in the absence of *M. tuberculosis*, fluorescence was measured in a VICTOR 3 Multilabel Plate Reader using excitation/emission wavelengths of 530/590 nm (PerkinElmer, Fremont, CA).

2.2.2.3 Inhibition of *M. tuberculosis* H37Rv *luxABCDE* by NADPH, $NADP^+$, NADH, NAD^+, HLM and RS9

NADPH, $NADP^+$, NADH, NAD^+, HLM and RS9, at final highest concentrations of 2 mM, 25 mM, 10 mM, 10 mM, 2 mg/ml and 2 mg/ml, respectively, were dissolved or suspended and serially diluted 2-fold in 7H12 medium. A stock of *M. tuberculosis* H37Rv *luxABCDE* was inoculated to achieve a final cell density of 8×10^5 cells/ml. After 5 days incubation at 37°C, luminescence was measured in a VICTOR 3 Multilabel Plate Reader (PerkinElmer, Fremont, CA).

2.2.2.4 Bactericidal Effect of NADPH, HLM and RS9 against the Growth of *M. tuberculosis* H37Rv *luxABCDE*

NADPH, HLM and RS9, at final highest concentrations of 2 mM, 2 mg/ml and 2 mg/ml, respectively, were dissolved or suspended and serially diluted 2-fold in 7H12 medium before inoculating with *M. tuberculosis* H37Rv *luxABCDE*, which have been growing in a 50 ml tube for 3 days from a density of 5 x 10^5 cells/ml at day 0. After 1 day incubation, luminescence was measured in a VICTOR 3 Multilabel Plate Reader (PerkinElmer, Fremont, CA).

2.2.2.5 Effect of Cofactors on the Efficiency of MGS for Type 4 Positive Control

HLM, MLM, RS9 and human liver S9 fractions (HS9) were incubated at a final concentration of 0.5 mg/ml in PBS with 1 μM LLK2-161 for 5 min at 37 °C before the reaction was initiated by addition of NADPH, NADH or NAD^+ at a final concentration of 1 mM to each of the enzyme systems. After 1 hr at 37 °C, the metabolic reactions were quenched and the relative amount of LLK2-161 and generated LLK2-150 was quantified by LC/MS/MS.

2.2.2.6 pH Dependence of MGS for Type 4 Positive Control

MLM were incubated at a final concentration of 0.2 mg/ml in PBS at pH 5.6, 6.0, 6.6, 7.0, 7.4 and 8.0 (adjusted by HCl), with 15.4 μM LLK2-161 at 37 °C for 5 min. The reactions were initiated by addition of NADH at a final concentration of 1 mM into MLM and the reaction mixtures were incubated at 37 °C for 24 hr. The concentration of the metabolite LLK2-150 generated was quantified by LC/MS/MS.

2.2.2.7 Optimization of MGS for Type 4 Positive Control

MLM were incubated at a final concentration of 1 mg/ml, 0.5 mg/ml, 0.1 mg/ml and 0.05 mg/ml in PBS with 15.4 µM LLK2-161 for 5 min at 37 °C. The reactions were initiated by addition of NADH at final concentrations of 2.5 mM, 1 mM, 0.5 mM, 0.25 mM, 0.1 mM, 0.05mM and the reactions were incubated at 37 °C for 6 hr. The concentration of the generated metabolite LLK2-150 was determined by LC/MS/MS.

2.2.2.8 Kinetics of Metabolite Formation in Optimized MGS for Type 4 Positive Control

MLM were incubated at a final concentration of 0.1 mg/ml in PBS with 15.4 µM LLK2-161 at pH 6.6. The reactions were initiated by addition of NADH at final concentrations of 0.1 mM and 0.05mM into MLM and the reactions were incubated at 37 °C for 24 hr. The formation of metabolite LLK2-150 was monitored at 10 hr, 15 hr and 20 hr. The concentration of the generated metabolite LLK2-150 was determined by LC/MS/MS.

2.2.2.9 Inhibition of *M. tuberculosis* H37Rv *luxABCDE* by MGS-Generated Type 4 Positive Control Metabolite

MLM were incubated at a final concentration of 0.1 mg/ml in PBS with 15.4 µM LLK2-161 at pH 6.6. The reactions were initiated by addition of NADH at a final concentration of 0.1 mM into MLM and the reaction mixtures were incubated at 37 °C for 20 hr. The concentration of the generated metabolite LLK2-150 was determined by LC/MS/MS. The reaction mixtures were extracted with acetonitrile (ACN), solvent removed in a speed vacuum and precipitate dissolved in sterile water at the same volume as the reaction system. The dissolved metabolites were serially diluted 2-fold before inoculating with *M. tuberculosis* H37Rv *luxABCDE*, the stock of which was suspended in a 2X 7H12 medium to achieve a density of 8 x 10^5 cells/ml. After 5

days incubation, luminescence was measured in a VICTOR 3 Multilabel Plate Reader (PerkinElmer, Fremont, CA).

2.2.2.10 Optimization of MGS with NADH-regenerating System for Type 4 Positive Control

MLM (0.1 mg/ml, suspended in PBS at pH 6.6 containing 8 mM $MgCl_2$ and 20 mM glucose-6-phosphate (G-6-P)) were incubated with LLK2-161 (15.4 µM) and RS9 at final concentrations of 5%, 2%, 1%, 0.5% and 0.1% for 5 min at 37 °C. The reactions were initiated by addition of NAD^+ at a final concentration of 5 mM, 2.5 mM, 1.0 mM, and 0.5 mM into each concentration of MLM and the reactions were incubated at 37 °C for 6 hr. The concentration of the generated metabolite LLK2-150 was determined by LC/MS/MS.

2.2.2.11 Kinetics of Type 4 Positive Control Metabolite Formation in Optimized MGS

MLM (0.1 mg/ml, suspended in PBS at pH 6.6 containing 8 mM $MgCl_2$ and 20 mM G-6-P) were incubated with LLK2-161 (15.4 µM) and RS9 at final concentrations of 1% and 0.5% for 5 min at 37 °C. The reactions were initiated by addition of NAD^+ at final concentrations of 2.5 mM and 1.0 mM for MGS with 1% RS9 fractions, and 1 mM for MGS with 0.5% RS9. The reactions were incubated at 37 °C for 10 hr and the formation of metabolite LLK2-150 was monitored at 2 hr, 6 hr and 10 hr. The concentration of the generated metabolite LLK2-150 was determined by LC/MS/MS.

2.2.2.12 Inhibition of *M. tuberculosis* H37Rv *luxABCDE* by Type 4 Positive Control Metabolite Produced in MGS with NADH-regenerating System

MLM (0.1 mg/ml, suspended in PBS at pH 6.6 containing 0.5% RS9, 8 mM $MgCl_2$ and 20 mM G-6-P) was incubated with 15.4 µM LLK2-161 as the inhibition positive control and negative control, and without 15.4 µM LLK2-161 as the inhibition blank control. The reactions were initiated by addition of NAD^+ at a final concentration of 1.0 mM into MLM into the inhibition positive control and blank control. A same volume of buffer was added instead for the inhibition negative control. All the reactions were incubated at 37 °C for 6 hr. The concentration of the generated metabolite LLK2-150 was determined by LC/MS/MS. The reaction mixtures were extracted by ACN, the solvent removed in speed vacuum dissolved in sterile water at the same volume as the reaction system. The dissolved metabolite was serially diluted 2-fold before inoculating with *M. tuberculosis* H37Rv *luxABCDE*, the stock of which was suspended in a 2X 7H12 medium to achieve a density of 8×10^5 cells/ml. After 5 days incubation, luminescence was measured in a VICTOR 3 Multilabel Plate Reader (PerkinElmer, Fremont, CA).

2.2.2.13 Exploration of Inhibitory Components in MGS

$MgCl_2$, G-6-P, NADH, and NAD^+ were dissolved at final concentrations of 60 mM, 35 mM, 10 mM and 10 mM and serially diluted 2-fold in sterile water before inoculating with *M. tuberculosis* H37Rv *luxABCDE*, the stock of which was suspended in a 2X 7H12 medium to achieve a density of 8×10^5 cells/ml.

Sterile 1X PBS at pH 5.6, 6.0, 6.6, 7.0, 7.4 and 8.0 were serially diluted 2-fold in sterile water before inoculating with *M. tuberculosis* H37Rv *luxABCDE*, the stock of which was suspended in a 2X 7H12 medium to achieve a density of 8×10^5 cells/ml.

After 7 days incubation at 37 °C, luminescence was measured in a VICTOR 3 Multilabel Plate Reader (PerkinElmer, Fremont, CA).

2.2.2.14 Inhibition of *M. tuberculosis* H37Rv *luxABCDE* by Type 4 Positive Control Metabolites Formed in Optimized MGS with NADH-regenerating System

MLM (0.1 mg/ml, suspended in PBS at pH 6.6 containing 0.5% RS9, 8 mM $MgCl_2$ and 20 mM G-6-P) was incubated with 15.4 μM LLK2-161 as the inhibition positive control and negative control, and without 15.4 μM LLK2-161 as the inhibition blank control. The reactions were initiated by addition of NAD^+ at a final concentration of 2.0 mM into MLM into the inhibition positive control and blank control. The same volume of buffer was added instead for the inhibition negative control. All the reactions were incubated at 37 °C for 6 hr. The concentration of the metabolite LLK2-150 generated was quantified by LC/MS/MS. The reaction mixtures were extracted by MeOH, solvent removed in a speed vacuum and precipitate dissolved in sterile water at the same volume as the reaction system. The dissolved metabolite was serially diluted 2-fold before inoculating with *M. tuberculosis* H37Rv *luxABCDE*, the stock of which was suspended in a 2X 7H12 medium to achieve a density of 8 x 10^5 cells/ml. After a 5-day incubation, luminescence was measured in a VICTOR 3 Multilabel Plate Reader (PerkinElmer, Fremont, CA).

2.2.2.15 Optimization of MGS for Type 3 Positive Control

HLM, at a final concentration of 0.5 mg/ml, 0.25 mg/ml, 0.1 mg/ml and 0.05 mg/ml, were suspended in PBS at pH 7.4, containing 8 mM $MgCl_2$, 20 mM G-6-P, 10 ug/ml CLA and RS9 at 2%, 1% or 0.5%. After being pre-warmed at 37 °C for 5 min, reactions were initiated by addition of $NADP^+$ at a final concentration of 1 mM, and the reaction mixtures were incubated at 37 °C

for 6 hr. The relative amount of the metabolite 14-(*R*)-OH CLA generated was quantified by LC/MS/MS.

HLM, to a final concentration of 0.5 mg/ml, 0.25 mg/ml and 0.1 mg/ml, were suspended in PBS at pH 7.4 PBS, containing 8 mM $MgCl_2$, 20 mM G-6-P, 10 ug/ml CLA and 0.5% RS9. After being pre-warmed at 37 °C for 5 min, reactions were initiated by addition of $NADP^+$ at a final concentrations of 50 mM, 25 mM, 10 mM or 5 mM to HLM at each concentration, and the reaction mixtures were incubated at 37 °C for 6 hr. The relative amount of the generated metabolite 14-(*R*)-OH CLA was quantified by LC/MS/MS.

2.2.2.16 pH Dependence of MGS for Type 3 Positive Control

HLM were suspended to a final concentration of 0.5 mg/ml in PBS at pH 5.6, 6.0, 6.6, 7.0, 7.4 and 8.0 (adjusted by HCl), containing 8 mM $MgCl_2$ and 20 mM G-6-P, and incubated with 10 µg/ml CLA and 0.5% RS9 at 37 °C for 5 min. The reactions were initiated by addition of $NADP^+$ at a final concentration of 25 mM or 10 mM and incubated at 37 °C for 6 hr. The relative amount of the generated metabolite 14-(*R*)-OH CLA was quantified by LC/MS/MS.

2.2.2.17 Kinetics of Metabolite Formation in Optimized MGS for Type 3 Positive Control

HLM (0.5 mg/ml, suspended in PBS at pH 6.6 containing 0.5% RS9, 8 mM $MgCl_2$ and 20 mM G-6-P) were incubated with 10 µg/ml CLA (15.4 µM) for 5 min at 37 °C. The reactions were initiated by addition of $NADP^+$ at a final concentration of 25 mM. The reactions were incubated at 37 °C for 9.5 hr and the formation of the 14-(*R*)-OH CLA metabolite was monitored at 2 hr,

4hr, 6 hr and 9.5 hr. The relative amount of the generated 14-(*R*)-OH CLA metabolite was quantified by LC/MS/MS.

2.2.2.18 Inhibition of *M. tuberculosis* H37Rv *luxABCDE* by Type 3 Positive Control CLA and its Active Metabolite 14-(*R*)-OH CLA

The inhibitory activities of CLA and 14-(*R*)-OH CLA were assessed against *M. tuberculosis* H37Rv *luxABCDE* strain with rifampin and isoniazid as the positive controls. Beginning with maximum concentrations of 20 µg/ml for CLA and 40 µg/ml for 14-(*R*)-OH CLA, 2-fold serial dilutions were made with 7H12 medium in 96-well plates. After addition of the *M. tuberculosis* inoculum to achieve a density of 4 x 10^5 cells/ml, plates were incubated for 7 days at 37 °C and luminescence was measured in a VICTOR 3 Multilabel Plate Reader.

2.2.2.19 Quantification of 14-(*R*)-OH CLA Formed in Optimized MGS

HLM (0.5 mg/ml, suspended in PBS at pH 6.6 containing 0.5% RS9, 8 mM $MgCl_2$ and 20 mM G-6-P) were incubated with 10 µg/ml CLA (15.4 µM) for 5 min at 37 °C. The reactions were initiated by addition of $NADP^+$ at a final concentration of 25 mM. The reaction mixtures were incubated at 37 °C for 9.5 hr and the formation of metabolite 14-(*R*)-OH CLA was monitored at 4 hr and 6 hr. The relative amount of the metabolite 14-(*R*)-OH CLA generated was quantified by LC/MS/MS.

2.2.2.20 Protein Binding of LLK2-150 and LLK2-161 in HLM

MLM (0.1 mg/ml) solutions (100 µL) containing LLK2-161 and LLK2-150 (2 and 10 µg/ml) were placed into the sample chamber of Single-Use Rapid Equilibrium Dialysis plates with cutoff

molecular weight 8000 Da (Thermo Scientific-Pierce Biotechnology, Rockford, IL). Three hundred microliters of PBS dialysis buffer was added into the adjacent chamber. Samples were setup in triplicate. The content of organic solvent in the final microsomal solutions was kept below 1%. The plates were then covered with sealing tape (MicroAmpTM, Applied Biosystems, Foster City, CA) and incubated at 37 °C for 4 hours on an orbital shaker at 100 rpm. Aliquots (50 µL) were removed from each side of the insert and placed in separate tubes. The same volume (50 µL) of blank microsomes was added to the buffer samples and an equal volume of PBS was added to the collected microsomes samples for matrix matching. To each sample, 200 µL of acetonitrile containing sulfaphenazole was added. These samples were vortexed for 30 s and chilled on ice for 30 min, then centrifuged at 16,100g for 15 min at 4 °C. LLK2-161 and LLK2-150 concentrations in the supernatant were determined by LC/MS/MS.

2.2.2.21 Measurement of LLK2-150 and 14-(*R*)-OH CLA in LC/MS/MS

The concentrations of LLK2-150 and 14-(*R*)-OH CLA formed were determined by LC/MS/MS. A Shimadzu Prominence HPLC interfaced with ABSciex Qtrap 4000 “equipped with an electrospray ion source was used. Chromatographic separation was carried out with a Waters XTerra MS C18 column (2.1×50 mm, 3.5 µm; Waters Corporation, Milford, MA)”. For LLK2-150, mobile phase was delivered at 200 µl/min, and the gradient was initiated at 75% A : 25% B (A, 0.1% formic acid in H_2O; B, acetonitrile containing 0.1% formic acid). The proportion of mobile phase B was held at 25% for 1 min, and then increased to 95% over 2 min, held constant for another 1 min, and then restored to the initial composition. For 14-(*R*)-OH CLA, mobile phase was delivered at 200 µl/min, and the gradient was initiated at 72 % A - 28% B (A, 0.1% formic acid in H_2O; B, acetonitrile containing 0.1% formic acid). The proportion of mobile phase B was held at 28% for 2 min, and then increased to 90% over 1.5 min, held constant for another 1 min, and then restored to the initial composition. A positive mode was utilized. As shown in figure 2.2,

the selective reaction monitoring (SRM) transitions for LLK2-150 and 14-(*R*)-OH CLA were 195.2/170.1 and 748.6/158.1 as the quantifiers, and the qualifiers were 195.2/157.2 and 748.6/606.5, respectively. Sulfophenazole was used as the internal standard with a SRM transition of 315/158. The dwell time for each transition was 5 ms.

A.

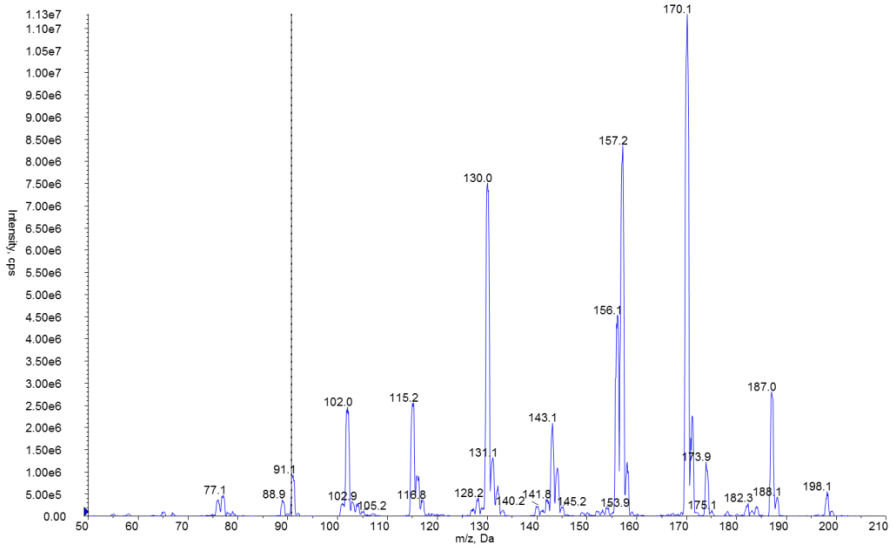

B.

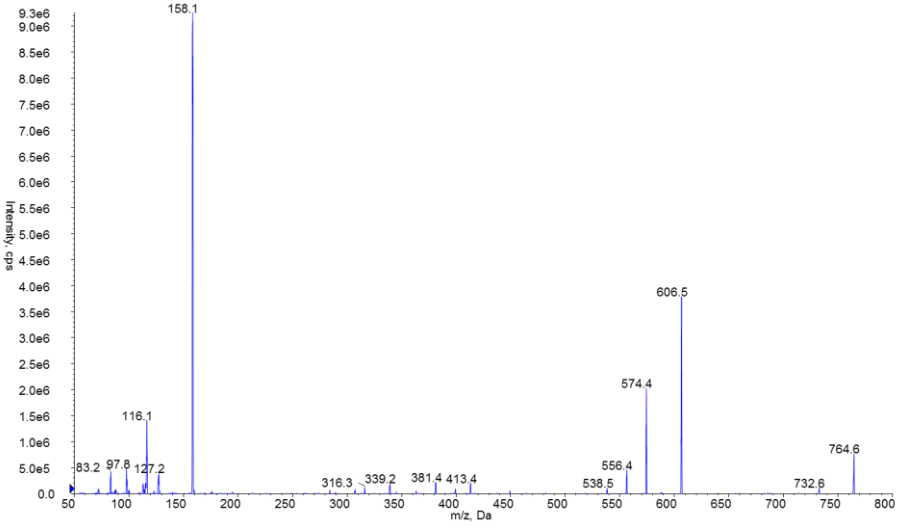

Figure 2.2 The spectrum of the product ions of LLK2-150 and 14-(*R*)-OH Clarithromycin.

2.2.3 Results

2.2.3.1 Interference of NADPH, HLM and RS9 in Fluorometric Readout

NADPH, HLM and RS9 were able to reduce Alamar Blue in a concentration-dependent pattern as determined by the relative fluorescence units (RFU) at Ex/Em of 530/590 nm (Figure 2.2).

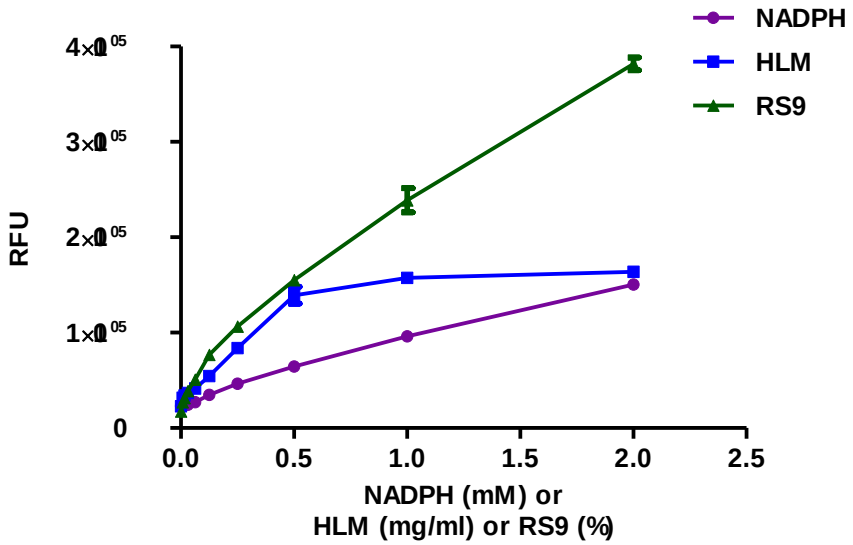

Figure 2.3 Fluorometric readout for resorufin reduced by NADPH, HLM and RS9. The data shown represent the mean ± S.D. from three replicates.

2.2.3.2 Inhibition of *M. tuberculosis* H37Rv *luxABCDE* by NADPH, $NADP^+$, NADH, NAD^+, HLM and RS9

The extent of inhibition of NADPH, $NADP^+$, NADH, NAD^+ HLM and RS9 on the growth of *M. tuberculosis* was calculated based on the ratio of the luminescence signal produced in the presence and absence of these assay components (Figure 2.3). NADPH, $NADP^+$, NADH, NAD^+, HLM and RS9 all showed a concentration-dependent inhibition against *M. tuberculosis* H37Rv *luxABCDE*. In order to avoid any background inhibition from the assay system, the highest

concentration of NADPH, $NADP^+$, NADH, NAD^+, HLM and RS9 acceptable in this assay under development is 0.1 mM, 6.25 mM, 5 mM, 5 mM, 0.25 mg/ml and 0.5 mg/ml, respectively.

A.

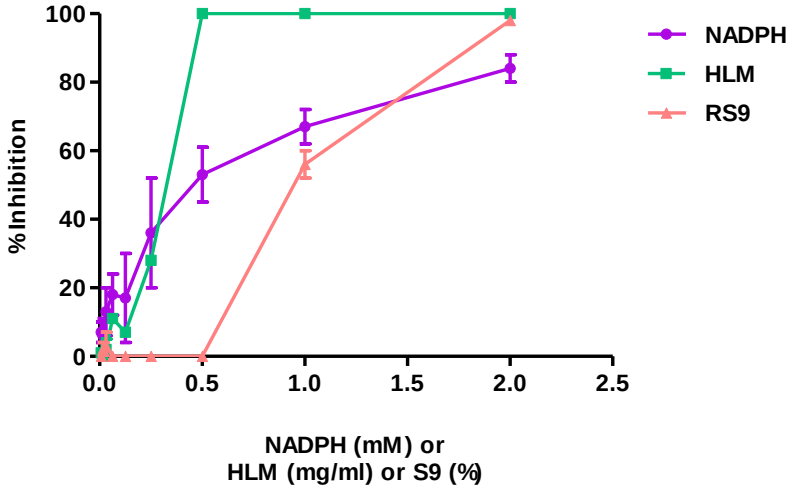

B.

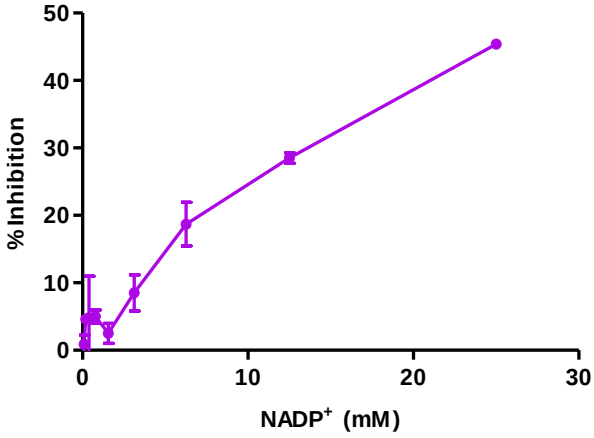

C.

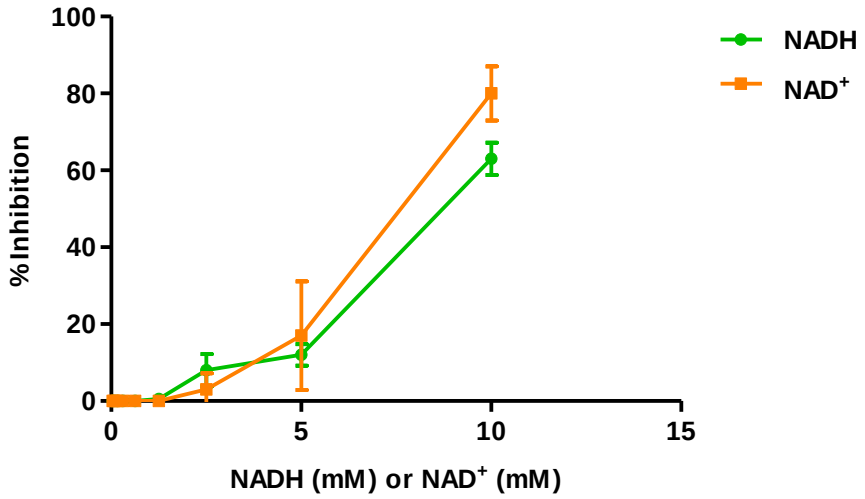

Figure 2.4 Inhibition of *M. tuberculosis* H37Rv *luxABCDE* by NADPH, HLM and RS9 (A) and $NADP^+$ (B) NADH and NAD^+ (C). The data shown represent the mean ± S.D. from three replicates.

2.2.3.3 Bactericidal Effect of NADPH and HLM against *M. tuberculosis* H37Rv *luxABCDE*

HLM effected a concentration-dependent reduction in luminescence signal relative to the bacterial control without HLM after 24 hr incubation (Figure 2.4). NADPH with the same concentration range as in the inhibition study did not show a killing effect, and the luminescence increase was the same in the absence and presence of NADPH at various concentrations. RS9 showed a concentration-dependent inhibition against the growing bacteria, however, even in the presence NADPH at 2.0 mM, *M. tuberculosis* H37Rv *luxABCDE* was still able to grow with an increase in relative luminescence units (RLU) of 2-fold.

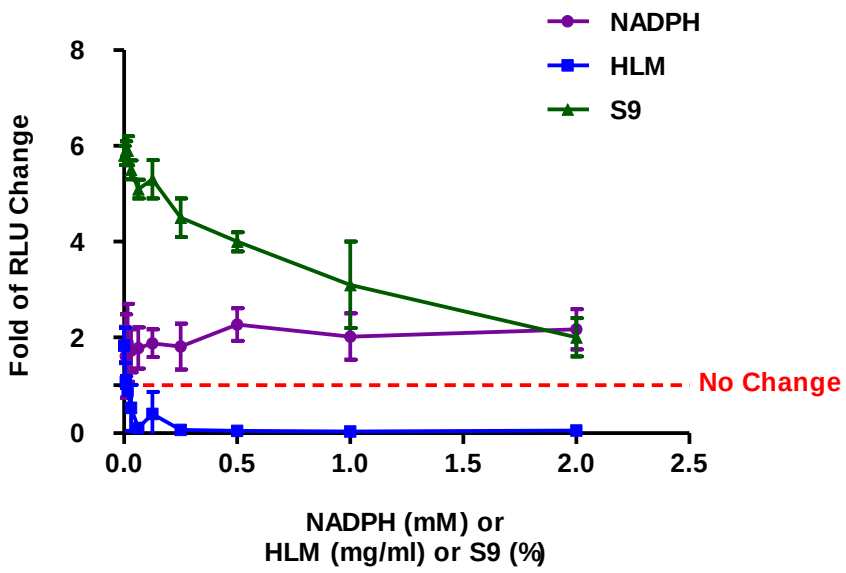

Figure 2.5 The effect of NADPH, HLM and RS9 on growing cultures of *M. tuberculosis* H37Rv *luxABCDE*. The data shown represent the mean ± S.D. from three replicates.

2.2.3.4 Effect of Cofactors on the Efficiency of MGS for Type 4 Positive Control

Using the value obtained without any cofactor as 100%, the percentage of remaining LLK2-161 was calculated for each MGS with different cofactors (Figure 2.5). MGS with MLM yielded the highest metabolism of LLK2-161, followed by RS9, compared to that with HLM or HS9, regardless of the cofactor (Figure 2.5A). With respect to the specific formation of metabolite LLK2-150, MLM with NADH as the cofactor led to a much higher formation than MLM with any other cofactor and any other subcellular fractions with any cofactor (Figure 2.5B).

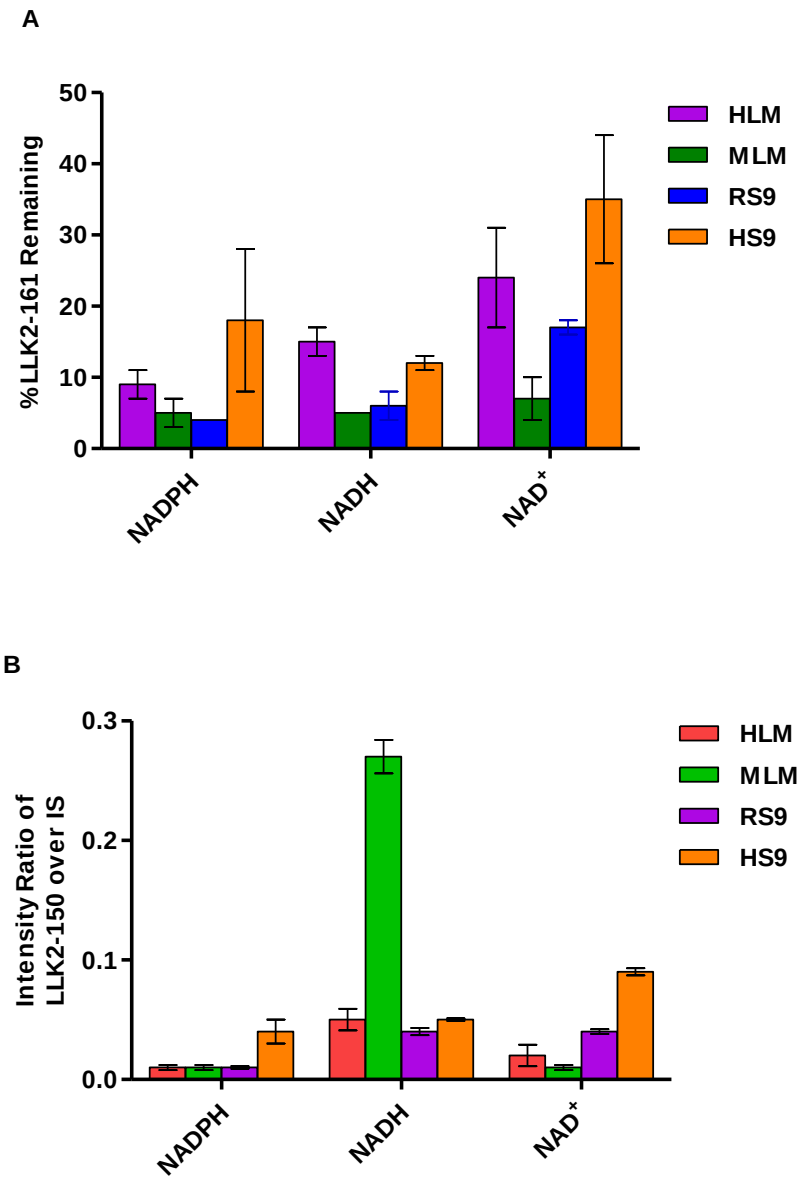

Figure 2.6 LLK2-161 metabolism (A) and LLK2-150 formation (B) in different MGS combinations. The data shown represent the mean ± S.D. from three replicates.

2.2.3.5 pH Dependence of MGS for Type 4 Positive Control

According to Saulter J, et al. 2005, the reduction of the amidoxime analog was more rapid at pH 6.5 compared to pH 7.4; therefore the pH range used in this experiment included and extended

beyond these values. The rate of LLK2-150 formation was most rapid at pH 6.0, achieving a maximum concentration as high as 8 µM at 3 hr (Figure 2.6). At higher pH values there was a corresponding decrease in rates of LLK2-150 formation. At pH 5.6-7, maximum LLK2-150 concentration was attained after 3 hours whereas at higher pH maxima were achieved at 12 hours.

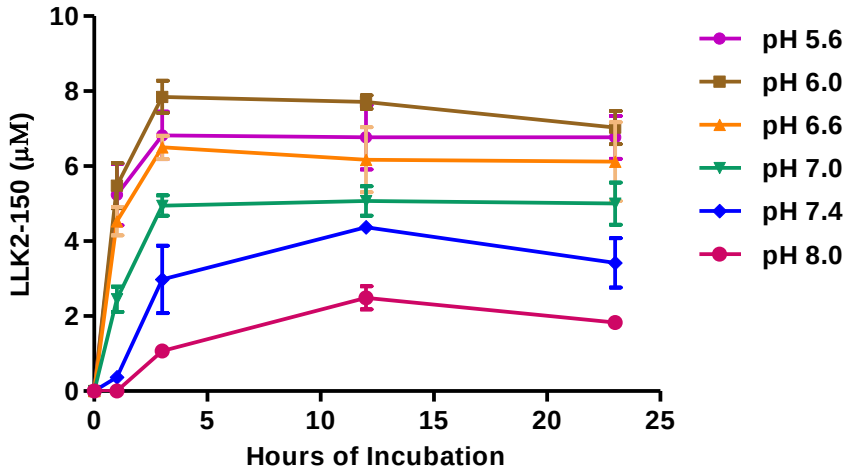

Figure 2.7 pH dependence of LLK2-150 formation in MLM with NADH. The data shown represent the mean ± S.D. from three replicates.

2.2.3.6 Optimization of MGS for Type 4 Positive Control

Using the optimal pH (6.0) for the reduction of the amidoxime LLK2-161, the MGS for this type 4 positive control was optimized with respect to the concentration of MLM and NADH. The production of amidine metabolite was inversely correlated with NADH at concentrations of NADH between 2.5 mM and 10 mM (Figure 2.7A). Optimal metabolite production was observed at 2 mg/ml MLM and 2.5 mM NADH. Therefore a lower concentration range of NADH and MLM was investigated in a subsequent experiment. The higher MLM concentrations of 1 and 2 mg/ml did not result in greater formation of the metabolite compared to that produced at 0.1 and 0.2

mg/ml (Figure 2.7B). The inhibition by NADH holds true over a range of NADH concentrations and it is more apparent at lower concentrations of MLM. For MLM at 0.1 or 0.2 mg/ml, this inverse correlation between the production of metabolite and the concentration of NADH exists within the concentration range of NADH of 0.25 mM to 2.5 mM. At lower concentrations of NADH, the production of amidine decreased slightly with a concentration of LLK2-150 still at approximately 4 µM. In summary, the optimal concentrations of MLM and NADH to form LLK2-150 are 0.1-0.2 mg/ml, and 0.25 mM, respectively.

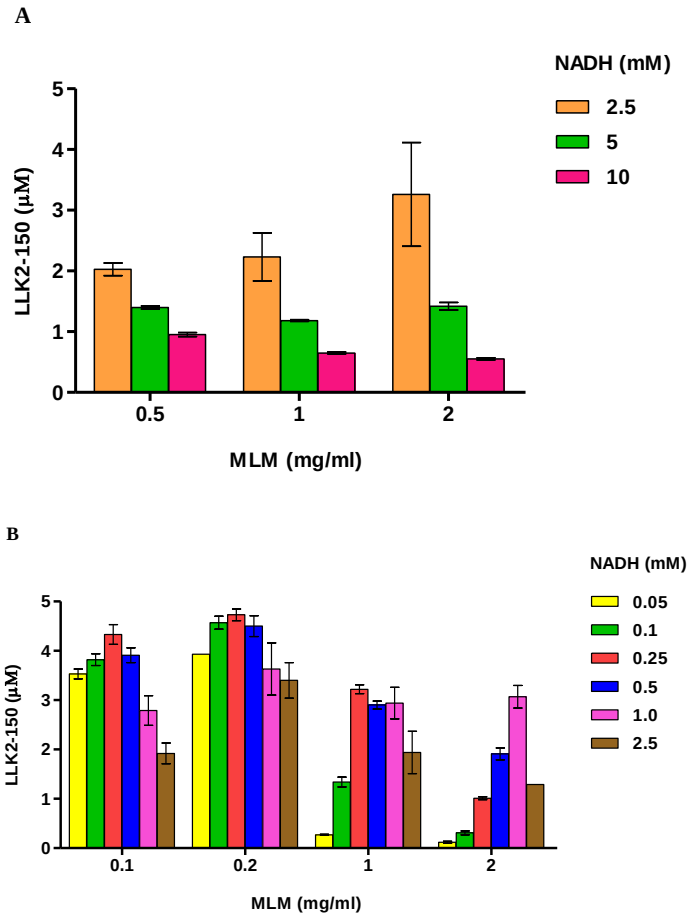

Figure 2.8 Formation of LLK2-150 at different concentrations of MLM and NADH. The data shown represent the mean ± S.D. from three replicates.

2.2.3.7 Kinetics of Metabolite Formation in Optimized MGS for Type 4 Positive Control

The formation of metabolite LLK2-150 was monitored over 20 hrs. With NADH at 0.1mM, the formation of metabolite continued increasing throughout the incubation achieving a maximum concentration of ~7 µM (Figure 2.8). At 0.05 mM NADH, metabolite yield plateaued as early as 10 hr at a maximum concentration of only 3 µM.

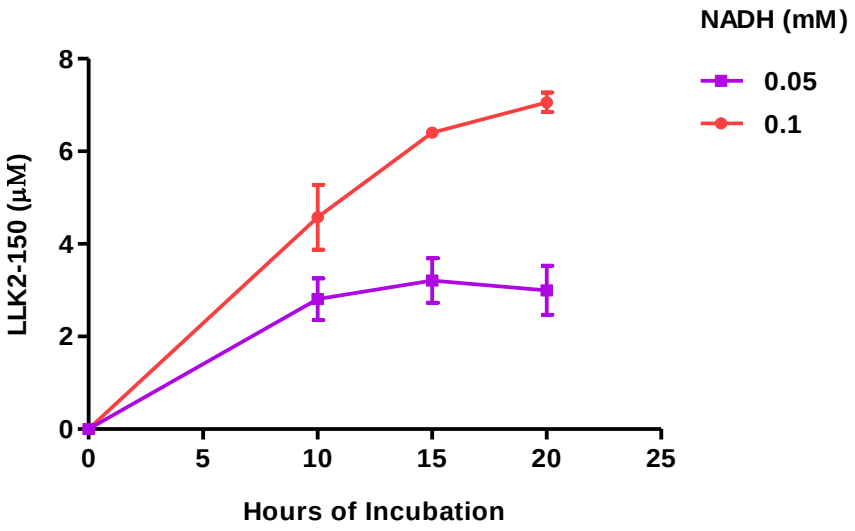

Figure 2.9 Time course of metabolite LLK2-150 formation. The data shown represent the mean ± S.D. from three replicates.

2.2.3.8 Inhibition of *M. tuberculosis* H37Rv *luxABCDE* by MGS-Generated Type 4 Positive Control Metabolite

The optimized MGS incubated with LLK2-161 achieved a concentration of 6.5 µM LLK-150. This was extracted from the MGS, reconstituted to the same concentration in the antibacterial assay and serially diluted. After 7 days incubation with *M. tuberculosis* H37Rv luxABCDE, the MIC was determined by measuring the luminescence of the treated cultures in comparison to bacterial controls without addition of metabolites. The MIC of LLK2-150 formed in the optimized MGS

was 1.5 µM (Figure 2.9). The negative control, from the same MGS without NADH, did not show any inhibition except for the 1st dilution which corresponds to the highest concentration of LLK2-161 (7.7 µM), which indicates that the background inhibition from the assay is negligible.

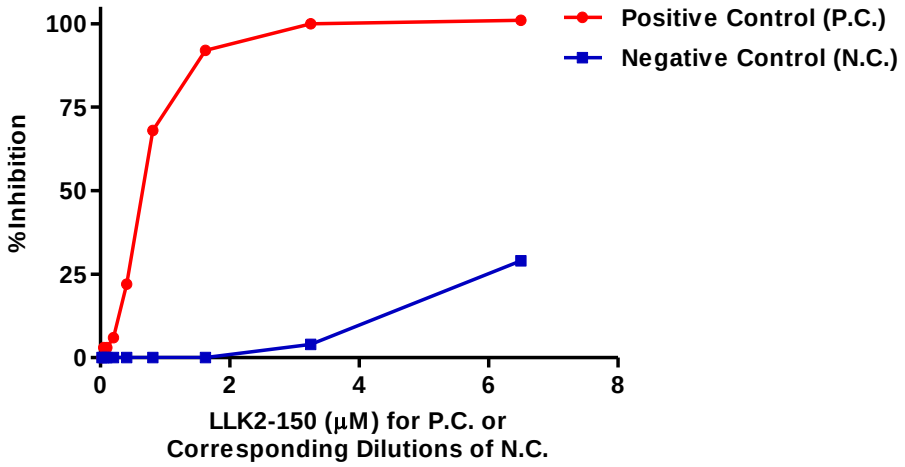

Figure 2.10 Inhibition profiles of LLK2-150 formed in MGS and the corresponding negative control. The negative control dilutions were compared to the same dilutions of positive control and profiled at the x-axis value of the corresponding positive control dilutions. The data shown represent the mean ± S.D. from two replicates.

2.2.3.9 Optimization of MGS with NADH-regenerating System for Type 4 Positive Control

The optimal NAD^+ concentration for LLK2-150 formation is 5.0 mM with RS9 at a concentration of 2%, 1% or 0.5% (Figure 2.10), with a maximum concentration of 9 µM LLK2-150 produced at 0.5% RS9. The highest (5%) and lowest (0.1%) concentrations of RS9 resulted in significantly lower yields of the amidine metabolite. At RS9 concentrations of 0.5-2%, there was a clear dose-response with respect to NAD^+ concentration.

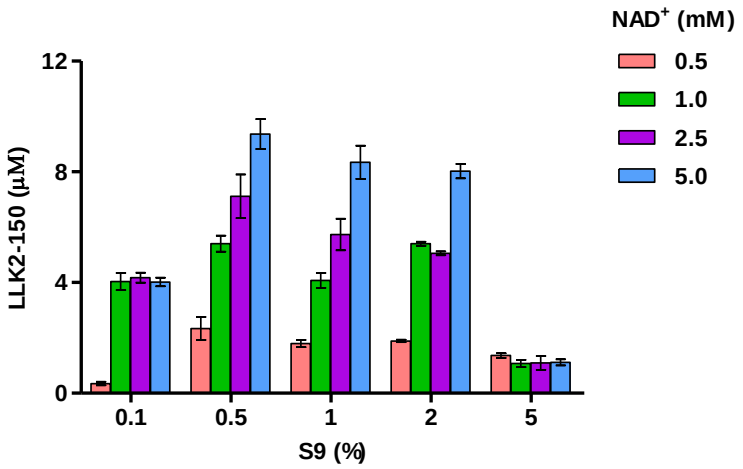

Figure 2.11 Formation of LLK2-150 at different concentrations of RS9 and NAD^+. The data shown represent the mean ± S.D. from three replicates.

2.2.3.10 Kinetics of Type 4 Positive Control Metabolite Formation in Optimized MGS

With the MGS containing 0.1 mg/ml MLM and three selected NADH-regenerating system conditions (2.5 mM NAD^+ plus 1.0% RS9, 1.0 mM NAD^+ plus 1.0% RS9, and 1.0 mM NAD^+ plus 0.5 % RS9), the formation of metabolite LLK2-150 was monitored. The latter reached a plateau at 6 hr, with a concentration as high as 7 µM (Figure 2.11). Considering that the amount of metabolite formed with NAD^+ at 1.0 mM plus RS9 at 0.5 % was comparable or superior to the other conditions, this lower concentration combination of NAD^+ and RS9 was chosen for the final optimized MGS.

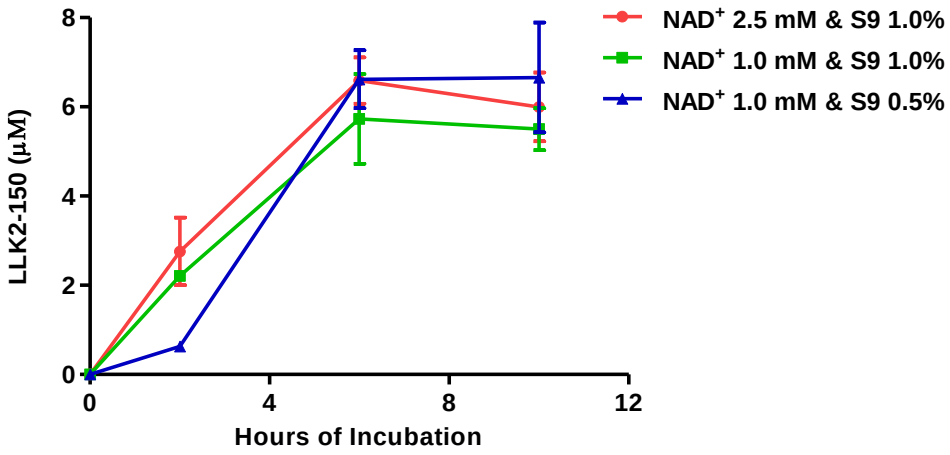

Figure 2.12 Time course of metabolite LLK2-150 formation with selected NADH-regenerating systems. The data shown represent the mean ± S.D. from three replicates.

2.2.3.11 Inhibition of *M. tuberculosis* H37Rv *luxABCDE* by Type 4 Positive Control Metabolite Formed in MGS with NADH-regenerating System

Using the optimized MGS containing a NADH-regenerating system, the metabolites formed from LLK2-161 were extracted and tested in the bacterial inhibition assay against *M. tuberculosis* H37Rv *luxABCDE*. The blank control included only the components of the optimized MGS with NADH-regenerating system in order to show that the MGS is not involved in the inhibition of bacteria. The negative control contained all the components (the MGS with NADH-regenerating system) in the blank control plus LLK2-161 at a final concentration of 15.4 µM, but no incubation was performed, in order to show the extent of inhibition by the combination of LLK2-161 and the optimized MGS. The positive control was of the same composition as the negative control but incubated for 6 hr at 37 °C to generate the expected metabolite and its inhibition was studied. However, the highest concentration of metabolites in the positive control and corresponding negative control and blank control made no difference in inhibiting bacterial growth with more

than 90% inhibition (Figure 2.12). For the positive control with generated metabolites, the inhibition difference on bacterial growth appeared for 2-fold to 32-fold compared to that of the negative control or blank control.

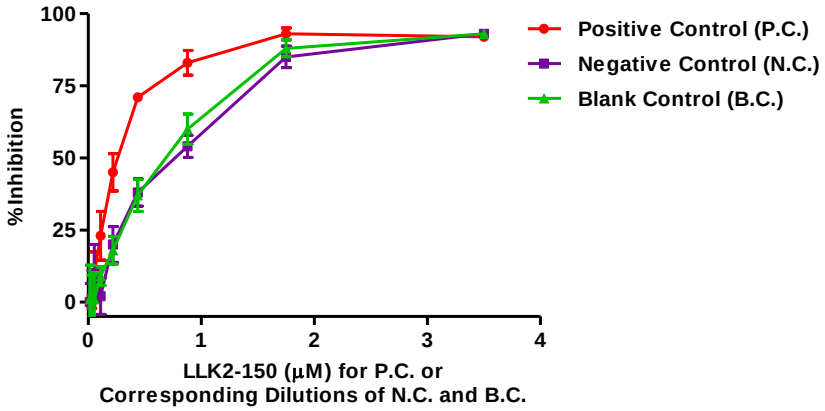

Figure 2.13 Bacterial growth inhibition of metabolites formed in positive control in comparison with negative control and blank control. The negative control and black control dilutions were compared to the same dilutions of positive control and profiled at the x-axis value of the corresponding positive control dilutions. The data shown represent the mean ± S.D. from three replicates.

2.2.3.12 Exploration of Inhibitory Components in MGS

PBS, adjusted by HCl, inhibited bacterial growth in a concentration and pH-dependent pattern on day 4 (Figure 2.13A). At low PBS concentrations, there was little difference in growth/inhibition regardless of the pH of the added PBS whereas at increasing PBS concentrations, more pronounced pH-related inhibition was observed. These effects were minimal at pH 6.6 to 7.0. When the incubation time was extended to 7 days, this pH-dependent inhibition of bacterial growth dropped below 30%, although the pH dependence was maintained (Figure 2.13B). Since the concentration of the salts in the commercial 1X PBS stock (0.137 mM

NaCl, 2.7 mM KCl, and 11.9 mM phosphate buffer) are comparable to that of the commercial mycobacterial medium, the inhibition from the blank control and negative control found in the inhibition study (refer to 2.2.3.11) should not be due to the salts in the buffer.

Besides the MLM and RS9, which were previously optimized, the remaining components in the MGS are $MgCl_2$ and G-6-P. $MgCl_2$ did not exhibit any inhibition up to 60 mM (data not shown). In contrast, G-6-P is inhibitory at concentrations exceeding 12 mM (Figure 2.14).

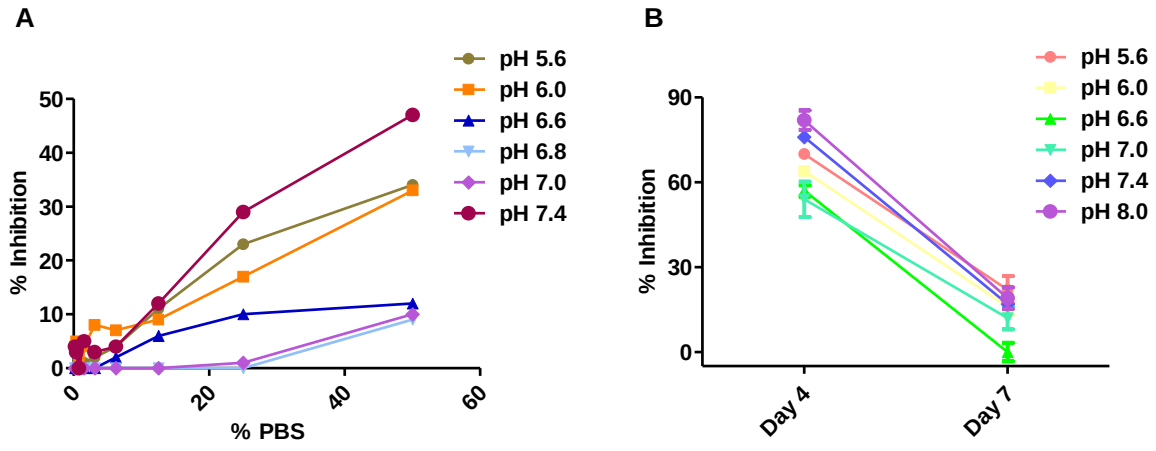

Figure 2.14 Inhibition of *M. tuberculosis* H37Rv *luxABCDE* growth by pH-adjusted PBS at Day 4 (A) and at an cxpanded pH range at 4-Day and 7-Day (B). The data shown represent the mean ± S.D. from two replicates.

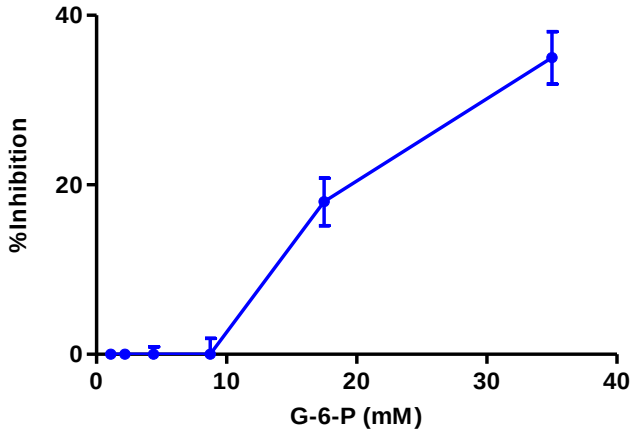

Figure 2.15 Inhibition of the growth of *M. tuberculosis* H37Rv *luxABCDE* by G-6-P. The data shown represent the mean ± S.D. from two replicates.

2.2.3.13 Inhibition of *M. tuberculosis* H37Rv *luxABCDE* by Type 4 Positive Control Metabolite Formed in Optimized MGS with NADH-regenerating System

When methanol was used as the organic solvent to extract the metabolites formed in the MGS, the blank control and negative control did not exhibit significant inhibition. The blank control included only the components of the optimized MGS with a NADH-regenerating system in order to show that the MGS is not involved in the inhibition of bacteria. The negative control contained all the components (the MGS with NADH-regenerating system) in the blank control plus LLK2-161 at a final concentration of 15.4 µM, but no incubation was performed, in order to show the extent of inhibition by the combination of LLK2-161 and the optimized MGS. The positive control had the same composition as the negative control but was incubated for 6 hr at 37 °C to generate the expected metabolite and its inhibition was studied. In comparison, the positive control effected a significant inhibition of *M. tuberculosis* from the formed metabolites of LLK2-161 with an MIC ~0.75 µM (Figure 2.15). In comparison to the result observed in 2.2.3.11, where the acetonitrile solvent may have been the cause of the significant inhibition of the blank

and negative controls, when methanol was used, no inhibition was observed with the negative control. Although the blank control exhibited a 30% inhibition, this may not be due to the MGS.

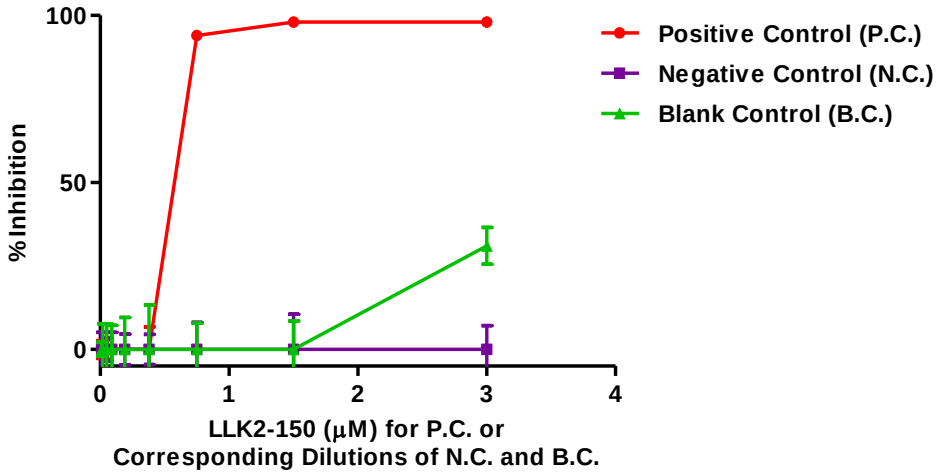

Figure 2.16 Inhibition of bacterial growth by the optimized MGS-generated LLK2-150 in comparison with negative control and blank control. The negative control and black control dilutions were compared to the same dilutions of positive control and profiled at the x-axis value of the corresponding positive control dilutions. The data shown represent the mean ± S.D. from three replicates.

2.2.3.14 Optimization of MGS for Type 3 Positive Control

CLA is metabolized by human liver CYP3A4 to 14-(*R*)-OH CLA, with the latter being more active against *M. tuberculosis* (Rodrigues D, et al 1997). Since this metabolite is absent in mice (Bédos, JP, et al, 1992), HLM was chosen to be the enzyme source for generating metabolites in using CLA as a positive control for type 3 compounds. Also, RS9 were included as the NADPH-regenerating system with $NADP^+$ as the cofactor. Higher yields of 14-(*R*)-OH CLA were obtained at higher concentrations of HLM and at the lowest concentration of RS9 (0.5%) (Figure 2.16A). At 0.5% RS9, the concentration of $NADP^+$ also affects metabolite formation for all

concentrations of HLM in a positive manner except at 50 mM, where no formation of 14-(*R*)-OH CLA was observed (Figure 2.16B). When incubated with 25 mM, 10 mM or 5 mM $NADP^+$, the generation of metabolite showed a positive concentration dependence on HLM in the range between 0.1 mg/ml and 0.5 mg/ml.

A

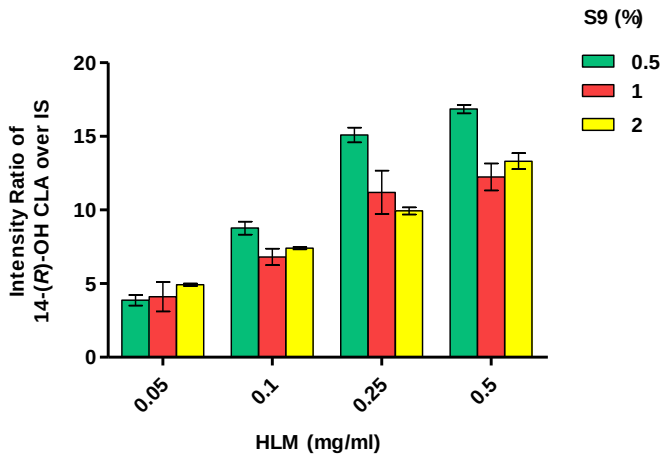

B

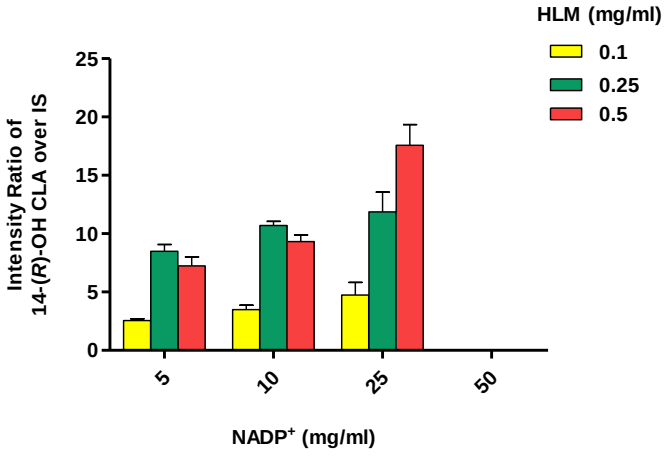

Figure 2.17 Optimization of MGS for type 3 positive control (A and B). The data shown represent the mean ± S.D. from three replicates.

2.2.3.15 pH Dependence of MGS for Type 3 Positive Control

The pH dependence for the formation of 14-(*R*)-OH CLA was studied in the same manner as that for LLK2-150. However, in this case there was no difference across the pH range in terms of the amount of metabolite formed (Figure 2.17). Since the pH of the incubation system could impart inhibition in the antibacterial assay and PBS at pH 6.6 was previously observed to produce the least inhibition, for subsequent experiments with 14-(*R*)-OH CLA formation, the same pH value (pH 6.6) was chosen.

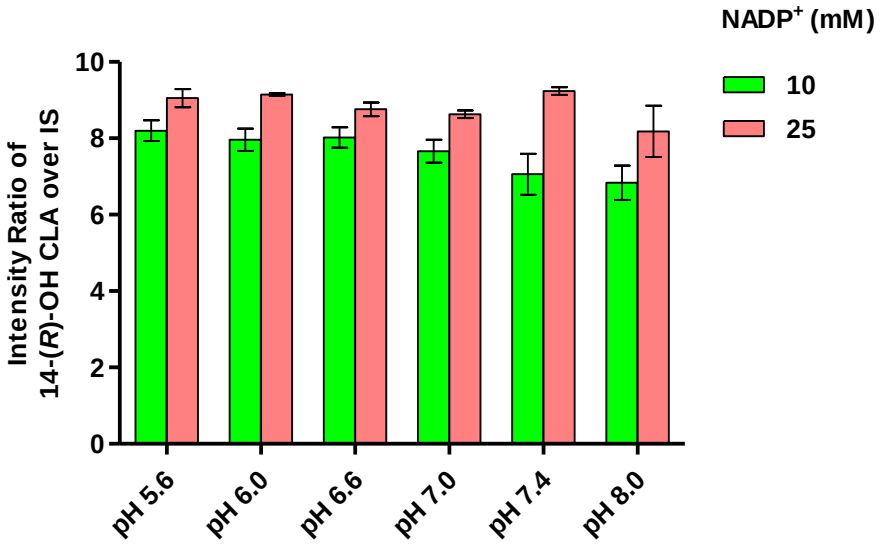

Figure 2.18 pH Dependence of 14-(*R*)-OH CLA Formation in HLM with $NADP^+$ and RS9. The data shown represent the mean ± S.D. from three replicates.

2.2.3.16 Kinetics of Metabolite Formation in Optimized MGS for Type 3 Positive Control

With the optimized MGS, the formation of 14-(*R*)-OH CLA was monitored over a period of 10 hours. The maximum concentration of 14-(*R*)-OH CLA was obtained at 6 hours (Figure 2.18).

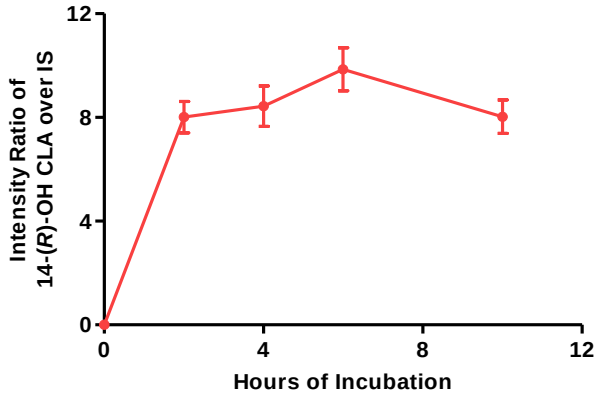

Figure 2.19 Time Course of 14-(*R*)-OH CLA Formation with Optimized MGS. The data shown represent the mean ± S.D. from three replicates.

2.2.3.17 Inhibition of *M. tuberculosis* H37Rv *luxABCDE* by Type 3 Positive Control CLA and its Active Metabolite 14-(*R*)-OH CLA

In the bacterial assay against the *luxABCDE* strain, the MIC of 14-(*R*)-OH CLA against *M. tuberculosis* H37Rv *luxABCDE* was 35 µM a value significantly higher than that (0.164 µM) reported previously for penicillin- and erythromycin-resistant *Streptococcus pneumonia* (Martin et al., 2001).

2.2.3.18 Quantification of 14-(*R*)-OH CLA Formed in Optimized MGS

In the optimized MGS, the concentration of 14-(*R*)-OH CLA (at both 2 hr and 6 hr) was ~3 µM when the starting concentration of CLA was 13.3 µM (10 µg/ml). This is comparable to a report that 14-(*R*)-OH CLA accounts for approximately 20% of the parent drug's metabolism (Langtry and Brogden, 1997).

2.2.3.19 Protein Binding of LLK2-150 and LLK2-161 in HLM

At the two concentrations of LLK2-150 and LLK2-161 tested, each had a $f_{u,m}$ of approximately 0.25-0.3, indicating that more than 70% of the molecules are bound to the microsomal proteins.

2.2.4 Discussion

In this chapter, a liver-enzyme based MGS was successfully developed with LLK2-161/LLK2-150 as the positive control (type 4). A high yield of the active amidine metabolite LLK2-150 from the prodrug - amidoxime analog was realized, a reaction catalyzed by NADH-dependent cytochrome b5 reductase, and the inhibitory activity of the generated active metabolite was confirmed. To summarize, a few key points are made as follows.

2.2.4.1 Rationale of Utilizing *M. tuberculosis* H37Rv *luxABCDE* as the Bacterial Strain in Active Metabolite Assay Development

The reductive potential of NADPH, MLM and RS9 were investigated for compatibility with MABA. In the classical anti-replicating bacteria assay MABA, *M. tuberculosis* H37Rv is used and the readout is fluorometric measurement of resazurin reduction. Considering that the metabolic reactions in liver are primarily oxidoreductions catalyzed by CYP450s, it was anticipated that the existence of these P450s in the MGS would be problematic with using the reduction of resazurin as the endpoint of bacterial viability in 2.2.3.2.

2.2.4.2 The Criteria for Determining the Components and Concentrations of MGS

The inhibitory effects of HLM, RS9 and NADPH/$NADP^+$, NADH/NAD^+ on the growth of *M. tuberculosis* and the concentration dependence of these inhibitions clearly indicate that the concentration of these enzymes and cofactors in the MGS should be as low as possible without compromising the yield of the expected metabolites. Considering that NADPH is more inhibitory than $NADP^+$ at the same concentration and the sustainability of the formation of metabolites, $NADP^+$ was chosen as the cofactor using a NADPH-regenerating system. Although the

inhibition of NADH is comparable to that of NAD^+, the latter is considered to be superior again due to the sustainability of metabolite generation with an NADH regeneration system.

The same rationale can apply to the RS9. As the supernatant obtained from the liver homogenate, RS9 contains cytosol and microsomes, which means it includes a diverse library of phase I and phase II metabolism enzymes.

Although HLM was reported to be able to generate the amidine metabolite with either NADPH or NADH and to be more efficient with the latter cofactor (Saulter et al., 2005), in our study, both conditions appeared to be incomparable to that of MLM with NADH. Also, it was found previously that cytochrome b_5 and b_5 reductase play an important role in catalyzing the reduction of amidoxime to form amidine with NADH as the cofactor. This might imply that MLM is richer in cytochrome b_5 and b_5 reductase than HLM. In addition, MLM has a significant advantage in cost for a HTS assay.

For drug metabolism studies, a typical pH value for incubation is 7.4 to reflect that in blood. It is known that the growth of *M. tuberculosis* in culture media is pH dependent with pH 6.6 ± 0.2 as the optimal range. (Piddington et al., 2000). Although this is a more acidic optimum than for many other bacteria, fortunately, this falls within the range for optimal yield of metabolites in the MGS.

The combination of MLM and NADH in MGS was studied in order to achieve a high yield of LLK2-150 and these studies revealed that NADH at a high concentration could inhibit the formation of the amidine metabolites. It is possible that NADH competes with amidoxime in binding the enzyme, and when the concentration of NADH increases, the binding of amidoxime to the protein decreases, which leads to a decreasing yield of metabolites. With regard to HLM, high protein concentrations are not always an advantage in generating metabolites. An increase in protein binding may reduce the free parent LLK2-161 and therefore decrease the yield of metabolites. When MLM exceeds a threshold concentration, the metabolic contribution of increased enzyme concentration may be offset by the enhanced protein binding of the parent compound. This same may be true with respect to the use of RS9 in MGS.

The dynamics of metabolite formation was monitored since it was found that metabolite LLK2-150 was relatively stable in microsomes (data not shown). However, the primary metabolite produced could degrade or be further metabolized upon extended incubation. It is unknown whether the formation rate of the metabolites in the late stage of the incubation will exceed its degradation rate. These dynamics appeared to vary in response to the composition of the MGS. At 0.1 mM NADH, the formation of metabolite continued to increase at 20 hr. In contrast, at 0.05 mM NADH the amount of LLK2-150 had decreased at 20 hr, compared to that at 15 hr. When a NADH-regenerating system is utilized, the concentration of LLK2-150 achieved plateau as early as 6 hr.

2.2.4.3 The Inhibition Activity of Amidine Metabolite Formed in MGS

The MIC of LLK2-150 (1.5 μM) generated from LLK2-161 in MGS was slightly higher than that of the pure synthetic LLK2-150 (0.2 μM). This discrepancy could however just be the result of

variability in the antibacterial assay, since MICs of the synthetic LLK2-150 varied from 0.2 µM to 0.9 µM. There was also variability over several runs in the LC/MS/MS quantification of LLK2-150 formed in the MGS.

2.2.4.4 The Drawback of Type 3 Positive Control – CLA

The MGS was also investigated for the formation of 14-(*R*)-OH CLA from CLA. This exploration ceased due to several reasons. First, the inhibitory activity of 14-(*R*)-OH CLA against replicating *M. tuberculosis* H37Rv *luxABCDE* is quite moderate compared to that of the parent CLA, with a MIC of 35 µM versus 1.8 µM. This was unexpected considering that this metabolite is known to have potency comparable to the parent compound against other bacteria. According to a previous study of CLA metabolism in HLM (Rodrigues et al., 1997), besides the formation of 14-(*R*)-OH CLA, there are several other metabolites, including N-desmethyl CLA and 14-(*S*)-OH CLA. The formation of N-desmethyl-CLA and 14-(*R*)-OH CLA both contribute greatly to the clearance of CLA with a V_{max}/K_M of 3.3 ± 0.53 µl/min/mg protein and 4.2 ± 0.21 µl/min/mg protein, which means that the percentage of 14-(*R*)-OH CLA formed from CLA in humans is only around 56% at most. If so, in order to achieve a concentration above 70 µM of 14-(*R*)-OH CLA from CLA in MGS, the parent concentration should be at least 125 µM. Even if the yield of 14-(*R*)-OH CLA is 100%, the concentration of CLA in MGS would still need to be as high as 70 µM in order to realize a 90% inhibition in the antibacterial assay with a metabolite concentration of 14-(*R*)-OH CLA at 35 µM. However, in this case, the negative control, containing 35 µM CLA, would be too inhibitory to come up with a data analysis method to correlate bioassay-generated data with type-4 positive control inhibition profile. Secondly, with 25 mM $NADP^+$ as the optimal concentration to generate the active metabolite of CLA, the background inhibition from the MGS will be as high as 45%, which is not acceptable for the assay control. HLM at the optimal

concentration of 0.5 mg/ml could still be an inhibition factor even if solvent extraction could get rid of most of it.

2.2.4.5 Protein Binding of Metabolites

High protein binding is frequently seen with drug molecules. For the type-4 positive control (LLK2-161) and its active metabolite (LLK2-150), more than 70% were bound to the proteins in the assay system at the two concentrations tested. The properties of these molecules imply that an extraction of the metabolites from the MGS is necessary or even critical in order to obtain free and active metabolites. Unfortunately this precludes the use of a one-pot assay and creates additional challenges for true HTS.

2.2.4.6 The Overall Disadvantages of Liver Enzyme-based MGS for the Assay

Although the metabolite of the positive control for type 4 compounds was successfully obtained at a high yield and its antibacterial activity confirmed with *M. tuberculosis* H37Rv *luxABCDE*, the procedures to complete this assay are complicated and would take 2~3 days in addition to the time required for the antibacterial assay. This involves the incubation of the MGS with the parent compounds, the extraction of the metabolites formed and parent compounds, and the evaporation of the extraction solvent. Therefore, the development of this assay for HTS would first require the successful automation of these procedures.

2.3 An Alternative anti-TB Assay Development Approach using HepaRG-Derived Active Metabolites

2.3.1 Introduction

M. tuberculosis is a facultative intracellular pathogen that, like all such organisms, depends upon the host for nutrients when residing intracellularly (Smith, 2003). Although macrophages, as phagocytic immune cells, are responsible for engulfing TB pathogens to destroy them, they also attract mononuclear cells and T lymphocytes by inducing a localized pro-inflammatory response after infection resulting in a granuloma, which is the hallmark tissue reaction of TB (Gengenbacher and Kaufmann, 2012). Several methods are available to determine the viability of phagocytosed *M. tuberculosis* for the purpose of TB drug discovery. The most common method involves the plating on agar-based media of a defined volume of serially diluted, infected macrophage cell lysates followed by CFU analysis (Parish and Brown, 2008). Infected macrophages are cultured in Dulbecco's modified Eagle's medium, which is a typical mammalian cell culture medium. It is likely that *M. tuberculosis* is also able to grow in mammalian cell culture medium. In this chapter, an alternative MGS, an immortal mammalian HepaRG cell line, was utilized to generate metabolites.

HepaRG is a new human hepatoma cell line derived from a differentiated tumor. Seeded at low density (2.6×10^4 cells/cm^2), HepaRG cells rapidly proliferate, and differentiate toward hepatocyte-like and biliary-like cells when they reach confluence (Le Vee et al., 2006; Cerec et al., 2007). Addition of 1% ~ “2% dimethyl sulfoxide (DMSO) and 50 µM hydrocortisone hemisuccinate to the culture medium induces the differentiation of the hepatocyte-like cells into more granular cells, closely resembling typical adult primary hepatocytes with one or two nuclei and bile canaliculi-like structures”. The differentiated cells could transdifferentiate into bipotent

hepatic progenitors when seeded at low density (2.6×10^4 cells/cm^2), and this can be avoided by seeding differentiated cells at high density (0.46×10^6 cells/cm^2).

The differentiated HepaRG cells express “various nuclear receptors (aryl hydrocarbon receptor, pregnane X receptor, constitutive androstane receptor, peroxisome proliferator-activated receptor), CYP450s (CYP1A2, 2C9, 2D6, 2E1, 3A4), phase II enzymes (UGT1A1, GSTA1, GSTA4, GSTM1) and other liver-specific functions”, the corresponding mRNA levels of which are comparable to those in human primary hepatocytes. The functional resemblance of HepaRG cells to human primary hepatocytes, including the basal activities of P450s, their response to prototypical inducers, metabolic profiles and cytotoxicity was confirmed (Aninat et al., 2006)”. The “expression and function of drug transporters in differentiated HepaRG cells has also been studied and was demonstrated to be close to that in primary human hepatocytes (Le Vee et al., 2006). Because of all of these hepatocyte-like characteristics, multiple assays have been developed with HepaRG cells as a human primary hepatocyte surrogate for studies of liver metabolism, induction and cytotoxicity (Guillouzo et al., 2007; Jossé et al., 2008; Pernelle et al., 2011). In our lab, the HepaRG cell line had been evaluated for liver drug metabolism and induction assays for anti-TB drug discovery (Song, 2011). In addition, the culture medium of HepaRG had been customized and optimized in order to shorten the culture time to 2 weeks and to reduce the cost of the cellular assay, especially at a HTS level.

In this subchapter, the potential of HepaRG cells as a screening assay to detect liver enzymes-derived active metabolites against *M. tuberculosis* was explored.

2.3.2 Materials and Methods

2.3.2.1 Materials

Williams' Medium E, GlutaMAX™-I Supplement, HepaRG™ Thaw, Plate, & General Purpose Medium Supplement, HepaRG™ Maintenance/Metabolism Medium Supplement, fetal calf serum (FCS) was purchased from Invitrogen (Carlsbad, CA). Human insulin, hydrocortisone, and DMSO were purchased from Sigma-Aldrich (St Louis, MO).

2.3.2.2 Compatibility of HepaRG Culture Medium with the Growth of *M. tuberculosis* H37Rv *lux ABCDE*

In-housed customized medium was prepared with Williams' medium E supplemented with 10% FCS, 1% DMSO, 5 μg/ml human insulin, 2 mM glutamine, and 50 μM hydrocortisone.

The commercial HepaRG Metabolism Medium or the in-house customized medium or D.I. water were added into the wells of 96-well white plates at a volume from 0 μl to 190 μl into 2X 7H12 medium at a volume from 190 μl to 0 μl to arrive at a percentage of cell culture medium in the total volume (200 μl) from 0% to 95%. Bacterial stock of *M. tuberculosis* H37Rv *luxABCDE* was diluted into 2X 7H12 medium, 10 μl of which then was inoculated into each well of the plates. The final bacterial density was 4×10^5 cells/ml. After the incubation at 37 °C for 7 days, luminescence from each well was measured in a VICTOR 3 Multilabel Plate Reader (PerkinElmer, Fremont, CA).

2.3.2.3 Metabolism of Type 3 and 4 Positive Controls in HepaRG Cells

In-housed customized medium was prepared with Williams' medium E supplemented with 10% FCS, 1% DMSO, 100 units/ml penicillin, 100 µg/ml streptomycin, 5 µg/ml human insulin, 2 mM glutamine, and 50 µM hydrocortisone.

Differentiated HepaRG cells were seeded into 96-well plates at a high density of 1.45×10^6 cells/ml (~0.46×10^6 cells/cm^2) in the in-house customized medium. The medium was replenished every 2 ~ 3 days. On day 7, the adherent and differentiated cells were replenished with 100 µl medium containing the type-3 positive control at final concentrations of 0.5, 1.0, 2.0 and 4.0 µg/ml and the type-4 positive control at final concentrations of 2.5, 5.0, 10 and 20 µg/ml. The culture supernatants were collected at 0 hr, 24 hr, 48 hr and 72 hr in order to monitor the metabolite formation. An equal volume of acetonitrile containing internal standard was added to extract the metabolites. The samples were then centrifuged for 30 min at 2200 g and 4 °C, and the supernatant was collected and analyzed by LC/MS/MS to quantify the formed metabolites.

2.3.2.4 Optimization of MGS with HepaRG Cells for Type 3 Positive Control in 96-well Plates

HepaRG cells were cultured as described above in 2.3.2.3. On day 7, the differentiated cells were treated with 100 µl medium containing the type-3 positive control, CLA, at 2 and 4 µg/ml. The culture supernatants were collected at 0 hr, 24 hr, 48 hr, 72 hr, 96 hr, 120 hr, 144 hr and 168 hr in order to monitor the metabolite formation. Metabolite extraction and analysis was performed as described above in 2.3.2.3.

2.3.2.5 Optimization of MGS with HepaRG Cells for Type 3 Positive Control in 24-well Plates

HepaRG cells were cultured as described above in 2.3.2.3. On day 7, the differentiated cells were treated with 250 µl medium containing type-3 positive CLA at 2 µg/ml. The medium supernatant of corresponding wells was collected at 0 hr, 24 hr, 48 hr, 72 hr, 96 hr and 120 hr in order to monitor the metabolite formation. Metabolite extraction and analysis was performed as described above in 2.3.2.3.

HepaRG cells were cultured as described above in 2.3.2.3. On day 7, the differentiated cells were treated with 150 µl and 250 µl medium containing type-3 positive CLA at 2 µg/ml. The medium supernatant of corresponding wells was collected at 0 hr, 72 hr and 144 hr in order to monitor the metabolite formation. Metabolite extraction and analysis was performed as described above in 2.3.2.3.

2.3.2.6 Quantitation of 14-(*R*)-OH CLA Formed in Optimized MGS

HepaRG cells were cultured as described above in 2.3.2.3. in both in-house and commercial medium, individually. On day 7, the differentiated cells were treated with 150 µl medium containing type-3 positive CLA at 2 µg/ml. The medium supernatant of corresponding wells was collected at 0 hr, 72 hr and 144 hr in order to quantify the metabolite formation. Metabolite extraction and analysis was performed as described above in 2.3.2.3.

2.3.2.7 Measurement of LLK2-150 and 14-(*R*)-OH CLA in LC/MS/MS

Refer to 2.2.2.21 (Page 39).

2.3.2.8 Inhibition of *M. tuberculosis* H37Rv *luxABCDE* by Type 3 Positive Control CLA and its Active Metabolite 14-(*R*)-OH CLA

Refer to 2.2.2.18 (Page 38).

2.3.2.9 Detection of LLK2-150 as the impurity of LLK2-161 in LC/MS/MS

The detection of LLK2-150 as the impurity in LLK2-161 powder was performed in mass spectrometer. The LC/MS/MS method for LLK2-150 quantifier and qualifier as decribed in section 2.2.2.21 was used to analyze the pure LLK2-161 solution sample which was dissolved in acetonitrile.

2.3.3 Results

2.3.3.1 Compatibility of HepaRG Culture Medium with the Growth of *M. tuberculosis* H37Rv *lux ABCDE*

The metabolites are mostly extracellular after their formation and release from the cells. In order to improve the efficiency of this assay, metabolites are not extracted from the culture medium. Instead, the supernatant, which is composed of the medium and metabolites released from the adherent cells, is incubated with the bacteria directly. The cell culture medium alone should not affect the growth of *M. tuberculosis* in the antibacterial assay.

The commercial HepaRG metabolism medium, when mixed with 2X 7H12 medium at any ratio between 0.05 ~ 0.95, was inhibitory for the growth of *M. tuberculosis* (data not shown). Commercial cell culture medium typically contains streptomycin (which is active against *M. tuberculosis)* as the antibacterial reagent and this was detected in the commercial medium by LC/MS/MS (data not shown). In contrast, the extent of growth of *M. tuberculosis* when cultured in a mixture of the in-house customized medium without antibiotic and 2X 7H12 medium, was not much different than that obtained when the 2X 7H12 was diluted with water when the proportion of in-house medium or H_2O was ≤ 0.3 (Figure 2.19). When the 2X 7H12 medium is diluted 1:1 with water (proportion of water in the final medium of 0.5) the optimum level of growth was obtained as expected and both lower and higher proportions of water decreased the overall extent of growth, in the latter case completely inhibiting growth at a proportion of 0.95. In contrast, the in-house medium, regardless of proportion, yielded growth that was approximately 50% of the of the 1X 7H12. Overall, the in-house customized medium without antibiotic can be used as the HepaRG cell culture medium for developing MGS.

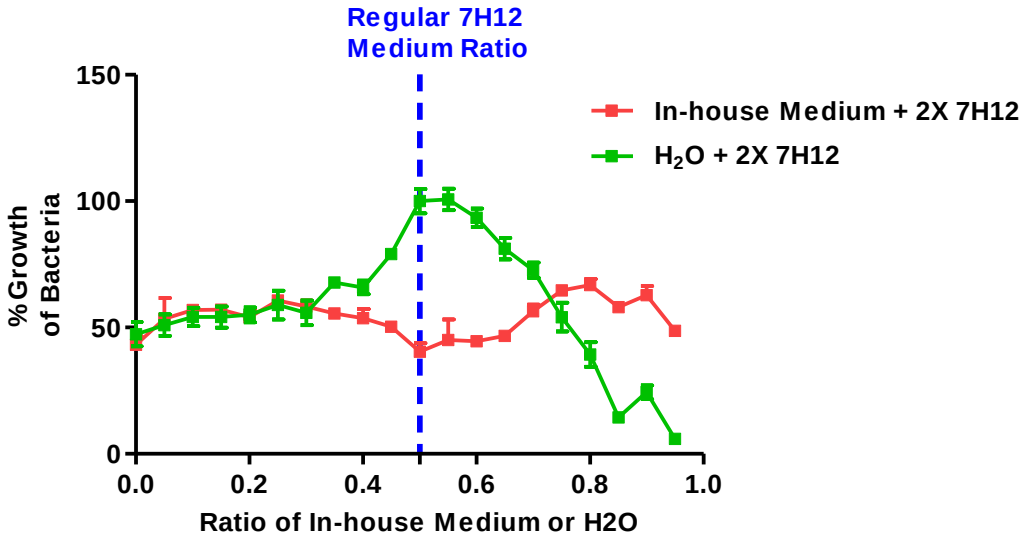

Figure 2.20 Growth of *M. tuberculosis* in mixtures of 2X 7H12 medium plus in-house HepaRG medium or H_2O. The data shown represent the mean ± S.D. from three replicates.

2.3.3.2 Metabolism of Type 3 and 4 Positive Controls in HepaRG Cells

Since the positive controls of type 3 and type 4 compounds generate active metabolites, their metabolism was investigated to maximize the yield of the expected metabolites. With a regular high cell plating density and culture conditions, increases of the metabolite LLK2-150 from the type 4 positive control LLK2-161 were not observed during the 72-hour incubation regardless of the initial LLK2-161 concentration (Figure 2.20A). Instead, LLK2-150 was found to be an impurity in the parent powder LLK2-161, which was proven in LC/MS/MS as shown in Figure 2.22. Both of the LLK2-150 quantifier and qualifier transitions could be detected in the pure LLK2-160 solution sample. As the impurity of LLK2-161, LLK2-150 was slightly metabolized further. In contrast, increases in the 14-(*R*)-OH CLA metabolite of the type 3 positive control, were detected throughout the entire incubation at all tested concentrations (Figure 2.20B).

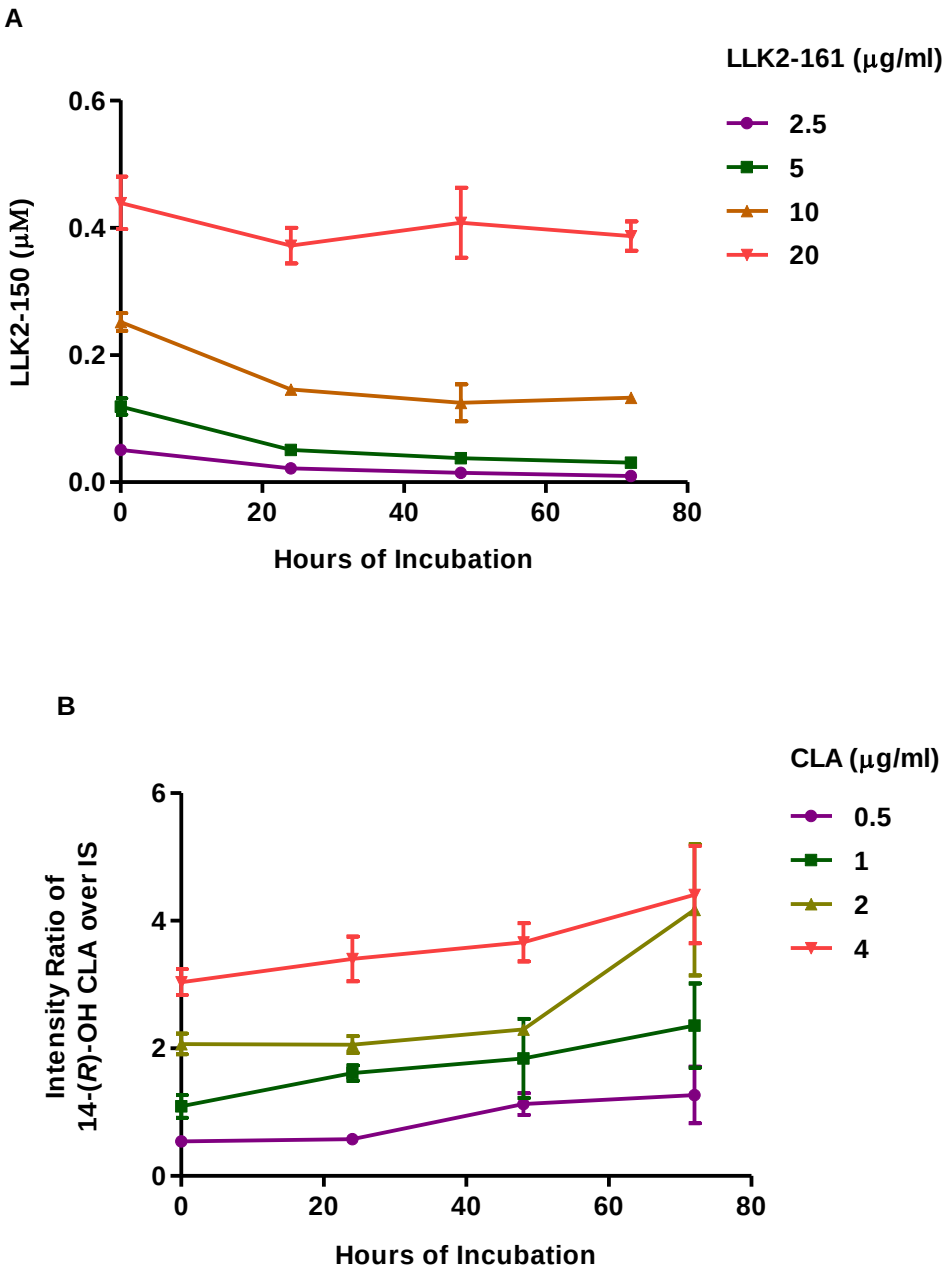

Figure 2.21 Formation of metabolite LLK2-150 (A) and 14-(*R*)-OH CLA (B) in HepaRG cells. The data shown represent the mean ± S.D. from two replicates.

A

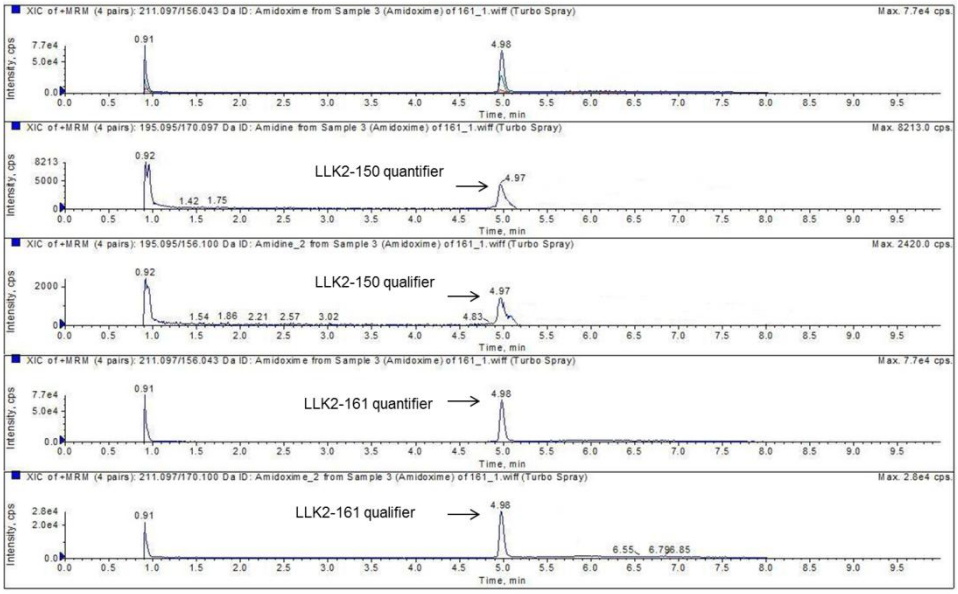

B

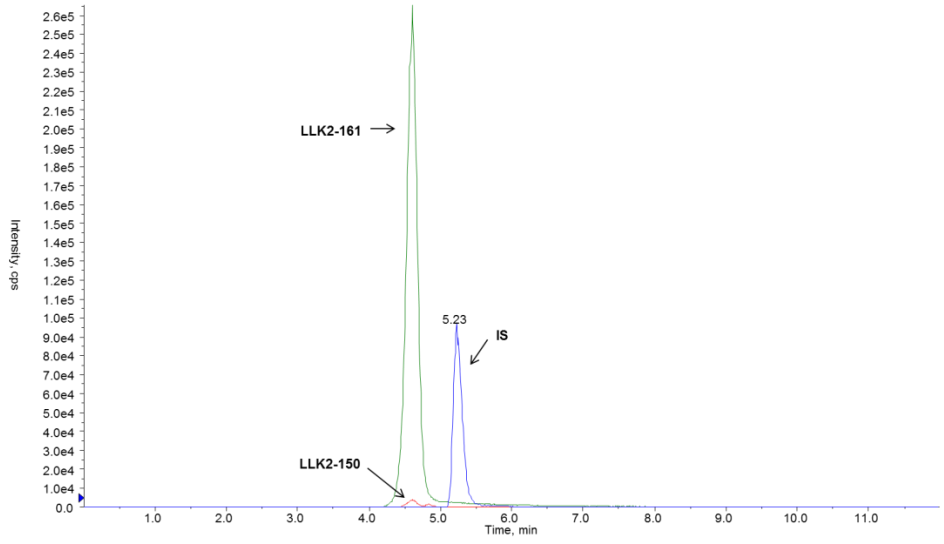

Figure 2.22 Detection of LLK2-150 as the impurity in LLK2-161 in LC/MS/MS (A) and the chromatography of the mixture of LLK2-150 and LLK2-161 in LC/MS/MS (B).

2.3.3.3 Optimization of MGS with HepaRG Cells for Type 3 Positive Control in 96-well Plates

Due to the lack of the chemical standard of metabolite 14-(*R*)-OH CLA for the time being, the ratio of metabolite formed over IS in terms of their responses in LC/MS/MS was compared throughout the incubation (Figure 2.21). Significant increases in metabolite occurred within the first 24 hr (day 1) for both concentrations of 2 and 4 µg/ml CLA and then remained essentially unchanged for the following 144 hr. However, compared to the response ratio of CLA at 2 µg/ml (~ 2.7 µM) over IS, it can be anticipated that the metabolite formed is far below the MIC of 14-(*R*)-OH CLA in *M. tuberculosis* (35 µM) and therefore would be undetectable by bioassay with *M. tuberculosis*.

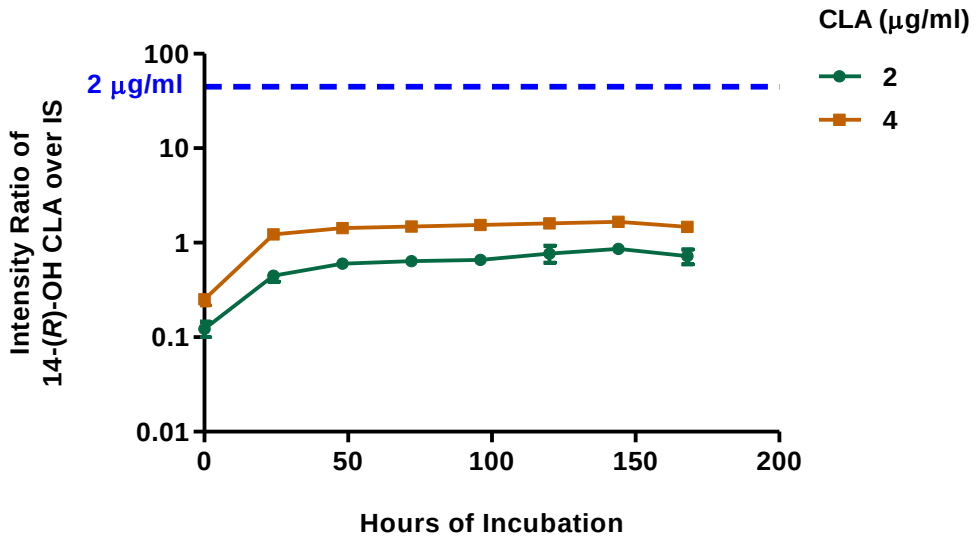

Figure 2.23 Formation of metabolite 14-(*R*)-OH CLA from CLA in HepaRG cells in 96-well plates with a volume of 100 µl. The data shown represent the mean ± S.D. from three replicates.

2.3.3.4 Optimization of MGS with HepaRG Cells for Type 3 Positive Control in 24-well Plates

It has been reported that a high plating density of cells (0.46×10^6 cells/cm^2) and the presence of DMSO (1~2%) are required for the expression of metabolizing enzymes and transporters (Le Vee et al., 2006; Cerec et al., 2007; Guillouzo et al., 2007). In order to achieve high expressions of these metabolizing enzymes, it is not advised to manipulate the conditions of culturing HepaRG cells. An alternative approach to increase metabolite production is to increase the total cell number.

When 500 µl cells were cultured in high density in 24-well plates for 7 days and was then replaced with 250 µl medium containing 2 µg/ml CLA, metabolite formation significantly increased until 96 hr (Figure 2.22). When the volume of medium containing 2 µg/ml CLA decreased to 150 µl, the concentration of 14-(*R*)-OH CLA was much higher than that of 250 µl at 72 hr and 144 hr (Figure 2.23), which indicated that a higher ratio of cells over parent molecules does help in generating metabolites.

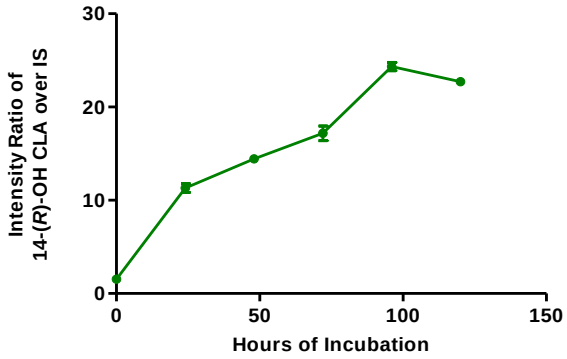

Figure 2.24 Formation of 14-(*R*)-OH CLA metabolite from CLA in HepaRG in a 24-well plate with a volume of 250 µl. The data shown represent the mean ± S.D. from two replicates.

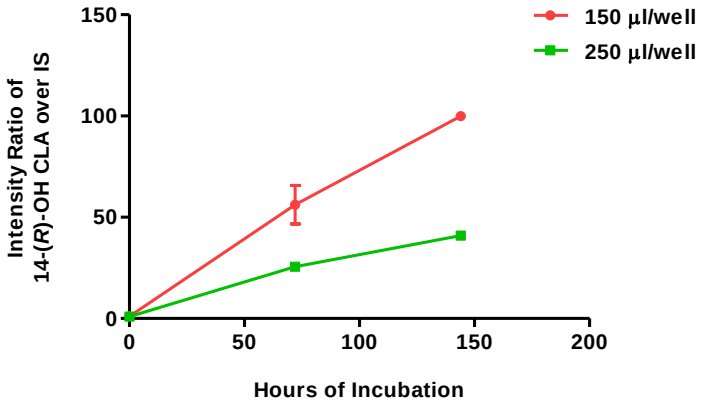

Figure 2.25 Formation of 14-(*R*)-OH CLA metabolite from CLA in HepaRG cells in a 24-well plate with a volume of 150 µl and 250 µl. The data shown represent the mean ± S.D. from two replicates.

2.3.3.5 Quantitation of 14-(*R*)-OH CLA Formed in Optimized MGS

The formation of metabolite 14-(*R*)-OH CLA in cells growing in commercial medium and in-house customized medium was compared (Figure 2.24). It was evident that at the two time points of 72 hr and 144 hr, the amount of metabolite formed in in-house medium was ~2x that found in commercial medium (0.053 µM vs 0.026 µM at 72 hr and 0.116 µM vs 0.050 µM at 144 hr), indicating the in-house medium was superior in supporting a higher yield of metabolite.

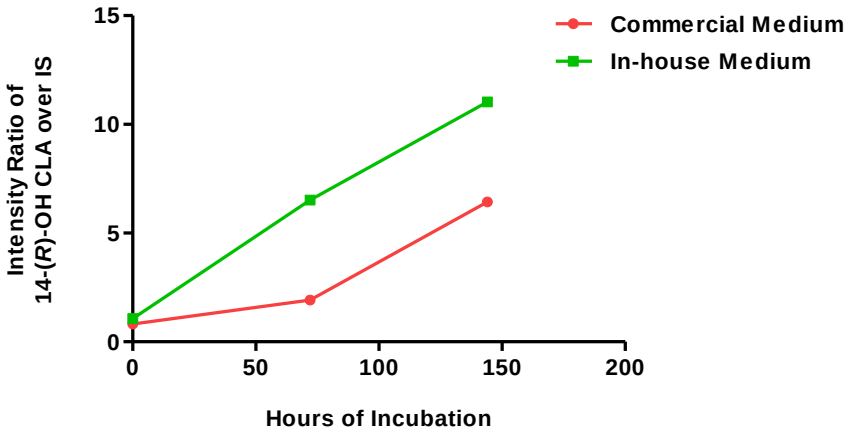

Figure 2.26 Formation of metabolite 14-(*R*)-OH CLA from CLA in HepaRG cells growing in commercial medium and in-house medium. The data shown represent the mean ± S.D. from two replicates.

2.3.3.6 Antibacterial Activity of 14-(*R*)-OH CLA Formed in HepaRG Cells

The anti-tuberculosis activity of the metabolites formed after 144-hr incubation of Hepa-RG with CLA in in-house medium was tested. The highest concentration of metabolite generated in this MGS was 0.116 µM (from parent at 3.7 µM), which failed to effect any inhibition in the bacterial assay (data not shown). Subsequently the MIC of the synthetic 14-(*R*)-OH CLA metabolite was determined to be as high as 35 µM, which was found to be 10.5 µM and 42 µM for strains MO-1 and LV-2 of the *M. avium* complex, respectively (Cohen et al., 1992). Therefore, with this optimized MGS, the amount of metabolite generated is far below that required to serve as the positive control for type 3 compounds.

2.3.4 Discussion

HepaRG cells have been utilized as the liver metabolic enzyme source to generate metabolites. The specific cell culture method is critical to ensure the expression of the metabolizing enzymes and transporters. For the type 3 positive control CLA/14-(*R*)-OH CLA, in the in-house customized medium, the formation of metabolite 14-(*R*)-OH CLA was higher than that in the commercial medium. Other advantages are the lower cost and the lack of streptomycin which is found in commercial medium. However, the yield of the metabolite of CLA in the optimized assay was still too low to inhibit *M. tuberculosis* even when this yield was improved by raising the ratio of cell numbers versus the parent molecules. In addition, the MIC of 14-(*R*)-OH CLA for *M. tuberculosis* H37Rv *lux ABCDE* is much higher than that of the parent (35 µM vs 0.9 µM), an unexpected results which makes CLA unsuitable for use as a positive control, for type 3 compounds.

Chapter 3. The Inhibition of Drug Metabolism

3.1 Introduction

3.1.1 Introduction to Inhibitory Drug-drug interactions

To achieve the desired therapeutic plasma or tissue concentration and maintain it for a certain period of time, a balance must be reached between the amount of administered drug and the rate of drug clearance (Fowler and Zhang, 2008). Since hepatic metabolism is the major clearance pathway for small molecule drug substances, the inhibition of these enzymes by coadministered drug(s) can cause overexposure to the victim drugs and thus increased toxicities, i.e., leading to drug-drug interactions (DDIs) (Danton et al., 2013). Both phase I and phase II enzymes can be inhibited by drugs. Pharmacokinetic DDIs have been observed with the inhibitor drugs, which require cautions when they are coadministered with the victim drugs. For example, clarithromycin inhibits CYP3A4 through a mechanism-based inactivation, and the coadministration of clarithromycin incurred significant AUC increases of midazolam (a CYP3A4 substrate) following i.v. and oral dosing by 3.2-fold and 8.0-fold, respectively (Quinney et al., 2008; Quinney et al., 2010). Also, fluconazole and voriconazole are reversible inhibitors of CYP3A4, CYP2C9 and CYP2C19, and these two drugs increased AUC of S-(+)-ibuprofen (a CYP2C9 substrate) by 105% and 83%, respectively (Hynninen et al., 2006). Atazanavir reversibly inhibits UGT1A1-mediated bilirubin glucuronidation, and hyperbilirubinemia was observed in subjects administered with atazanavir (Bissio and Lopardo, 2013). Mibefradil that inhibits CYP3A4 and CYP2D6 was shown to interact with more than 26 marketed drugs in humans and have been withdrawn from market since 1998 (Po and Zhang, 1998).

3.1.2 Reversible Inhibition of Drug-Metabolizing Enzymes (DME)

Inhibition of drug metabolizing enzymes including CYP450s and UGTs may occur through different mechanisms. When the inhibitor binds the enzyme non-covalently, this inhibition is

reversible. Based on the interactions among inhibitor, substrate, and enzyme, reversible inhibition can be further characterized as competitive, noncompetitive, uncompetitive or mixed inhibition (Kakkar et al., 1999).

3.1.2.1 Competitive Inhibition

Inhibitor only binds the unbound enzyme and the binding of the inhibitor to the active site of the enzyme prevents binding of the substrate and vice versa (Figure 3.1, Pathway 1). For example, sulfaphenazole inhibits diclofenac 4'-hydroxylation by binding to the catalytic site of CYP2C9 and preventing diclofenac's binding to CYP2C9 (Zweers-Zeilmaker et al., 1997).

3.1.2.2 Uncompetitive Inhibition

Inhibitor cannot bind to the free enzyme, but to the complex formed between the enzyme and the substrate (the E-S complex) (Figure 3.1, Pathway 2).

3.1.2.3 Noncompetitive Inhibition

Inhibitor binds to both unbound and substrate-bound enzyme at the site(s) different from the substrate-binding site. The inhibitor binding to the enzyme reduces the enzyme activity (Figure 3.1, Pathways 1 and 2). Examples include the inhibition of noscapine against (*S*)-warfarin 7-hydroxylation by CYP2C9 (Fang et al., 2010).

3.1.2.4 Mixed Inhibition

Inhibitor binds, similarly “as the noncompetitive, but possibly at the site(s) overlapped with substrate-binding site, the unbound and the substrate bound enzyme with potentially different affinities” (Figure 3.1, Pathways 1, 2 and 3). Felodipine and fluoxetine both exhibited mixed inhibition toward 1’-hydroxylation of midazolam (Foti et al., 2010).

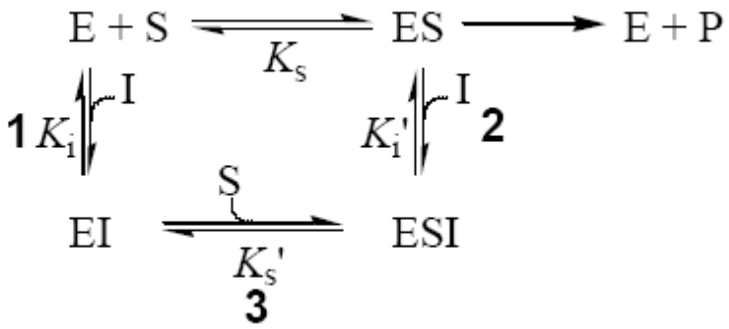

Figure 3.1 Reversible Enzyme Inhibitions Follows Michaelis - Menten Kinetics

3.1.3 Mechanism-based inhibition of CYP450s

This mechanism can be divided into the following three categories based on the underlying biochemical reactions: (1) covalent modification of apoproteins, (2) covalent modification of haem, and (3) quasi-irreversible inactivation involving the formation of metabolic-intermediate complex (MIC) (Figure 3.2). The former two involve the formation of a covalent bond between the enzyme and the activated inhibitor while the latter one refers to the formation of a metabolic intermediate that chelates the haem iron (Venkatakrishnan et al., 2007). A series of functional groups have been found to be associated with mechanism-based inactivation of CYP450 enzymes, including alkene, alkyne, 2-alkylimidazole and methylenedioxyphenyl (Orr et al., 2012a).

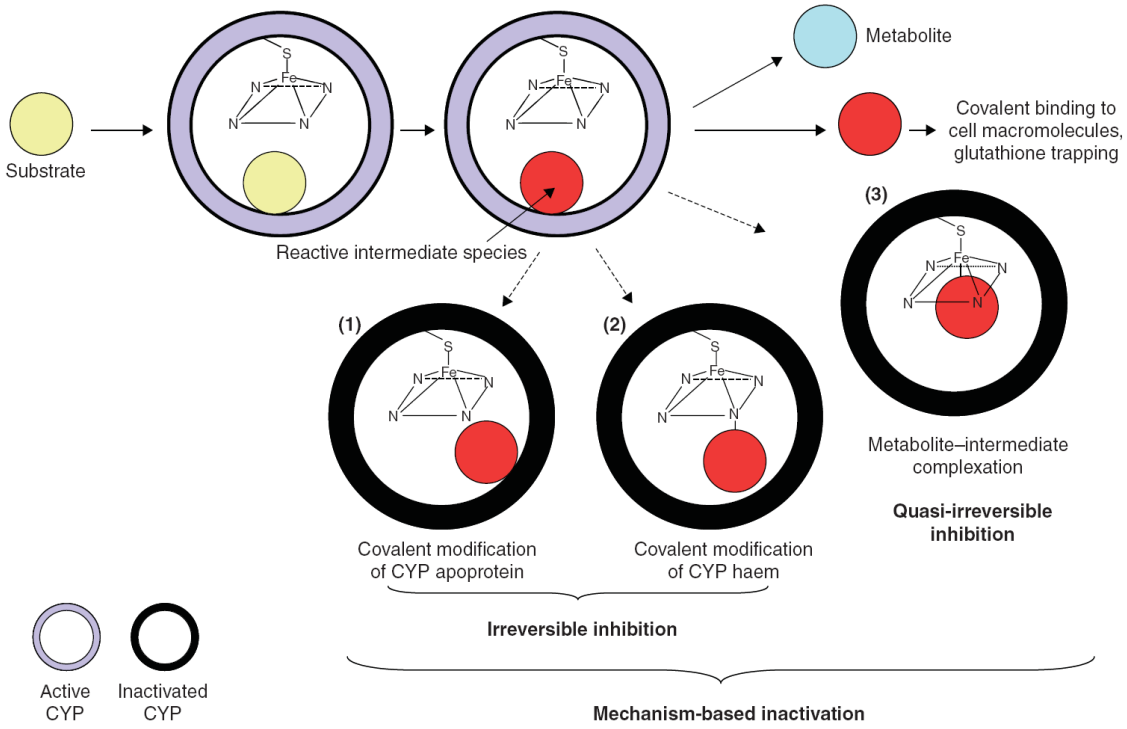

Figure 3.2 Mechanism-based inhibition of CYP450s.

3.1.4 Methodology of the Study of DME inhibition

Recombinant proteins for drug-metabolizing enzymes and freshly isolated primary hepatocytes have been well-established tools for DME inhibition studies. *In vitro* studies using the tools can be used to identify metabolizing enzymes inhibited by drugs and to estimate the risk of drug-drug interactions.

3.1.4.1 *In Vivo* Consequences of Reversible Inhibition of DME

The inhibition constant K_i of the inhibitor is calculated by nonlinear regression based on different inhibitory mechanisms of competitive inhibition (eq. 1), uncompetitive inhibition (eq. 2), noncompetitive inhibition (eq. 3), or mixed inhibition (eq. 4) (Zhang and Wong, 2005).

$$v = \frac{V_{max}S}{K_m\left(1+\frac{I}{K_i}\right)+S} \qquad (1)$$

$$v = \frac{V_{max}}{1+\frac{I}{K_i}+\frac{K_m}{S}} \qquad (2)$$

$$v = \frac{V_{max}S}{(K_m+S)\left(1+\frac{I}{K_i}\right)} \qquad (3)$$

$$v = \frac{V_{max}S}{K_m\left(1+\frac{I}{K_i}\right)+S\left(1+\frac{I}{K_i'}\right)} \qquad (4)$$

When the plasma concentration of inhibitor is higher than K_i, the inhibitor might inhibit the hepatic metabolism and clearance of victim drugs and cause overexposure of the victim drug, which might incur toxicity *in vivo*. However, how much the overexposure of the victim drug is and whether the overexposure is high enough to cause adverse reactions *in vivo* cannot be determined from the difference between the value of K_i and the plasma concentration of the inhibitor. A calculation of AUC change of the victim drug in plasma due to the inhibition of its clearance has to be made. For competitive or noncompetitive inhibition, the AUC change of the victim drug will be calculated using eq. 5 when the victim drug concentration in plasma is much lower than the K_m (Brown et al., 2005b), where D is the dose of victim drug. When the victim drug is eliminated by the metabolic pathway by a fraction (f_m), AUC change upon coadministration of the inhibitor can be calculated using eq. 6 (Brown et al., 2005a).

$$\frac{AUC_i}{AUC} = \frac{\frac{D}{CL_i}}{\frac{D}{CL}} = \frac{CL}{CL_i} = \frac{V_{max}/(s+K_m)}{V_{max}/(s+K_m\left(1+\frac{I}{K_i}\right))} = 1+\frac{I}{K_i} \qquad (5)$$

$$\frac{AUC_i}{AUC} = 1/(f_m/(1+\frac{I}{K_i}) + (1-f_m)) \quad (6)$$

3.1.4.2 *In Vivo* Consequences of Irreversible Inhibition of DME

The prediction of drug-drug interaction by irreversible inhibition is based on the studies of mechanism-based enzyme inactivators (Silverman, 1995). The mechanism-based inactivation of metabolizing enzymes involves the synthesis and degradation of the affected enzyme, besides the inactivation by the precipitant drug (Figure 3.3). As described previously, upon binding to an enzyme, the inactivator (I) is destined to one of three fates: it can be converted to a product and released from the enzyme or released from the enzyme through reversible binding, or it can inactivate the enzyme by forming an irreversible complex (E•MI) (Mayhew et al., 2000).

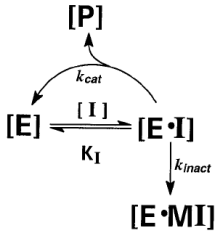

Figure 3.3 Inactivation of enzyme by inhibitors

The rate of enzyme inactivation at a given inactivator concentration is referred to as the apparent inactivation rate constant k_{inact}, denoted by λ and the mathematical model of the rate of enzyme inactivation is as eq. 7 (Tudela et al., 1987):

$$\lambda = \frac{I * k_{inact}}{I + K_I} \qquad (7)$$

k_{inact} is the maximum inactivation rate constant (when the inactivator concentration is close to infinity), and K_I is the inhibitor concentration that produces half the maximal rate of inactivation.

The steady-state concentration of enzyme (in the absence of inhibitors) is defined by the eq. 8:

$$E_{SS} \propto \frac{k_{synth}}{k_{degrad}} \qquad (8)$$

where k_{synth} is the rate constant for enzyme synthesis and k_{degrad} is the rate constant for enzyme degradation.

In the presence of a mechanistic inactivator, an additional pathway for enzyme degradation needs to be included (Figure 3.4) and the new steady-state concentration of enzyme is defined by the eq. 9:

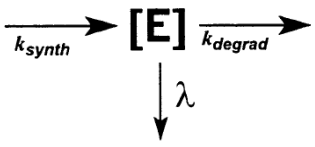

Figure 3.4 A steady-state model of enzyme content in synthesis, degradation and inactivation

$$E_{SS}{}' \propto \frac{k_{synth}}{k_{degrad} + \lambda} \qquad (9)$$

Since intrinsic clearance (CL_{int}) is proportional to $[E]_{ss}$ and CL_{int} is inversely proportional to AUC_{po}, the AUC change for mechanism-based inactivation can be expressed as eq. 10 (Wilkinson and Shand, 1975; Houston, 1981).

$$\frac{AUC'}{AUC} = \frac{E_{SS}}{E_{SS}'} = \frac{k_{degrad} + \frac{I * k_{inact}}{I + K_I}}{k_{degrad}} \qquad (10)$$

For the metabolic pathway responsible for a fraction (f_m) of the clearance of the victim drug, AUC change can be calculated as eq. 11 (Obach et al., 2006).

$$\frac{AUC'}{AUC} = \frac{1}{\frac{f_{m(450)}}{1 + \frac{I_{in\ vivo} * k_{inact}}{K_I * k_{degrad}}} + (1 - f_{m(450)})} \qquad (11)$$

3.1.5 Overall Research Objective

The inhibitory DDIs with the increased exposure of victim drugs can be predicted through the calculation of AUC change of the victim drugs. A clear understanding of the inhibition mechanism of precipitant drug against the metabolizing enzymes with the victim drug as the substrate is critical in estimating the AUC change.

In this chapter, the inhibitory DDIs through the reversible inhibition and mechanism-based inactivation were investigated. The reversible inhibition study is to explore the potential risk of DDIs by investigating the inhibition kinetics of four commonly used TKIs against the glucuronidation of a panel of UGT isoforms. The mechanism-based inactivation study of

noscapine is also to identify the inhibition mechanism of noscapine toward (*S*)-warfarin 7-hydroxylation by CYP2C9. By determining the inactivation parameters of noscapine in three CYP2C9 variant proteins, AUC change of (*S*)-warfarin was predicated and a dose adjustment was calculated for these variant carriers from different populations.

3.2 Reversible Inhibition of Tyrosine Kinase Inhibitors on UDP-glucuronosyltransferase Glucuronidation

3.2.1 Introduction

Tyrosine-kinase inhibitors (TKIs) are anticancer drugs. Tyrosine kinases phosphorylate the tyrosine residues of proteins involved in the activation of signal transduction cascades that play key roles in biological processes including growth, differentiation and apoptosis in cancer cells (Paul and Mukhopadhyay, 2004). Currently, 17 FDA-approved TKIs are used clinically. More than 80 % of cancer cases are developed in patients older than 60 years old (Howlader et al., 2013) who are subject to other diseases that require drug treatment (Christensen et al., 2009). As a result, TKIs have been commonly combined with other drugs in cancer patients for the treatment of multiple diseases (Bressler and Bahl, 2003; Costa and Huberman, 2006), and drug-drug interaction involving TKIs is a potential clinical concern.

UDP-glucuronosyltransferases (UGT), a class of phase II enzymes, catalyze the conjugation of glucuronic acid to endogenous substances and exogenous compounds. "UGT-catalyzed glucuronidation reactions are responsible for the metabolism of approximately 35% of all drugs metabolized by phase II enzymes" or "one-seventh of the drugs prescribed" in the United States in 2002 (Williams et al., 2004). The human UGT superfamily involved in xenobiotics metabolism is comprised of 2 families: UGT1 and UGT2 (Izukawa et al., 2009). UGT1A1, 1A3, 1A4, 1A6, 1A9, 2B7 and 2B15 are major UGTs responsible for metabolism of drugs (Miners et al., 2010). UGT1A7, 1A8, 1A10 and 2B4 have also been found to metabolize drugs including lorazepam, FYX-051, GV150526 and Z-338 (Gilissen et al., 2000; Furuta et al., 2004; Omura et al., 2007; Uchaipichat et al., 2013). The distribution of UGT isoforms is quite broad and most of them were

found in liver except UGT1A7, 1A8 and 1A10, which are expressed mainly in intestine (Strassburg et al., 1997; Harbourt et al., 2012).

The attentions to the inhibition of glucuronidation by UGT have been drawn recently. Although there have been many findings about the inhibition of UGT *in vitro*, the clinical observations of DDIs involving UGTs and the correlations with the clinically relevant interactions in humans are quite rare (Midgley et al., 2007; Liu et al., 2010c; Fujita et al., 2011; Ai et al., 2013). The reason for the low frequency is that UGT substrate drugs are often metabolized by multiple UGTs and have high K_m values *in vitro* when compared with substrates of P450 enzymes. The *in vitro* data also suggest that the ratio of inhibitor plasma concentration over K_i would be low. In addition, only 10 % of the top 200 drugs prescribed in US in 2002 are cleared by UGT glucuronidation (Williams et al., 2004). Even if the inhibition of UGT glucuronidation happens, the AUC change of the victim drug as the UGT substrate is usually less than 2-fold, except that of probenecid inhibited by zomepirac (AUC change>4-fold), which has been withdrawn from market.

Previous *in vitro* and *in vivo* studies indicate that TKIs may alter the hepatic elimination of co-administered drugs by inhibiting their metabolism. For example, nilotinib and erlotinib inhibit UGT1A1 activity whereas gefitinib inhibits UGT1A1, UGT1A7, UGT1A9 and UGT2B7 activities (Liu et al., 2010a; Liu et al., 2010b; Fujita et al., 2011). A clinical study also showed that co-administration of lapatinib with irinotecan leads to a ~40% increase in the AUC of SN-38 (an active metabolite of irinotecan and a UGT1A1 substrate) (Midgley et al., 2007), suggesting the inhibition of UGT1A1 activity by lapatinib. However, whether these TKIs affect activities of others UGT isoforms and whether other TKIs affect UGTs remain unknown.

In this study, four commonly used TKIs − axitinib, imatinib, lapatinib and vandetanib (Figure 3.5) − were evaluated for their capabilities to inhibit UGT activities. The inhibition kinetics of each compound was characterized with a non-selective substrate except for UGT1A4. Based upon inhibition potency, an inhibition kinetics study of selected TKIs against certain UGT isoforms with corresponding drugs or endogenous molecules as the substrate was performed. In the end, the risks of the inhibition of UGT glucuronidation activities by TKIs in clinical were estimated.

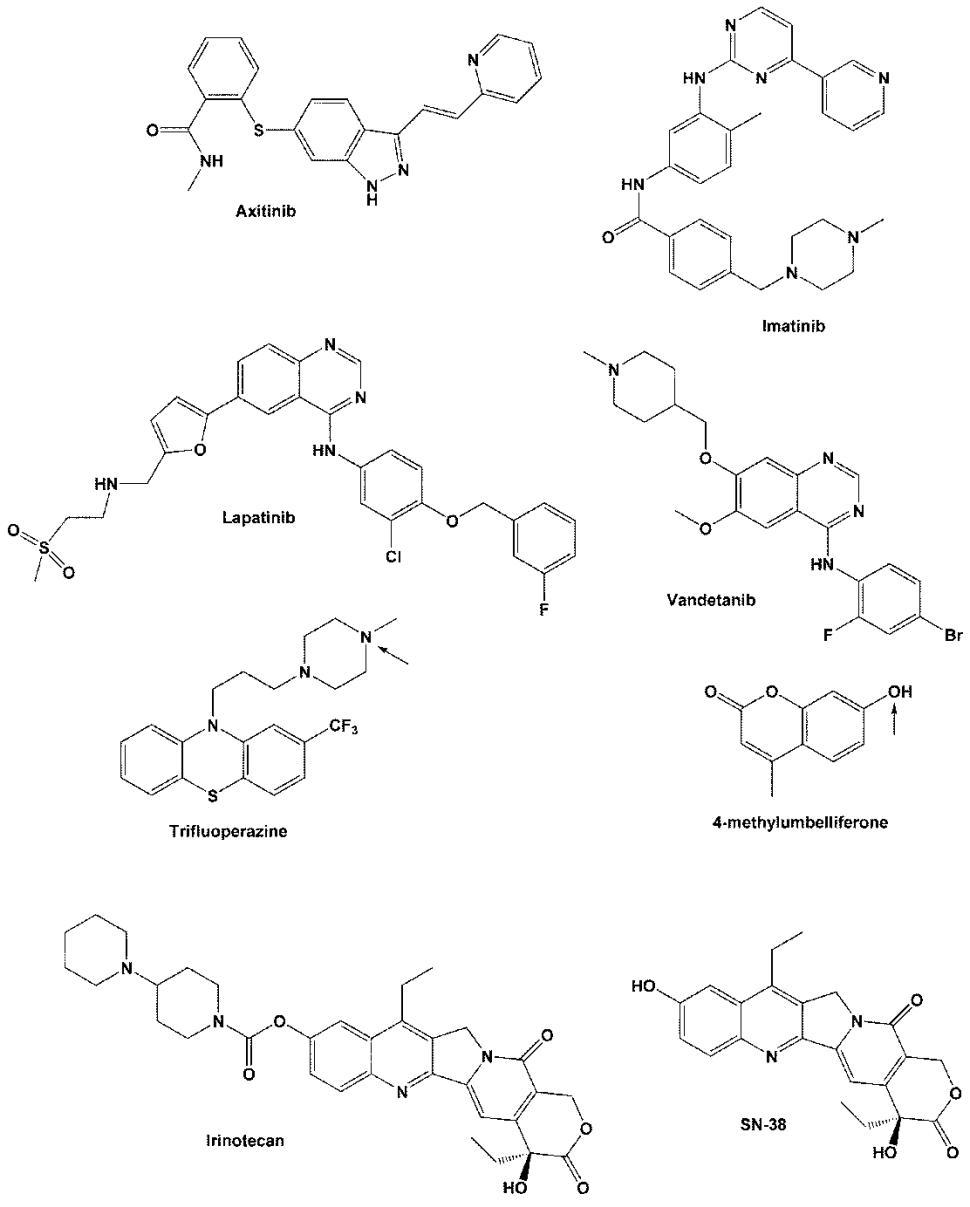

Figure 3.5 Structures of TKIs and UGT substrates

3.2.2 Materials and Methods

3.2.2.1 Materials

Axitinib, imatinib, lapatinib, vandetanib, SN-38 and SN-38 glucuronide (SN-38G) were purchased from Toronto Research Chemicals, Inc (Toronto, Ontario, Canada). Tris-HCl, 4-methylumbelliferone (4-MU), 4-methylumbelliferone-β-D-glucuronide (4-MUG), and uridine 5-diphosphoglucuronic acid trisodium salt (UDPGA) were purchased from Sigma-Aldrich (St. Louis, MO). Trifluoperazine (TFP) was from purchased Enzo Life Science (Farmingdale, NY). All other reagents were of high-performance liquid chromatography (HPLC) grade or the highest grade commercially available. "A panel of recombinant human UGT supersomes (UGT1A1, 1A3, 1A4, 1A6, 1A7, 1A8, 1A9, 1A10, 2B4, 2B7, 2B15, and 2B17) expressed in baculovirusinfected insect cells was purchased from BD Gentest" (Woburn, MA). HLM (n=50 donors) were purchased from Invitrogen (Carlsbad, CA).

3.2.2.2 Inhibition of UGT Glucuronidation Assay

The nonselective substrate of UGTs, 4-MU, was used as a probe substrate for all UGT isoforms except for UGT1A4. "A typical incubation mixture with a total volume of 100 μl contained recombinant UGT isoform (final concentration: 0.1, 0.15, 0.05, 0.01, 0.01, 0.01, 0.01, 0.5, 0.05, 0.15 and 0.1 mg/ml for recombinant UGT1A1, 1A3, 1A6, 1A9, 2B4, 2B7 and 2B15, respectively)", 10 mM UDPGA, 5 mM $MgCl_2$, 100 mM Tris-HCl buffer (pH 7.4), and 4-MU in the absence or presence of 100 μM TKI. "Incubations with 4-MU were performed at the final concentration corresponding to the apparent K_m or S_{50} value reported for each isoform (110, 1200, 110, 15, 750, 30, 80, 1200, 350, 250, and 2000 μM 4-MU for UGT1A1, 1A3, 1A6, 1A7, 1A8, 1A9, 1A10, 2B4, 2B7, 2B15, and 2B17, respectively)" (Liu et al., 2010a). For UGT1A4, TFP was selected as the substrate. At a final concentration of 10 μM, TFP was incubated with four TKIs individually and 0.025 mg/ml UGT1A4. The following known UGT inhibitors were used

as positive controls (at 100 μM): diclofenac for UGT1A1, 1A6, 1A7, and 1A9; hecogenin for UGT1A4, androsterone for UGT1A3, 2B7, and 2B15; and phenylbutazone for UGT1A8 and 1A10, respectively (Uchaipichat et al., 2004; Uchaipichat et al., 2006; Liu et al., 2010a). As there are no inhibitors of UGT2B4 and 2B17 that are previously reported, positive controls for these enzymes were not included. All the inhibitors and 4-MU or TFP were dissolved in DMSO. The final concentration of DMSO in the incubation system was 1% (v/v). The UGT reaction mixtures were pre-incubated at 37 °C for 5 min, and reactions were initiated by adding UDPGA. Incubation time differed among the UGT isoforms based on the linear formation of product as follows: it was 120 min for UGT1A1, 1A10, 2B4, 2B7, 2B15, and 2B17, 75 min for UGT1A3, 45 min for UGT1A4 and 30 min for UGT1A6, 1A7, 1A8, and 1A9. All the reactions were quenched by adding 100 μl of chilled acetonitrile containing 1 μM phenytoin as an internal standard. The sample mixtures were centrifuged at 16,000 g for 16 min to obtain the supernatant. Samples were then analyzed in LC/MS/MS. The relative rate of 4-MUG or trifluoperazine glucoronide (TFPG) formation for each isoform was linear with respect to protein concentration and incubation time.

3.2.2.3 Inhibition of SN-38 glucuronidation assay

SN-38 glucuronidation activity was determined with a slight modification of a previously published method (Liu et al., 2010d). SN-38 was incubated in the absence or presence of different concentrations of lapatinib (0-200 μM). Reactions were performed in 0.1 mg/ml UGT1A1 or 0.4 mg/ml pooled HLM. “After preincubation of the reaction mixture for 5 min, the reaction was started by adding UDPGA for a final concentration of 5 mM. Incubation was performed at 37°C for 30 min”.

3.2.2.4 Determination of IC_{50}

The same incubation condition as for the preliminary inhibition study was used for each UGT isoform, except that the concentration of each inhibitor was ranged from 0 μM to 200 μM. SN-38 was also included for the inhibition of UGT1A1 by lapatinib. At a concentration of 4 μM and 2.5 μM, SN-38 was preincubated with lapatinib (0 μM to 200 μM) in 0.1 mg/ml UGT1A1 or 0.2 mg/ml HLM for 5 min before addition of UDPGA to initiate the reaction (Liu et al., 2010d).The relative formation rate of 4-MUG, TFPG or SN-38G as compared to the absence of inhibitor was estimated, and the half maximal inhibitory concentration (IC_{50}) value for each TKI was estimated by using GraphPad Prism 5 software (La Jolla, CA).

3.2.2.5 Determination of K_i

4-MU at four concentrations (ranging from $0.5\times K_m$ to $4\times K_m$) was incubated with recombinant UGT1A1, 1A3, 1A7, 1A8, 1A9, 1A10, 2B7, 2B15 or 2B17 at a final protein concentration as described in the UGT glucuronidation inhibition assay in the absence or presence of TKI at four different concentrations (ranging from $IC_{50}/4$ to $4\times IC_{50}$) to determine the inhibition constant (K_i) values. The inhibition kinetics of lapatinib against SN-38 glucuronidation by UGT1A1 and HLM was also investigated. SN-38 (2 μM, 4 μM, 10 μM or 20 μM) was incubated with 0.1 mg/ml for UGT1A1 or 0.4 mg/ml for HLM (final concentrations) in the presence of lapatinib (0 μM, 0.1 μM, 0.5 μM, 1 μM or 2 μM). The incubation time for each UGT isoform was the same as that used to determine IC_{50}. K_i values were calculated with nonlinear regression according to the equations for competitive inhibition (eq. 1), noncompetitive inhibition (eq. 3), or mixed inhibition (eq. 4) (Copeland, 2000), where *v* is the reaction rate, and S “and I are the concentrations of substrate and inhibitor, respectively. K_i is the inhibition constant of the inhibitor for the enzyme, and K_m is the substrate concentration at half of the maximum velocity (V_{max}) of the reaction. The type of inhibition was determined from the fitting of data to the enzyme inhibition models. Goodness of

fit to kinetic and inhibition models was assessed from the F statistic, r^2 values, parameter standard error estimates and 95% confidence intervals by using GraphPad Prism 5 software". Kinetic constants are reported as the mean value ± standard error of the parameter estimate.

3.2.2.6 Calculation of TKI Concentrations

The average systemic plasma concentration ($[I]_{av}$), the maximum systemic plasma concentration ($[I]_{max}$), the maximum unbound systemic plasma concentration ($[I]_{max,u}$), the maximum hepatic input concentration ($[I]_{in}$) and the maximum unbound hepatic input concentration ($[I]_{in,u}$) of TKIs after repeated oral administration were estimated based on the following equations (eq. 12 ~ 16) (Ito et al., 2004).

$$[I]_{av} = (D/\tau)/(CL/F) \quad (12)$$

$$[I]_{max} = ([I]_{av}\, k\, \tau)/(1 - exp^{-k\,\tau}) \quad (13)$$

$$[I]_{max,u} = ([I]_{av}\, k\, \tau\, f_u)/(1 - exp^{-k\,\tau}) \quad (14)$$

$$[I]_{in} = [I]_{av} + k_a\, F_a \frac{D}{Q_h} \quad (15)$$

$$[I]_{in,u} = f_u\, ([I]_{av} + k_a\, F_a \frac{D}{Q_h}) \quad (16)$$

"where D and τ represent dose and dosing interval of inhibitors used in the *in vivo* interaction study, respectively; *k* is the elimination rate constant; k_a is the absorption rate constant; F_a is the fraction absorbed from the gut into the portal vein; Q_h is the hepatic blood flow rate; and f_u is the unbound fraction. The values of k_a, F_a and f_u for TKIs were obtained from the literature" (Brunton et al., 2005; Peng et al., 2005; Rugo et al., 2005; USFDA, 2007; Smith et al., 2009; EMA, 2011;

Martin et al., 2012; Garrett et al., 2013). Q_h value of 1610 ml/min (Ito et al., 2004) was used for estimation.

3.2.2.7 Determination of $f_{u,m}$

Single-Use Rapid Equilibrium Dialysis plate from Thermo Scientific-Pierce Biotechnology (Rockford, IL) with cutoff molecular weight 8000 Da was used. HLM (0.4 mg/ml) solutions (100 µL) containing Lapatinib (0.1 µM, 0.5 µM, 1 µM, 5 µM) were placed into the sample chamber and 300 µL PBS dialysis buffer was added into the adjacent chamber in triplicate. The content of organic solvent in the final microsomal solutions was kept below 1%. The plates were then covered with sealing tape (MicroAmpTM, Applied Biosystems, Foster City, CA) and incubated at 37 °C for 4 hours on an orbital shaker at 100 rpm. Aliquots (50 µL) were removed from each side of the insert and placed in separate tubes. The same volume (50 µL) of blank microsomes was added to the buffer samples and an equal volume of PBS was added to the collected microsomes samples for matrix matching. To each sample, 100 µL of acetonitrile containing phenytoin (1 µM; internal standard) was added. These samples were vortexed for 30 sec and chilled on ice for 30 min, then centrifuged at 16,100 *g* for 15 min at 4 °C. Lapatinib concentrations in the supernatant were determined by LC/MS/MS.

3.2.2.8 Prediction of AUC Change for UGT Substrates

The magnitude of the inhibition of TKIs was estimated as the ratio of the area under the curve (AUC_i/AUC) of UGT substrates in the presence and absence of the inhibitor. The ratio was calculated based on the eq. 17 for drugs orally administered (Ito et al., 2004):

where AUC_i and AUC are the AUC in the presence and absence of inhibitor, respectively; K_i is inhibition constant from the *in vitro* inhibition experiment; f_m is the fraction of the UGT substrate "metabolized by the inhibited enzyme; and [I] is the TKI concentration at the enzyme active site."

"In view of the general assumption that only unbound drug is available for interaction with the enzyme active site, and the consideration that the aim of DDI research is to exclude the highest risk, we used in this study the maximum unbound hepatic input concentration ($[I]_{in,u}$) as the inhibitor concentration at the active site of the UGT isoforms mainly distributed in liver", and the maximum unbound systemic plasma concentration ($[I]_{max,u}$) was used for the isoforms mainly in gastrointestinal track, such as UGT1A7. The prediction of AUC ratio is for any potential UGT substrates with undetermined f_m, a range of f_m between 0.1 and 1 was included for calculating AUC_i/AUC ratio.

3.2.2.9 LC/MS/MS Quantification Method

4-MUG concentrations were determined by using an Agilent 1200 HPLC interfaced with Applied Biosystems Qtrap 3200 "equipped with an electrospray ion source. Chromatographic separation was carried out with a Waters XTerra MS C18 column" (2.1×50 mm, 3.5 µm; Waters Corporation, Milford, MA). Mobile phase was delivered 250 µl/min, and the gradient was initiated at 85% A-15%B (A, 0.1% formic acid in water; B, acetonitrile). The proportion of mobile phase B was increased to 90% over 1 min, held constant for 1.5 min, and then restored to the initial composition until 10 min. 4-MUG was detected by using SRM transition (353/177), and phenytoin was used as the internal standard (253/182) in positive ion mode (Yuan et al., 2009; Donato et al., 2010) . The dwell time for each transition was 5 ms.

Signals for TFPG were detected by using Applied Biosystems Qtrap 4000 with an electrospray ion source interfaced with a Shimazu Prominence Modular HPLC. The mobile phase consisted of 0.1% formic acid in water (A) and acetonitrile (B). The column was first equilibrated at 25% mobile phase B for 1.5 min at a 200 µl/min flow rate. The elution was then ramped linearly to 90% mobile phase B over 1.5 min, maintained for 5 min, and followed by a return to initial conditions. TFPG was detected using SRM pair of 584/408 in positive ionization mode (Gagez et al., 2012). Phenytoin was used as the internal standard (Yuan et al., 2009). The dwell time for each transition was 5 ms.

The quantification of SN-38G was performed in AB SCIEX 5500 QTRAP (AB SCIEX, Foster City, CA) equipped with a turbo ionspray ionization source coupled to an automated Agilent 1200 series liquid chromatograph and autosampler (Agilent Technologies, Wilmington, DE). The SRM transition setting for SN-38G was 569.2/393.2 in the positive mode (Corona et al., 2010). The same internal standard phenytoin was used for quantification (Yuan et al., 2009). The mobile phase consisted of 0.1% formic acid in water (A) and acetonitrile (B). The column was first equilibrated at 10% mobile phase B for 1 min at a 250 µl/min flow rate. The elution was then ramped linearly to 90% mobile phase B over 2 min, maintained for 2 min, and followed by a return to initial conditions. The dwell time for each transition was 5 ms.

3.2.3 Results

3.2.3.1 Inhibition of UGT Glucuronidation Assay

As a preliminary study, the UGT inhibitory potentials of TKIs were examined. To this end, axitinib, imatinib, lapatinib or vandetanib (at 100 μM) was incubated with a UGT substrate (4-MU for all UGTs except for UGT1A4 for which TFP was used) and a panel of recombinant UGT enzymes (UGT1A1, 1A3, 1A6, 1A7, 1A8, 1A9, 1A10, 2B4, 2B7, 2B15, and 2B17), and the changes in the extent of glucuronide metabolite production were examined. The results showed that at 100 μM concentration, axitinib reduced the glucuronidation of UGT1A3, 1A4 and 1A7 by greater than 50% while having insignificant effects on the remaining UGTs (Figure 3.6). On the other hand, imatinib exhibited greater than 50% inhibition of UGT1A1, 1A7, 1A8, 1A10, 2B7, 2B15 and 2B17 activities. The inhibition of UGT1A1 and 1A7 activity by lapatinib and that of UGT1A7 and 1A9 activity by vandetanib were also found to be greater than 50%.

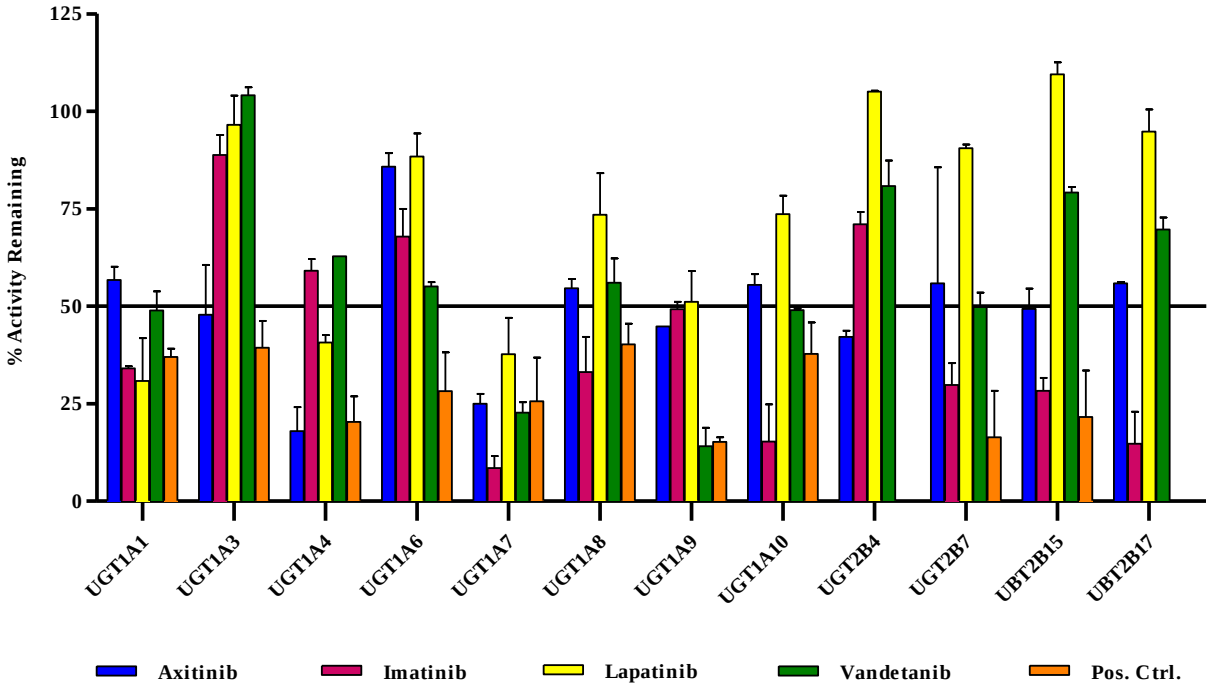

Figure 3.6 The inhibition of axitinib, imatinib, lapatinib, and vandetanib on recombinant UGT activities. The data shown represent the mean ± S.D. from two replicates. (The

following “known UGT inhibitors were used as positive controls (at 100 μM): diclofenac for UGT1A1, 1A6, 1A7, and 1A9; hecogenin for UGT1A4, androsterone for UGT1A3, 2B7, and 2B15; and phenylbutazone for UGT1A8 and 1A10, respectively” (Uchaipichat et al., 2004; Uchaipichat et al., 2006; Liu et al., 2010a). As there are no inhibitors of UGT2B4 and 2B17 that are previously reported, positive controls for these enzymes were not included.)

For these UGTs that are inhibited by TKIs (100 μM) by greater than 50%, IC_{50} values of TKIs were further estimated. To this end, recombinant UGTs were incubated with one of the TKIs at different concentrations, and the extent of 4-MU or TFP (for UGT1A4) glucuronidation was examined. The results showed that axitinib inhibited UGT1A7 and 1A9 with an IC_{50} of 3.3 μM and 3.6 μM, respectively (Figure 3.7 A). Imatinib inhibited UGT2B17 activity with an IC_{50} as low as 0.81 μM (Figure 3.7 B). Lapatinib has a different inhibition profile with an IC_{50} of 0.50 μM against UGT1A1 and 2.7 μM against UGT1A7 toward 4-MU glucuronidation (Figure 3.7 C), while vandetanib inhibiting 4-MU glucuronidation by UGT1A9 is as high as 5.0 μM (Figure 3.7 D). The IC50 values of four TKIs are summarized in Table V.

	Axitinib (μM)	**Imatinib (μM)**	**Lapatinib (μM)**	**Vandetanib (μM)**
UGT1A1	N.D.	11.0	0.46	14.5
UGT1A3	N.D.	N.D.	N.D.	N.D.
UGT1A4	14.2	N.D.	N.D.	N.D.
UGT1A7	3.3	19.5	2.7	38.9
UGT1A8	N.D.	22.9	N.D.	N.D.
UGT1A9	3.6	N.D.	N.D.	5.0
UGT1A10	N.D.	47.3	N.D.	N.D.
UGT2B7	N.D.	68.4	N.D.	N.D.
UGT2B15	N.D.	91.0	N.D.	N.D.
UGT2B17	N.D.	0.81	N.D.	N.D.

Table V. THE IC_{50} OF TKIS IN THE INHIBITION OF UGT ACTIVITIES. The data shown represent the mean ± S.D. from two replicates. N.D., not determined.

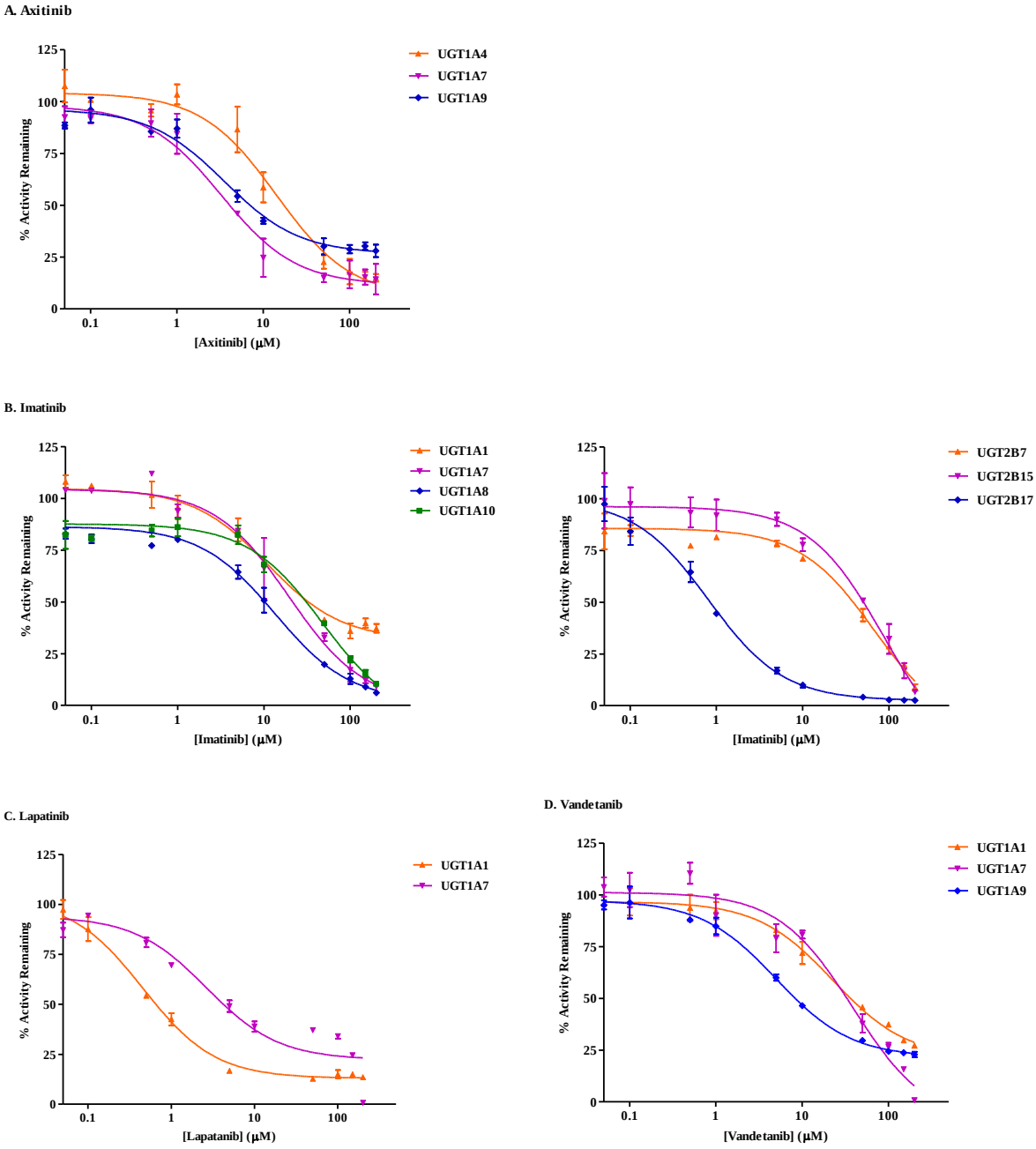

Figure 3.7 The IC_{50} of axitinib (A), imatinib (B), lapatinib (C) and vandetanib (D) against the glucuronidation of recombinant UGT isoforms. The data shown represent the mean ± S.D. from two replicates.

3.2.3.2 Inhibition Kinetics of TKIs against Recombinant UGT Isoforms

In order to characterize these inhibitors, kinetics studies were performed with the corresponding UGT isoforms. The C_{max} values of TKIs tested in this study are at the micromolar level (Brunton et al., 2005) except that of axitinib (USFDA, 2012c). For TKIs that exhibit IC_{50} values lower than 10 μM (i.e., imatinib against UGT1A1 and 2B17; lapatinib against UGT1A1, 1A7, and 1A9; and vandetinib against UGT1A9), their UGT inhibitory kinetics profiles were further characterized using 4-MU. Because axitinib's IC_{50} values were much higher than its C_{max} (i.e., 0.16 μM) (USFDA, 2012c), axitinib was not included in this study.

The representative Lineweaver-Burk plots for the inhibition of 4-MUG formation by imatinib and analysis of the parameters of the enzyme inhibition model suggested that the inhibition type of imatinib against UGT1A1 and UGT2B17 was both competitive (Figure 3.8A and 3.8C). K_i values of imatinib were estimated to be 19.1 μM and 0.39 μM against the UGT1A1 and UGT2B17, respectively (Figure 3.8B and 3.8D). Lapatinib exhibits a potent competitive inhibition against UGT1A1 with a K_i of 0.5 μM (Figure 3.9A and 3.9B), a non-competitive inhibition with a K_i of 4.5 μM against UGT1A7 (Figure 3.9C and 3.9D) and a mixed inhibition with a K_i of 3.0 μM against UGT1A9 (Figure 3.9E and 3.9F). Vandetanib showed a mixed inhibition against UGT1A9 with a K_i of 9.0 μM (Figure 3.10A and 3.10B).

3.2.3.3 Inhibition of Lapatinib on SN-38 Glucuronidation

Lapatinib inhibition of UGT1A1 activity was one of the most potent among all UGT inhibition by TKIs (second lowest K_i next to imatinib inhibition of UGT2B17). To estimate clinical relevance of the finding, UGT1A1 inhibition was examined using a clinically used UGT substrate, SN-38 (there are no clinically used UGT2B17 substrates currently available). To this end, IC50 values

were estimated for lapatinib inhibition of SN-38 glucuronidation in human microsomes and UGT1A1 proteins, and their kinetic parameters were estimated. Lapatinib showed strong inhibition against SN-38 glucuronidation, the IC50 of which is 0.33 µM in UGT1A1 and 0.42 µM in HLM (Figure 3.11A). Kinetic experiments were performed to further characterize the inhibition of SN-38 glucuronidation by lapatinib. The K_i were 0.56 µM and 1.6 µM for UGT1A1 and HLM (Figure 3.11B – 3.11E), respectively, which are similar to the K_i for inhibition of 4-MU glucuronidation by lapatinib. Interestingly, the kinetic profile of lapatinib inhibition of SN-38 glucuronidation was different from that of 4-MU glucuronidation in UGT1A1. In both UGT1A1 and HLM, lapatinib showed a non-competitive inhibition against SN-38 glucurnidation.

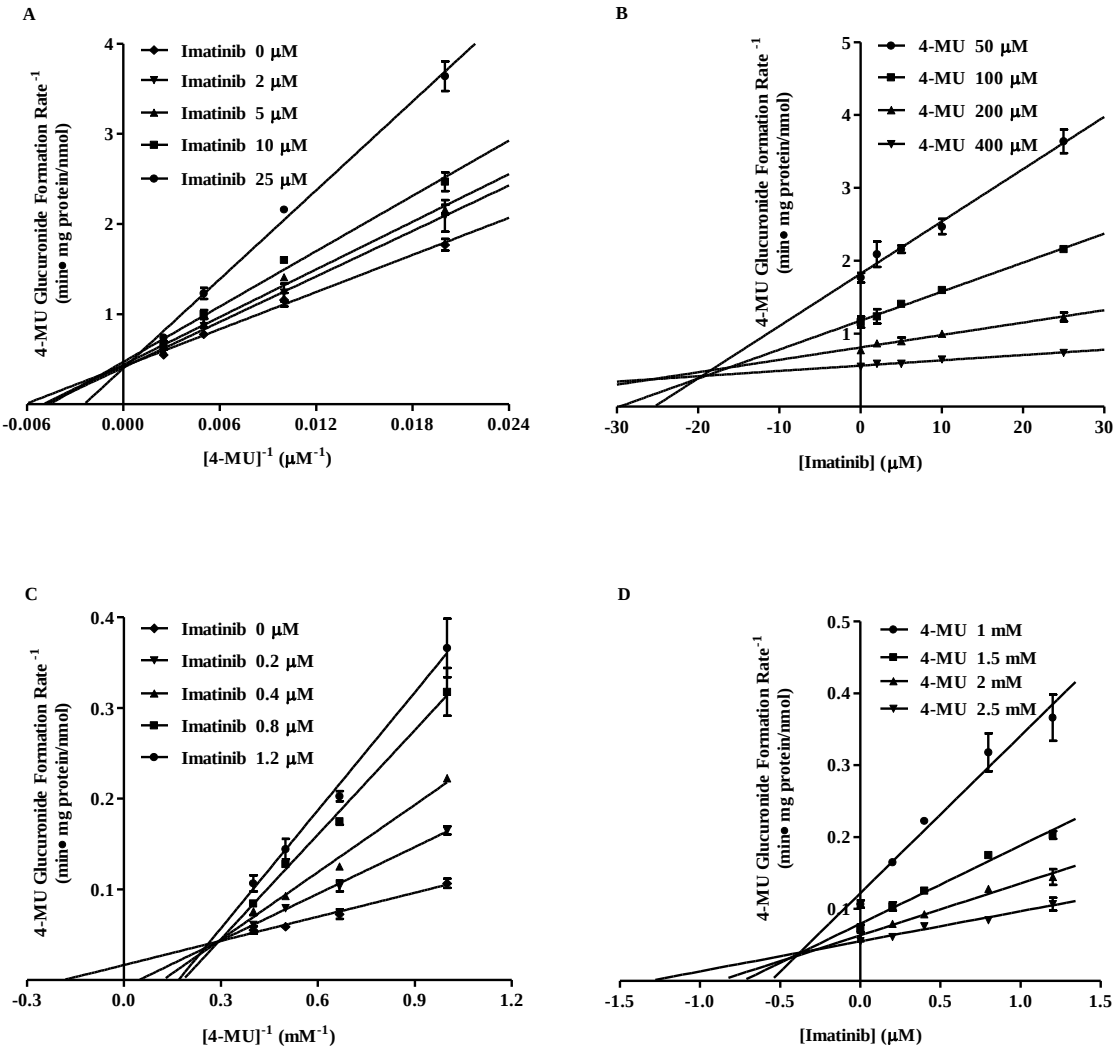

Figure 3.8 Representative Lineweaver-Burk plots and Dixon plots showing the effects of imatinib on 4-MU glucuronidation in UGT1A1 (A and B) and UGT2B17 (C and D). The data shown represent the mean ± S.D. from two replicates.

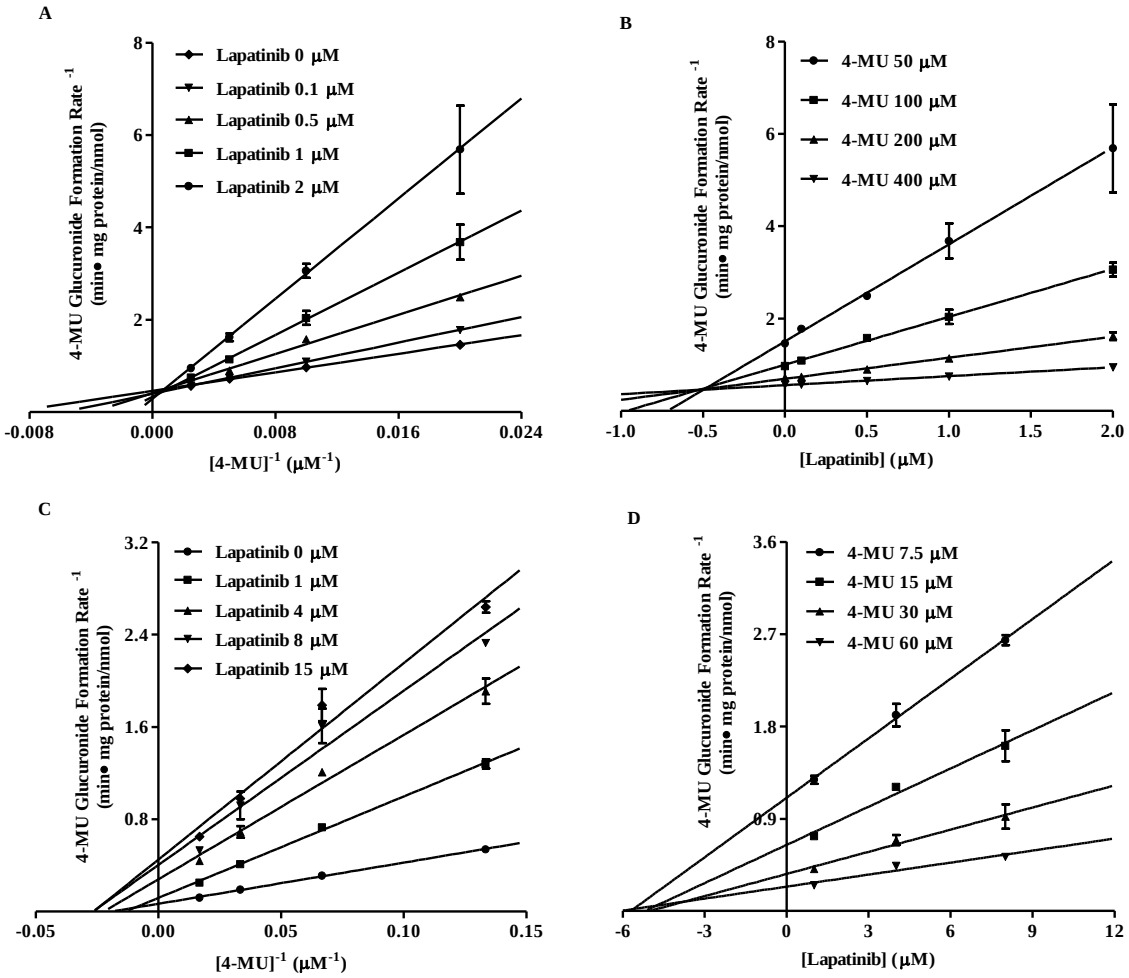

Figure 3.9 Representative Lineweaver-Burk plots and Dixon plots showing the effects of lapatinib on 4-MU glucuronidation in UGT1A1 (A and B), UGT1A7 (C and D) and UGT1A9 (E and F). The data shown represent the mean ± S.D. from two replicates.

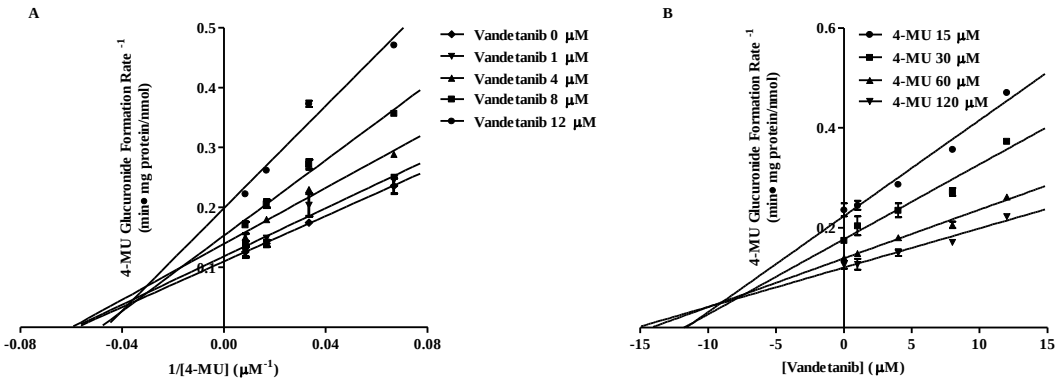

Figure 3.10 Representative Lineweaver-Burk plots and Dixon plots showing the effects of vandetinib on 4-MU glucuronidation in UGT1A9 (A and B). The data shown represent the mean ± S.D. from two replicates.

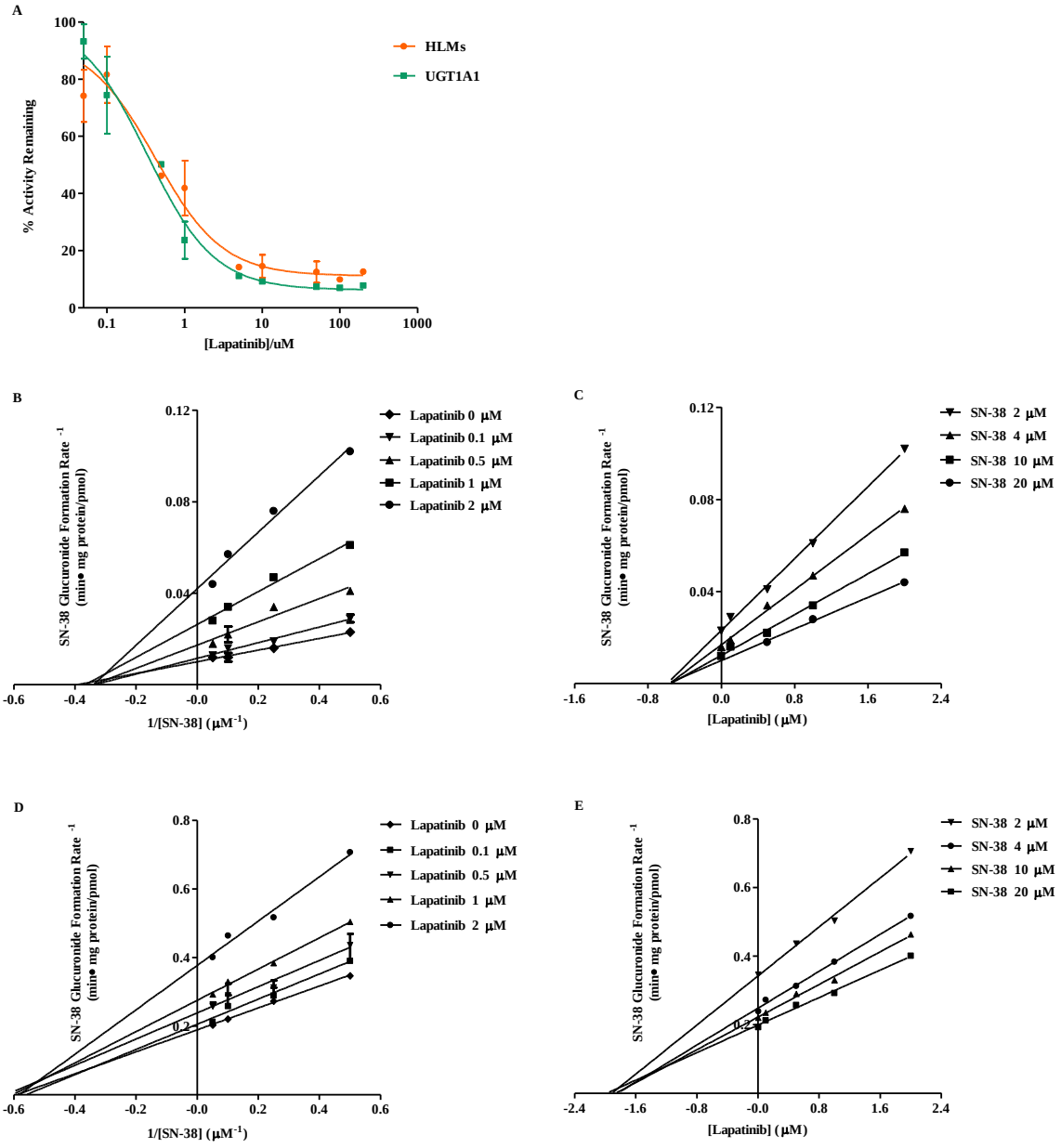

Figure 3.11 The IC_{50} of lapatinib against SN-38 glucuronidation by recombinant UGT1A1 and HLM (A). Representative Lineweaver-Burk plots and Dixon plots showing the effects of lapatinib on SN-38 glucuronidation in UGT1A1 (B and C) and HLM (D and E). The data shown represent the mean ± S.D. from two replicates.

3.2.3.4 Concentrations of TKIs with Repeated Oral Administration in Liver or GI Track

In order to estimate the AUC change of the victim drugs due to the inhibition of UGT isoforms, the hepatic or systemic concentrations of each TKI were first estimated using previously reported clinical pharmacokinetic data (Table VI). For the inhibitions of UGT1A1 by lapatinib, UGT1A9 by vandetanib and UGT2B17 by imatinib, the maximum unbound hepatic input concentrations of inhibitors were estimated. For lapatinib that inhibits UGT1A7, which is mainly expressed in intestines, systemic drug concentration was estimated.

3.2.3.5 Quantitative Prediction of DDI Potential (AUC_i/AUC) with Nonselective Substrate

The risk of DDIs due to the inhibition of TKIs on UGTs was evaluated by predicting the ratio of AUC of a victim drug (whose f_m may range from 0.1 to 1.0) in the presence and absence of the inhibitors (i.e., AUC_i/AUC). To this end, the hepatic or systemic concentrations of each TKI were first estimated using previously reported clinical pharmacokinetic data (Table VI). For the inhibitions of UGT1A1 by lapatinib, UGT1A9 by vandetanib and UGT2B17 by imatinib, the maximum unbound hepatic input concentrations of inhibitors were estimated. For lapatinib that inhibits UGT1A7, which is mainly expressed in intestines, systemic drug concentration was estimated. The AUC ratios of each inhibitor were estimated based on K_i values obtained in this study and the calculated hepatic or plasma concentrations of TKIs. The results showed that the predicted AUC changes of the UGT2B17 substrate by imatinib (at the time for C_{max}) were found significant; when f_m of the victim drug was 90%, UGT2B17 inhibition by imatinib was predicted to increase the AUC of 4-MU by 137% (Figure 8A). On the other hand, the AUC_i/AUC ratios of 4-MU were less than 1.25 for imatinib, lapatinib, and vandetanib against UGT1A1, UGT1A7 and UGT1A9, respectively (data not shown), suggesting minor clinical impacts of the TKIs on the pharmacokinetics of their substrates according to the FDA guideline (USFDA, 2012b). Also, lapatinib was predicted to cause ~21% increase in AUC of UGT1A1 substrates (4-MU) when the

f_m of 4-MU is 0.9 (Figure 3.12B), which is considered to be a potential risk with marginal significance. With concerns of clinical DDIs between drug substrate and lapatinib, SN-38 was also included for this evaluation. When HLM is at 0.4 mg/ml, the $f_{u,m}$ of lapatinib is 0.032 ± 0.0033, and the $K_{i,u}$ in HLM is calculated to be 0.051 µM. The AUC change of SN-38 due to the inhibition of lapatinib when f_m is 0.81 (Hanioka et al., 2001), is predicted to be 133% increase (Figure 3.12C).

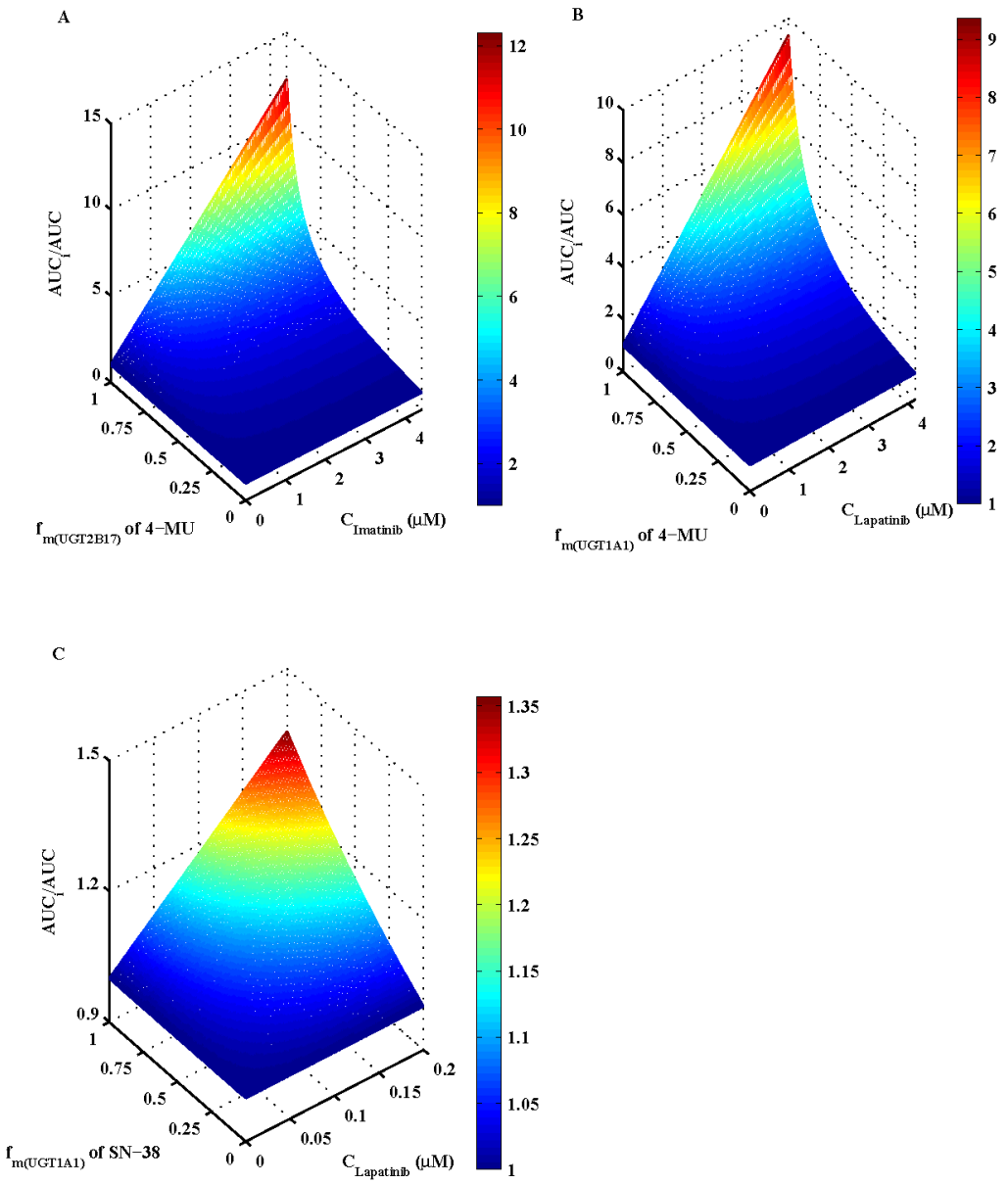

Figure 3.12 3-Dimensional plots for the calculated AUC_i/AUC ratios of 4-MU by imatinib (A) and lapatinib (B) and AUC_i/AUC ratio of SN-38 by lapatinib (C)

Drugs	Dose (mg)	Dosing Interval (hr)	Cmax (μM)	Absorption Rate Constant (k_a, h^{-1})	Fraction absorbed (F_a)	Plasma Unbound Fraction ($f_{u,p}$)	Oral CL (L/h)	$t_{1/2}$ (h)	Calculated Concentrations			Reference
									I_{av} (μM)	$I_{max,u}$ (μM)	$I_{in,u}$ (μM)	
Axitinib	5	12	0.16	0.523	0.88	0.01	45	3.2	0.024	0.00067	0.00086	(Rugo et al., 2005; USFDA, 2012c; Garrett et al., 2013)
Imatinib	400	24	4.41	1.64	1	0.05	11.2	22	2.52	0.18	0.70	(Brunton et al., 2005; Peng et al., 2005; van Erp et al., 2007)
Lapatinib	1250	24	4.2	0.7	0.73	0.01	114	24	0.79	0.011	0.12	(USFDA, 2007; Smith et al., 2009)
Vandetanib	300	24	3.32	0.3	0.935	0.06	13.2	456	1.99	0.12	0.23	(EMA, 2011; Martin et al., 2012)

Table VI. OBSERVED AND CALCULATED PHARMACOKINETIC PARAMETERS OF TKIS

3.2.4 Discussion

Previous *in vitro* studies have shown that several TKIs including erlotinib, efitinib, and sorafenib inhibit UGTs (Liu et al., 2010a; Liu et al., 2010b; Peer et al., 2012). Sorafenib and lapatinib were also shown to increase AUC of SN-38, which is a UGT1A1 substrate by 120% and 41% (Midgley et al., 2007; Mross et al., 2007). In the present study, we investigated the effects of four TKIs, including axitinib, imatinib, lapatinib, and vandetanib, on UGT activities.

Our data offer *in vitro* evidence that lapatinib is a potent inhibitor of UGT1A1 and also an intermediate inhibitor of UGT1A7. UGT1A1 is broadly expressed in human organs including liver, intestines, and kidney (Ritter et al., 1991; Strassburg et al., 1998a; Strassburg et al., 1998b) although the expression levels in the intestines and kidney are one third as high as that in liver (Harbourt et al., 2012). UGT1A1 is the only isoform involved in bilirubin glucuronidation, and UGT1A1 inhibition by antiviral agents (atazanavir and indinavir) and a TKI (erlotinib) is known to cause hyperbilirubinemia (Jakacki et al., 2008; Liu et al., 2010a), suggesting that the inhibition of UGT1A1 by lapatinib is associated with hyperbilirubinemia. Indeed, clinical studies have shown that the administration of lapatinib with capetitabine could trigger hyperbilirubinemia in 34.6% of 52 metastatic breast cancer patients with a dose of lapatinib at 1250 mg once daily and capecitabine at 2000 mg/m^2 per day (Xu et al., 2011). However, in our study it was found that lapatinib did not exhibit inhibition against bilirubin glucuronidation in UGT1A1 up to 200 µM, “although it potently inhibited 4-MU glucuronidation in UGT1A1. This finding further confirms the observation that the inhibition of UGT1A1 activity might vary with the substrate” (Udomuksorn et al., 2007). The absence of *in vitro* inhibition of bilirubin glucuronidation by lapatinib suggests there might be other causes to the observed hyperbilirubinemia. Another clinical study showed that HLA-DQA1*02:01 might be a risk factor for lapatinib-induced hepatotoxicity resulting in

hyperbilirubinemia (Spraggs et al., 2011). In addition, capecitabine was also found to cause hyperbilirubinemia in cancer patients (Abdel-Rahman et al., 2013).

About 15% of top 200 prescribed drugs in the United States in 2002 are eliminated mainly via glucuronidation by UGT1A1 (Williams et al., 2004). The inhibition of UGT1A1 can have clinically significant impacts on therapy using a narrow therapeutic index drug such as irinotecan. Irinotecan is a chemotherapeutic agent commonly used, alone or in combination, for the treatment of colorectal cancer. Irinotecan requires metabolic activation by carboxylesterase 2 to the active metabolite SN-38. SN-38 is eliminated via glucuronidation by UGT1A1, 1A3, 1A6, and 1A9. UGT1A1 shows the highest activity of SN-38 glucuronidation (Hanioka et al., 2001). However, considering that the inhibition of UGT1A1 is substrate- dependent (Udomuksorn et al., 2007), the effects of lapatinib on SN-38 glucuronidation in HLM and recombinant UGT1A1 were also investigated in this study. The inhibition potential in UGT1A1 is similar to that when 4-MU was the substrate.

Our study has revealed that imatinib is a broad inhibitor of several UGTs. Imatinib is a potent inhibitor of UGT2B17; an intermediate inhibitor of UGT1A1; and a weak inhibitor of UGT1A7, 1A8, 1A9, 1A10, 2B7, and 2B15. The human UGT2B enzymes are involved in the metabolism of steroid hormones as well as bile acids, acidic steroids, and fatty acids (Radominska-Pandya et al., 1999). Among UGT2Bs, UGT2B17 exhibits high levels of activity against androgens and xenobiotics including carcinogens, coumarins, anthraquinones, flavonoids, nonsteroidal anti-inflammatory drugs, monoterpenoids, and phenols (Turgeon et al., 2003). Individuals lacking the expression of UGT2B17 was shown to exhibit altered clearance rates of suberoylanilide hydroxamic acid (SAHA) or exemestane, both of which are UGT2B17 substrates (Balliet et al.,

2009; Sun et al., 2010). Therefore, the inhibition of UGT2B17 by imatinib could potentially have a significant clinical effect on the metabolism of UGT2B17 substrates.

Different from above two TKIs, vandetanib was found as an intermediate inhibitor of UGT1A9, which is also involved in the glucuronidation of a number of drugs (Kiang et al., 2005). UGT1A9 is expressed in both human liver and some extrahepatic tissues including the gastrointestinal tract (Kiang et al., 2005). Significant evidence exists supporting a role for gastrointestinal UGTs as modifiers of pharmacokinetics and biological responses to drugs and xenobiotics (Ritter, 2007). Our data show that vandetanib might influence the first-pass effect and bioavailability of more orally administered drugs. This issue requires additional attentions, especially when modern medicinal chemistry tends to synthesize polar chemicals to avoid the metabolism by CYPs, which makes Phase II enzymes become the main metabolizing enzymes such as UGTs.

The “quantitative prediction of DDI risk indicated that the coadministration of lapatinib or imatinib at clinical doses could result in a significant increase of AUC of drugs primarily cleared by UGT1A1 or UGT2B17, suggesting that lapatinib and imatinib can induce clinically significant DDI with co-administered UGT1A1 or 2B17 substrates”. Our prediction with SN-38 and lapatinib is consistent with the clinical observation that co-administration of lapatinib increased the AUC of SN-38 by an average of 41% (Midgley et al., 2007). In addition, the pharmacokinetic parameters used to calculate concentrations are mean values of the parameters reported, but inter-individual variability is high. Furthermore, *in vitro* data tend to underestimate inhibition of` drug glucuronidation *in vivo* (Uchaipichat et al., 2006). Therefore, the actual effects of lapatinib and imatinib might be different than those calculated here.

In summary, the present findings highlight the need to pay more attention to UGT-mediated DDIs by TKIs, and also shed light on the mechanisms underlying clinically adverse effects associated with TKIs. Our study provides the basis for further clinical studies investigating the DDI potential between TKIs with UGT substrates.

3.3 Mechanism-based Inhibition of Noscapine on Liver Metabolism of Warfarin

3.3.1 Introduction

Noscapine (Figure 3.13), a non-addictive phthalideisoquinoline alkaloid obtained from opium poppy latex, has been broadly recognized as a safe and promising oral antitussive agent (Karlsson et al., 1990). Recently, noscapine has shown antiproliferative activity against a wide variety of tumor cell types (Mahmoudian and Rahimi-Moghaddam, 2009). Pretreatment with oral noscapine was also proven to limit lymphatic metastasis of PC3 human prostate cancer in nude mouse models (Barken et al., 2010).

Noscapine is currently undergoing phase I/II trials for non-Hodgkin's lymphoma or hematological malignancies treatment (Aneja et al., 2007), and combination chemotherapy regimens with noscapine are being investigated for human non-small lung cancer and triple negative breast cancer (Chougule et al., 2011a; Chougule et al., 2011b). As an anticancer agent, noscapine is used at 6- to 15-fold higher doses than as a cough suppressant [MedInsight Research Institute, http://www.pcref.org/MedInsight%20-%20PCREF%20Noscapine%20Review.pdf]. In humans, the pharmacokinetic behavior of noscapine shows a relatively high interindividual variation, as well as extensive "first pass" metabolism due to C-C cleavage, O-demethylation, monohydroxylation and demethylenation reactions (Tsunoda and Yoshimura, 1981). Several cytochrome P450 (CYP) enzymes (CYP1A2, CYP2C9, CYP2C19, and CYP3A4/5) and flavin-containing mono-oxygenase 1 are responsible for these reactions (Fang et al., 2012).

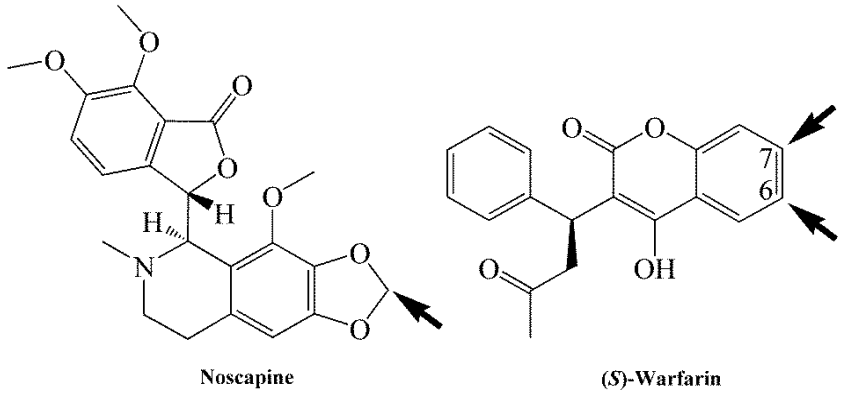

Figure 3.13 Chemical structures of noscapine and (*S*)-warfarin. Arrows denote the proposed oxidation sites by CYP2C9.

Venous thromboembolism (VTE) is a common complication of cancer and its therapy (Streiff, 2009). The prevalence of VTE in cancer patients is 2- to 6-fold higher than in the general population (Rahme et al., 2013). The anticoagulant warfarin is frequently prescribed for the initial phase treatment of VTE, and used for long-term treatment to prevent recurrent thrombosis (Lee, 2009). Of note, warfarin is a narrow therapeutic index drug that can cause life-threatening bleeding; thus, better understanding of factors that can influence the pharmacokinetics of warfarin is essential to achieve optimal warfarin therapy. Clinical evidence indicates that noscapine causes significant drug-drug interactions (DDI) with warfarin when administrated as an antitussive agent (Ohlsson et al., 2008; Scordo et al., 2008; Myhr, 2009). Considering the higher doses of noscapine used for cancer treatment (Madan et al., 2011), clinically significant interactions between noscapine and warfarin are therefore expected. However, the magnitude and underlying mechanisms of noscapine-warfarin interaction remain unknown.

Warfarin is administrated as a racemic mixture and undergoes stereoselective metabolic clearance in the human liver. (*S*)-warfarin (Figure 3.13) has a 5-fold higher anticoagulant activity than the (*R*)-isomer (Hirsh et al., 2001), and is primarily metabolized by CYP2C9 to form 7- and 6-hydroxy warfarin as the major metabolites (Rettie et al., 1992). CYP2C9 is subject to several well studied genetic polymorphisms that affect enzyme activity and therefore affect the clearance of (*S*)-Warfarin (Redman, 2001). Although the relatively complex metabolic profile of both warfarin enantiomers might suggest that a range of CYP450 polymorphisms could affect metabolism and be therefore relevant to dose requirement, only CYP2C9 genotype appears relevant to dose requirement based on a large number of published studies to date (Daly, 2013). The most common variant alleles are CYP2C9*2 and *3, which are mainly among Caucasians with the frequency as high as 19% and 16.2%, respectively (Miners and Birkett, 1998; Yamazaki et al., 1998; Xie et al., 2002). Both alleles are associated with amino acid substitutions which appear to affect catalytic activity with (*S*)-warfarin. Besides the above two alleles, it was found that CYP2C9*5, *6, *8, *11 and *13 are also associated to warfarin response. Compared to the wildtype CYP2C9*1, CYP2C9*2, *3, *5, *6, *8, *11 and *13 showed decreased activities in metabolizing (*S*)-warfarin, which leads to a decrease in dose of (*S*)-warfarin accordingly (Daly, 2013).

A previous study demonstrated that noscapine inhibited CYP2C9 turnover in a noncompetitive and time-dependent manner in HLM when diclofenac was used as the probe substrate (Fang et al., 2010). Of note, CYP2C9 inhibitors have shown substrate-dependent differences in inhibitory potencies, with warfarin generally being more susceptible to CYP2C9 inhibition. For example, the reversible inhibition by CYP2C9 inhibitors including benzbromarone, sulfamethizole, and progesterone was greater with (*S*)- warfarin than phenytoin, tolbutamide and diclofenac was as probe substrates (Kumar et al., 2006). Also, (*S*)-warfarin was a more sensitive probe substrate

of CYP2C9 to mechanism-based inactivation (MBI), in comparison with (*S*)-flurbiprofen and diclofenac (Hutzler et al., 2009). In addition to exhibiting substratedependent inhibition kinetics, CYP2C9 also shows genotype-dependent inhibition patterns. For example, CYP2C9.3 (I359L), the enzyme product of a predominant CYP2C9 variant in Caucasians, was found to be less susceptible than the wild-type CYP2C9.1 to a reversible inhibitor fluconazole as compared to the wild-type CYP2C9.1 (Kumar et al., 2006), when fluriprofen was used as a probe substrate. Whether CYP2C9 variants exhibit different inhibition kinetics for warfarin metabolism remains unknown. Together, the inhibition kinetics of noscapine remains to be characterized specifically for warfarin considering its narrow therapeutic index.

In the present study, we examined the inhibitory mechanisms of noscapine against (*S*)-warfarin 7- hydroxylation at noscapine concentrations required for cancer treatment, and characterized the *in vitro* inhibition kinetics using pooled HLM and complementary DNA (cDNA)-expressed CYP2C9. Furthermore, we examined the effects of CYP2C9 genotype on the inhibitory potency of noscapine to guide warfarin dosage adjustment. The extent of the *in vivo* noscapine-warfarin interaction was then predicted from the obtained kinetic data.

3.3.2 Materials and Methods

3.3.2.1 Materials

(S, R)-Noscapine, (*S*)-warfarin, 7-hydroxywarfarin, mebendazole, phenytoin, phosphate-buffered saline (PBS), isocitric acid, magnesium chloride, isocitric acid dehydrogenase, 1-aminobenzotriazole (ABT), sulfaphenazole, nicotinamide adenine dinucleotide phosphate ($NADP^+$), and NADPH were purchased from Sigma-Aldrich (St. Louis, MO). Pooled HLM (n=50 donors) were from Invitrogen (Carlsbad, CA). cDNA-expressed CYP2C9.1 (wild-type), .2 (R144C), and .3 (I359L) co-expressing human NADPH-CYP reductase and human cytochrome b5 were obtained from BD Biosciences (Woburn, MA). Formic acid (ACS grade), acetonitrile and methanol (Optima grade) were purchased from Fisher Scientific (Pittsburgh, PA). All other reagents were of high performance liquid chromatography (HPLC) grade or the highest grade commercially available.

3.3.2.2 Determination of K_m

Pooled HLM (0.1 mg/ml) were incubated with (*S*)-warfarin (0 - 20 μM) in NADPH-regenerating system (5 mM isocitric acid, 0.2 unit/ml isocitric acid dehydrogenase, and 5 mM magnesium chloride in 100 mM Tris-HCl buffer, pH 7.4; 100 μl total volume). After preincubation at 37 ^oC for 5 min, the reactions were started by addition of $NADP^+$ (1 mM) and further incubated for another 20 min. The reactions were then terminated by adding 100 μL ice-cold acetonitrile containing mebendazole (1 μM) as internal standard and kept on ice for 30 min, followed by centrifugation at 16,100g for 15 min at 4 ^oC to obtain the supernatant. The concentrations of 7-hydroxywarfarin in the supernatants were measured using LC/MS/MS. 7- Hydroxywarfarin formation rates were determined, and the K_m values were estimated by using GraphPad Prism 5 software (La Jolla, CA). The incubations were performed in duplicate, and the experiments were repeated at least

two times. The final concentrations of organic solvent in the incubation media were kept below 1% (v/v) for all microsomal reactions.

3.3.2.3 Determination of IC_{50}

Pooled HLM (0.1 mg/ml) or recombinant enzymes (40 pmol/ml) were incubated with (*S*)-warfarin (2.5 μM) in the presence of noscapine (0-100 μM) in NADPH-regenerating system for 20 min. The warfarin concentration was selected based on the apparent K_m values in pooled HLM or cDNA-expressed CYP2C9 (2 - 9 μM) (Liu et al., 2012) and the clinically relevant concentration range (C_{max}, ~5 μM) (Maddison et al., 2013). 7-Hydroxywarfarin formation rates were determined, and the half maximal inhibitory concentration (IC_{50}) values were estimated.

3.3.2.4 Determination of K_i

(*S*)-warfarin (1.0, 2.5, 5.0, and 10 μM) was incubated with pooled HLM or recombinant CYP2C9.1 in the presence of noscapine at different concentrations (0 - 25 μM), and the concentration of 7-hydroxywarfarin was measured. The K_i values of noscapine were calculated via nonlinear regression of the data to the equations for competitive inhibition (eq. 1), noncompetitive inhibition (eq. 3), or mixed inhibition (eq. 4), using GraphPad Prism 5 software:

$$v = \frac{V_{max}S}{K_m\left(1 + \frac{I}{K_i}\right) + S} \qquad (1)$$

$$v = \frac{V_{max}S}{(K_m + S)\left(1 + \frac{I}{K_i}\right)} \qquad (3)$$

$$v = \frac{V_{max}S}{K_m\left(1 + \frac{I}{K_i}\right) + S\left(1 + \frac{I}{K_i'}\right)} \qquad (4)$$

where *v* represents the velocity of the reaction; S and I are the concentrations of substrate and inhibitor, respectively; and K_m is the substrate concentration that yields a half-maximal velocity (V_{max}). The inhibition type was determined from the Lineweaver-Burk plot, the Dixon plot, and fits to the enzyme inhibition kinetic models. Comparisons of goodness of the fits were determined by examination of the residues, R^2 values, the parameter standard error estimates, and 95% confidence intervals. Kinetic constants were reported as the mean ± S.E. of the parameter estimate. K_i values were further adjusted for nonspecific binding to 0.1 mg/ml microsomes to get unbound K_i ($K_{i,u}$) for calculation.

3.3.2.5 Time- and NADPH-Dependent Inhibition.

Noscapine (15 μM) was pre-incubated with CYP2C9.1, CYP2C9.2, or CYP2C9.3 (400 pmol/ml) for 30 min at 37 ^{o}C with regeneration system in the presence or absence of $NADP^+$. The concentration of noscapine was selected to be 10-fold higher than the concentration exhibiting 25% of maximum reversible inhibition according to a previous study (Obach et al., 2007). An aliquot of the inactivation mixture (10 μl) was then added to an incubation mixture containing (*S*)-warfarin (2.5 μM), $NADP^+$ and regeneration system for the measurement of residual CYP2C9 activity.

3.3.2.6 Determination of K_I and k_{inact}.

Noscapine (0 - 50 μM) was pre-incubated with pooled HLM (1mg/ml) or recombinant CYP2C9 enzymes (400 pmol/ml) in NADPH-regenerating system. At different time points (0-30 min), an aliquot (10 μl) was transferred into a secondary incubation system containing (*S*)-warfarin (25 μM), and 7-hydroxywarfarin concentrations were measured by LC/MS/MS. The concentration of warfarin in the secondary incubation system was determined to be >4 times higher than the

apparent Km values obtained from different enzyme sources (Hutzler et al., 2009; Liu et al., 2012). The observed rates of inactivation (k_{obs}) were determined from the slopes of residual CYP2C9 activity vs. time plot. Inactivation kinetic parameters (k_{inact} and K_I) were calculated using nonlinear regression of the data according to eq. 18.

$$k_{obs} = k_{obs[I]=0} + \frac{k_{inact}\,[I]}{K_I + I} \qquad (18)$$

where *[I]* represents the initial concentrations of noscapine in the inactivation preincubations; $k_{obs[I]=0}$ is the apparent inactivation rate constant measure in the absence of noscapine; kinact is the theoretical maximal inactivation rate; K_I is the inactivator concentration required for half the maximal inactivation rate; and unbound K_I ($K_{I,u}$) is K_I multiplied by $f_{u,m}$, where $f_{u,m}$ is the free fraction of noscapine in the primary microsomal incubation (1 mg/ml).

3.3.2.7 Effects of Ultrafiltration on CYP2C9 Inactivation

HLM (1 mg/ml) were pre-incubated with ABT (1 mM), noscapine (50 μM), sulfaphenazole (10 μM), or vehicle (control) in NADPH-regenerating system for 20 min at 37oC. The preincubation mixtures (100 μl) were chilled on ice, 5-fold diluted, and then filtered through Amicon Ultra-0.5 centrifugal filter devices (Millipore, Billerica, MA; cut-off of 30 kDa) according to the manufacturer's instructions. Samples were washed with 450 μl of 100 mM Tris-HCl buffer (pH 7.4), centrifuged at 14,000 *g* for 10 min, collected by a reverse spin at 1000 *g* for 2 min, and then resuspended with buffer to the original volume. Aliquots (10 μl) were removed and diluted 10- fold to determine the residual CYP2C9 activities by incubating with warfarin (2.5 μM).

3.3.2.8 Determination of $f_{u, m}$

Single-Use Rapid Equilibrium Dialysis plate from Thermo Scientific-Pierce Biotechnology (Rockford, IL) with cutoff molecular weight 8000 Da was used. HLM (0.1 mg/ml or 1 mg/ml) solutions (100 µL) containing noscapine (0.3 - 50 µM) were placed into the sample chamber and 300 µL PBS dialysis buffer was added into the adjacent chamber in triplicate. The content of organic solvent in the final microsomal solutions was kept below 1%. The plates were then covered with sealing tape (MicroAmpTM, Applied Biosystems, Foster City, CA) and incubated at 37^{o}C for 4 hours on an orbital shaker at 100 rpm. Aliquots (50 µL) were removed from each side of the insert and placed in separate tubes. The same volume (50 µL) of blank microsomes was added to the buffer samples and an equal volume of PBS was added to the collected microsomes samples for matrix matching. To each sample, 200 µL of acetonitrile containing phenytoin (1 µM; internal standard) was added. These samples were vortexed for 30 sec and chilled on ice for 30 min, then centrifuged at 16,100*g* for 15 min at 4 ^{o}C. Noscapine concentrations in the supernatant were determined by LC/MS/MS.

3.3.2.9 Measurement of 7-Hydroxywarfarin and Noscapine

7-Hydroxywarfarin concentrations in microsomal samples were determined by a LC/MS/MS method as previously described with slight modifications (Liu et al., 2012). An Agilent 1200 HPLC interfaced with Applied Biosystems Qtrap 3200 “equipped with an electrospray ion source was used. Chromatographic separation was carried out with a Waters XTerra MS C18 column” (2.1×50 mm, 3.5 µm; Waters Corporation, Milford, MA). Mobile phase was delivered 250 µl/min, and the gradient was initiated at 90% A-10%B (A, 5 mM ammonium acetate buffer, pH 4.6; B, acetonitrile). The proportion of mobile phase B was increased to 60% over 1 min, held constant for 1 min, and then restored to the initial composition. 7-Hydroxywarfarin was detected by MS/MS (323/176), and mebendazole was used as the internal standard (294/262) in negative

ion mode. The mobile phase for noscapine consisted of 0.1% formic acid in water (A) and acetonitrile (B). The column was first equilibrated at 25% mobile phase B for 1.5 min at a 200 µl/min flow rate. The elution was then ramped linearly to 90% mobile phase B over 1.5 min, maintained for 5 min, and followed by a return to initial conditions. SRM pair for noscapine (MS/MS 414/220) was performed in positive ionization mode, and phenytoin (MS/MS 253/182) was employed as the internal standard (Sproll et al., 2006; Yuan et al., 2009). The dwell time for each transition was 5 ms.

3.3.2.10 Spectral Analysis of Metabolite-Intermediate (MI) Formation

Recombinant CYP2C9.1 was diluted into buffer (0.1 M potassium phosphate buffer, pH 7.4) to yield a final concentration of 0.3 µM and a stock solution of reduced NADPH was added to yield a final concentration of 1 mM NADPH. The solution was split into sample and reference cuvettes and spectra recorded on an Olis-modernized Aminco DW-2 spectrophotometer (Olis, Bogart, GA). After 3 min of pre-incubation at 37°C, the experiment was initiated by adding vehicle to the reference cuvette (2 µl methanol) and substrate to the sample cuvette (2 µl of noscapine stock solution) to yield a final concentration of 50 µM noscapine. The final volume in both cuvettes was 0.40 ml and contained 0.5% methanol. The spectrophotometer was operated in split beam mode and repetitive scans were taken from 500 to 400 nm wavelength light (readings at 1 nm intervals) at 1, 2, 4, 8, and 16 min. Once MI complex formation had ceased, the incubation was quenched by adding a few crystals of dithionite to each cuvette. Following a 3 min incubation period, a new baseline scan was taken and the spectrum blanked. CO gas was then bubbled gently into the sample cuvette only and scans taken to determine the amount of residual CYP capable of binding CO. The amount of CO-bound CYP was quantified by applying a molar extinction coefficient of 91 cm^{-1} mM^{-1} to the 450 – 490 nm absorbance difference (OMURA and SATO, 1964a; OMURA and SATO, 1964b). Control runs were performed in the

absence of NADPH. The kinetic profile of metabolic intermediate (MI) complex formation was captured by measuring the absorbance at 458 nm and 490 nm from 0 min to 20 min and plotting the increase in difference in absorbance over time. The concentrations of MI complexes were approximately calculated by dividing the absorbance difference at 458 nm and 490 nm by the molar extinction coefficient of 65 cm^{-1} mM^{-1} (Manno et al., 1988). The initial rates of MI complex formation (k) and maximal concentration of MI complex (MIC_{max}) were calculated by fitting the data to the standard monoexponential function $MIC_t = MIC_{max}$ (1 - e^{-kt}), where MIC_t is the concentration of MI complex at each time point.

3.3.2.11 Quasi-irreversibility of the Inhibition of CYP2C9 by Noscapine

The preincubation was performed as in 3.3.2.2.4 in the presence or absence of 10 uM noscapine (Barbara et al., 2013). The preincubation mixtures of both types were 2-fold diluted into the buffer with or without 10 mM ferricyanide and incubated for 10 min at 37 °C before another 5-fold dilution into the reaction mixture containing the substrate. The final incubation was in the same oncidtion as that in 3.3.2.2.4.

3.3.2.12 Quantitative Predictions of *In Vivo* Drug Interactions

The relative changes in area under the curve (AUC) of (*S*)-warfarin upon co-administration of noscapine were predicted based on reversible inhibition (eq. 17) or TDI mechanism (eq. 18) (Brown et al., 2005a; Grimm et al., 2009).

$$AUC_i/AUC = 1/(f_m/(1 + [I]/K_i) + (1 - f_m)) \qquad (17)$$

$$AUC_i/AUC = 1/(f_m/(1 + \frac{k_{inact} \times [I]}{K_{I,u} \times k_{deg}}) + (1 - f_m)) \quad (18)$$

AUC_i/AUC is the predicted ratio of *in vivo* exposure of (*S*)-warfarin with vs. without coadministration of noscapine; $k_{deg(CYP2C9)}$ is the first-order rate constant of *in vivo* degradation of CYP2C9 [0.00026 min^{-1} (Obach et al., 2007)]; $K_{i,u}$ is K_i adjusted by the free fraction of noscapine in 0.1mg/ml pooled HLM (= $K_i \times f_u$); k_{inact} is the theoretical maximal inactivation rate; and $K_{I,u}$ is the unbound inhibitor concentration at 1 mg/ml microsomes yielding 0.5 times k_{inact}. $[I]_{in\ vivo}$ represents the inhibitor concentration at the enzyme active site. The unbound C_{max} at steady state (defined as $f_u \times C_{max}$, $C_{max,u}$) was used for $[I]_{in\ vivo}$ because $C_{max,u}$ yields the most accurate predictions of drug-drug interactions (Obach et al., 2007) and the use of total C_{max} typically leads to overprediction of DDI risk (Fujioka et al., 2012). The free fraction of noscapine (f_u) in pooled human serum is about 7% (Karlsson and Dahlstrom, 1990). In previous clinical pharmacokinetic studies of noscapine, single doses of 100 mg, 200 mg and 300 mg noscapine tablet led to the C_{max} values of 0.31 μM, 0.95 μM, and 2.1 μM, respectively (Karlsson et al., 1990). A recent clinical study with the dosage of 50 mg demonstrated that the noscapine concentration at 4 hours after dosing ranged from 0.02-0.19 μM (Rosenborg et al., 2010). Based on all these previous data, C_{max} values ranging from 0.02-2.1 μM were selected to estimate the AUC_i/AUC ratio.

The extent of CYP2C9-mediated metabolism in overall (*S*)-warfarin elimination ($f_{m(CYP2C9)}$) was estimated by using the following equations (Ito et al., 2005).

$$CL^{EM} = f_{m(CYP2C9)}{}^{EM} \times CL^{EM} + (1 - f_{m(CYP2C9)}{}^{EM})CL^{EM} \quad (19)$$

$$CL^{XM} = f_{m(CYP2C9)}{}^{XM} \times CL^{XM} + (1 - f_{m(CYP2C9)}{}^{EM})CL^{EM} \quad (20)$$

where *XM* refers to poor (PM, patients with *2/*2, *2/*3, or *3/*3 genotype), intermediate (IM, patients with *1/*2 or *1/*3 genotype) or extensive (EM, patients with *1/*1 genotype) metabolizer phenotype predicted based on CYP2C9 genotype information. Combining the eqs. 19 and 20, the following equation describes the $f^{XM}_{m(CYP2C9)}$ decrease by the CL^{EM}/CL^{XM} ratio:

$$f_{m(CYP2C9)}{}^{XM} = 1 - (1 - f_{m(CYP2C9)}{}^{EM}) \times CL^{EM}/CL^{XM} \qquad (21)$$

The $f^{EM}_{m(CYP2C9)}$ value was set as 0.82-0.92 based on the urinary recovery of metabolites, biliary excretion and the recovery of unchanged drug (Kunze and Trager, 1996). Then, the *XM* warfarin ranged from 0 to 0.92 for different CYP2C9 phenotypes, based on the previous *in vivo* (*S*)-warfarin clearance data obtained in subjects with different CYP2C9 genotypes (Scordo et al., 2002). AUC_i/AUC values were subsequently calculated and plotted against $[I]_{in\ vivo}$ and $f_{m(CYP2C9)}$ using MATLAB R2009b (Mathworks, Natick, MA). The fraction of warfarin dose required to obtain the same level of systemic exposure as in the wild-type carrier was predicted by using eq. 22 for the carriers of CYP2C9 variants (Castellan et al., 2013).

$$Dose\ Adjustment\ Factor_{Genotype} = \frac{AUC^{EM}}{AUC^{XM}} = 1 - f_{m(CYP2C9)}{}^{EM} \times (1 - FA) \qquad (22)$$

in which *FA* represents the fraction of remaining CYP2C9 activity of CYP2C9 variants. The combined effects of CYP2C9 genotypes and inhibition by noscapine on warfarin dose could be estimated using eq. 23.

$$Dose\ Adjustment\ Factor = Dose\ Adjustment\ Factor_{Genotype} \times \frac{AUC}{AUC_i} \qquad (23)$$

3.3.3 Results

3.3.3.1 Inhibition of (*S*)-warfarin 7-hydroxylation by Noscapine

To determine the (*S*)-warfarin concentration employed in inhibition assays, the enzyme kinetic studies were first performed by using pooled HLM. The apparent kinetic parameters K_m and V_{max} of 7-hydroxywarfarin formation were estimated to be 3.3 ± 0.3 μM and 6.9 ± 0.2 pmol/min/mg protein, respectively (Figure 3.14A). In the subsequent experiments using 2.5 μM (*S*)-warfarin, noscapine inhibited CYP2C9-mediated (*S*)-warfarin 7-hydroxyaltion with an IC_{50} of 6.5 ± 0.7 μM in pooled HLM (Figure 3.14B). In cDNA-expressed enzyme preparations of CYP2C9.1, the IC_{50} value was 2.6 ± 0.1 μM. Relatively small decreases in inhibition potency were noted in CYP2C9.2 and CYP2C9.3 enzymes (IC_{50}, 3.6 ± 0.2 μM and 4.9 ± 0.7 μM, respectively). As shown in Figure 3.15, results from the inhibition kinetic assays suggest that noscapine inhibited CYP2C9 activity in a competitive manner, with K_i values of 4.6 ± 0.4 μM (in pooled HLM, Figure 3.15A and 3.15B) and 1.0 ± 0.1 μM (in recombinant CYP2C9.1 Figure 3.15C and 3.15D). These results indicate that noscapine is a competitive inhibitor of (*S*)-warfarin metabolism by CYP2C9.

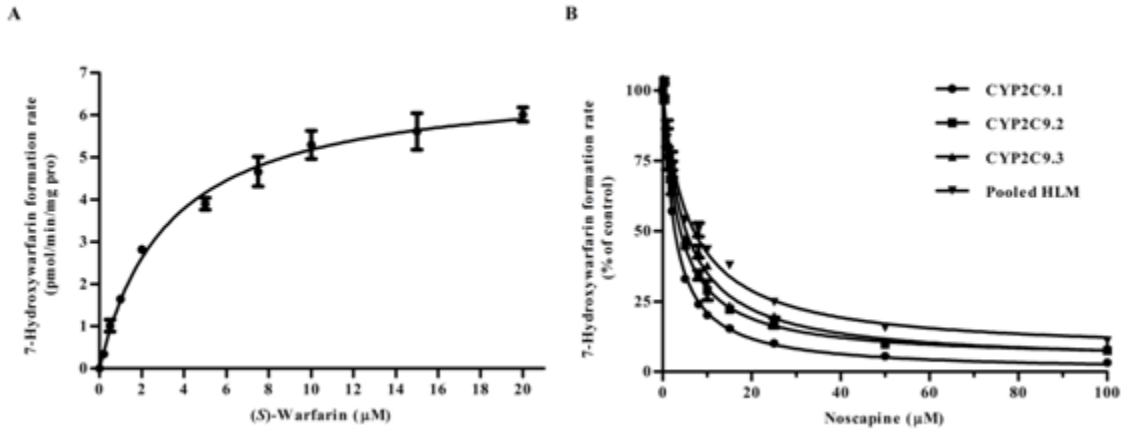

Figure 3.14 Enzyme kinetics of (*S*)-warfarin 7-hydroxylation in pooled HLM (A) and the inhibition of (*S*)-warfarin 7-hydroxylation by noscapine in HLM and recombinant CYP2C9 enzymes (B). The data shown represent the mean ± S.D. from two replicates.

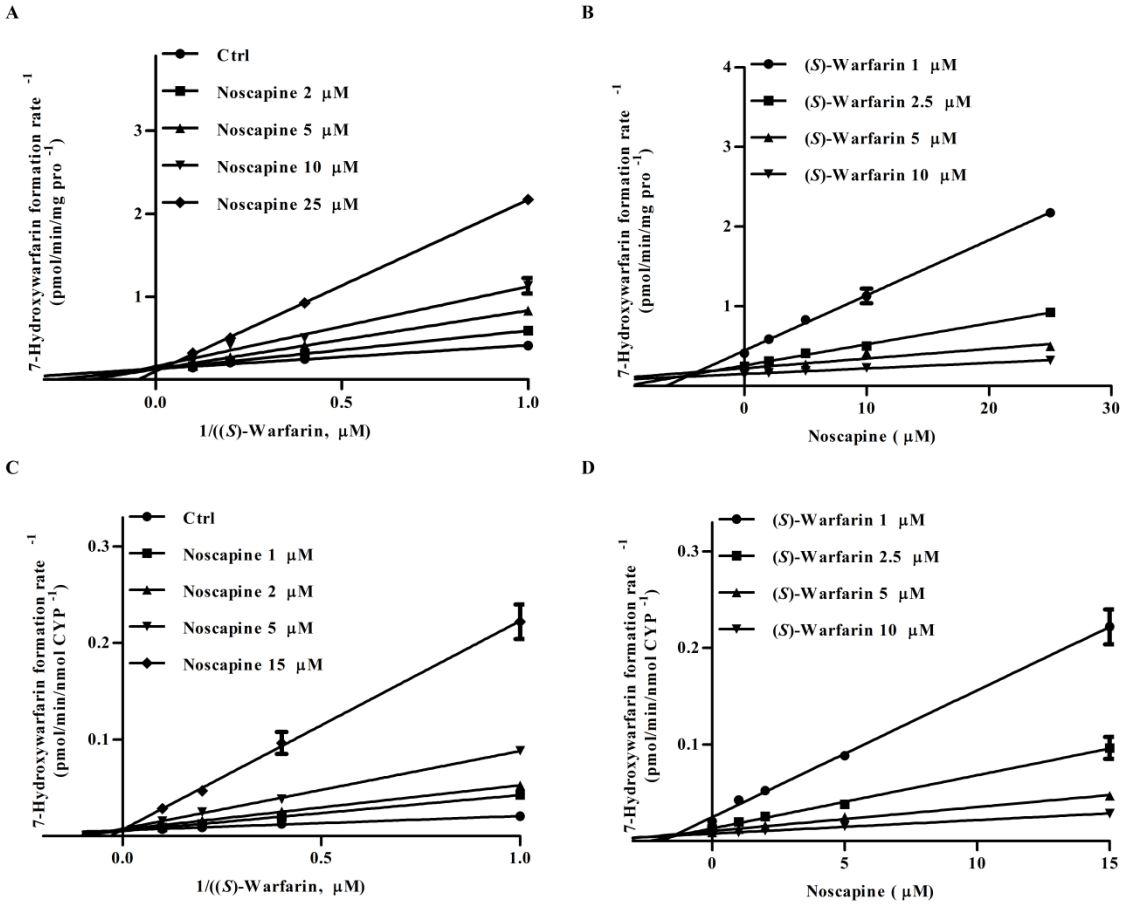

Figure 3.15 Representative Lineweaver-Burk plots and Dixon plots showing the effects of noscapine on (*S*)-warfarin 7-hydroxylation in pooled HLM (A and B) and recombinant CYP2C9.1 (C and D). The data shown represent the mean ± S.D. from two replicates.

3.3.3.2 Time- and NADPH-Dependent Inhibition of CYP2C9

Previously, noscapine was shown to inhibit diclofenac 4'-hydroxylation via a mechanism of time-dependent inhibition (Fang et al., 2010). To examine whether noscapine inhibits warfarin metabolism by a similar mechanism, noscapine at different concentrations was incubated with pooled HLM for different time periods, and the residual CYP2C9 activity was determined by using (*S*)-warfarin as the probe drug. The resulting inactivation kinetics was best fit to the

standard hyperbolic equation (Figure 3.16), with k_{inact} of 0.041 min^{-1} and K_I of 6.8 μM. The estimated k_{inact}/K_I was 6.0 ml/min/μmol, indicating high inactivation efficiency. To evaluate the effects of CYP2C9 genotypes on the time-dependent inhibition potential of noscapine, single point inactivation experiments were performed using recombinant wild-type CYP2C9 and its variants. To this end, a recombinant CYP2C9 protein was pre-incubated with noscapine (or vehicle) in the presence (or absence) of NADPH for 30 min, and then the residual CYP2C9 activity was determined by incubation with (*S*)-warfarin. A greater than 15% loss in CYP2C9 activity by preincubation with noscapine (when compared to the activity in the absence of NADPH) was used as a cut-off value for significant time-dependent inhibition (Obach et al., 2007). The percentage of CYP2C9.1 activity loss in the presence of NADPH was calculated to be 42 ± 5% (Figure 3.16A), indicating significant inactivation of the enzyme by noscapine.

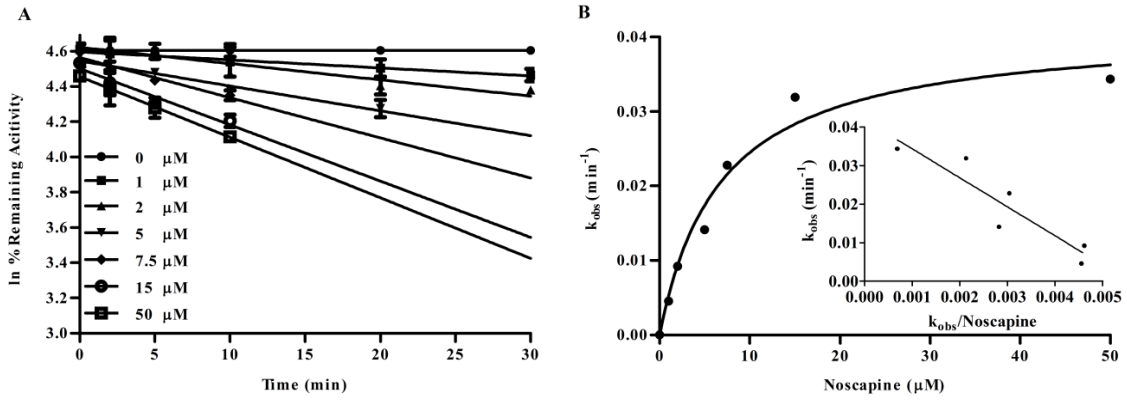

Figure 3.16 Time- and concentration-dependent inhibition of (*S*)-warfarin 7-hydroxylation by noscapine (0-50 μM) in pooled HLM incubations. The data shown represent the mean ± S.D. from two replicates.

Interestingly, the CYP2C9 variants associated with the PM phenotype were found to be more susceptible to inactivation by noscapine than the wild type; the decrease in activity was 71 ± 7%

(CYP2C9.2, p<0.01) and 59 ± 5% (CYP2C9.3, p<0.05) (Figure 3.17A). Similar results were also observed when inactivation kinetics was compared among different CYP2C9 variants (Figure 3.17B through 3.17D). CYP2C9.1 was inactivated by noscapine with K_I of 4.4 μM and k_{inact} of 0.013 min^{-1}. Although K_I values for CYP2C9.2 (5.7 μM) and CYP2C9.3 (2.6 μM) were similar to that of CYP2C9.1, their k_{inact} values increased noticeably (0.033 min^{-1} for CYP2C9.2 and 0.022 min^{-1} for CYP2C9.3), resulting in moderately higher inactivation efficiencies in comparison with that of the wild-type enzyme (i.e., 2-fold and 3-fold for CYP2C9.2 and CYP2C9.3, respectively).

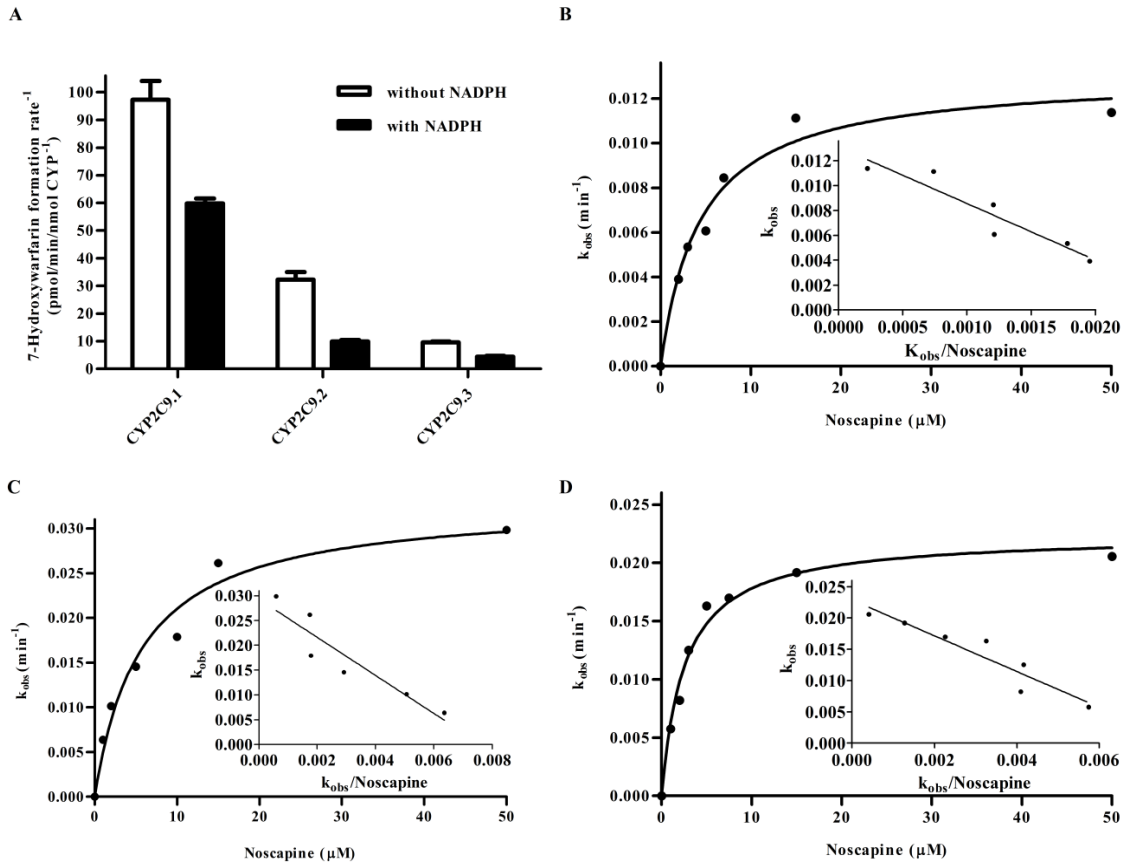

Figure 3.17 NADPH-dependent inactivation of (*S*)-warfarin 7-hydroxylation by noscapine (15 μM) in recombinant CYP2C9 (A). Kinetic plots demonstrating observed rates of inactivation (k_{obs}) by noscapine (0-50 μM) in recombinant CYP2C9.1 (B), CYP2C9.2 (C), and CYP2C9.3 (D). The data shown represent the mean ± S.D. from two replicates.

Taken together, noscapine is both a competitive and time-dependent inhibitor of CYP2C9, and its inhibitory potency differs among CYP2C9 variants.

3.3.3.3 Effect of Ultrafiltration on CYP2C9 Inactivation by Noscapine

To determine the reversibility of the inactivation of CYP2C9 by noscapine, NADPH, unbound noscapine and its metabolites were removed from the preincubation samples by ultrafiltration, and the remaining CYP2C9 activity was determined by measuring (*S*)-warfarin 7-hydroxylation rates. ABT (a mechanism-based inactivator of CYPs) and sulfaphenazole (a reversible inhibitor of CYP2C9) were used as controls in parallel. The filtered samples of microsomes preincubated with noscapine and ABT showed less than 10% recovery of (*S*)-warfarin 7-hydroxylase activity after ultrafiltration, whereas >30% recovery was detected with sulfaphenazole (Figure 3.18). Together, these results indicate that noscapine-mediated CYP2C9 inhibition is irreversible and that similarly to ABT, noscapine inhibits CYP2C9 by mechanism-based inactivation (MBI).

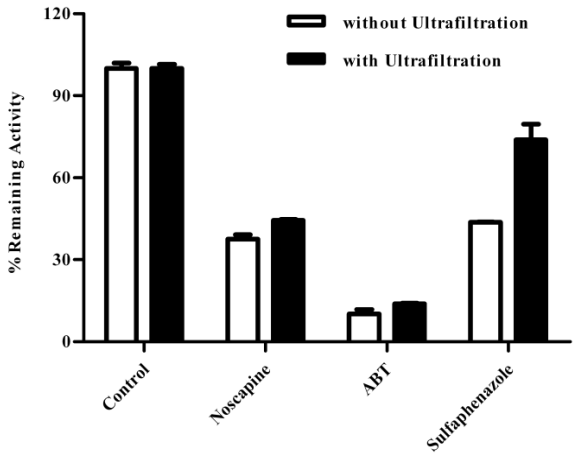

Figure 3.18 Effects of ultrafiltration on the time- and NADPH-dependent inhibitory potential of noscapine towards CYP2C9-mediated (*S*)-warfarin 7-hydroxylation. The data shown represent the mean ± S.D. from two replicates.

3.3.3.4 Spectral Analysis of MI Complex Formation

In order to examine MI complex formation, absorption spectra of the incubation mixtures of recombinant CYP2C9.1 with noscapine were monitored. A time dependent increase in the Soret peak at 458 nm, characteristic of MI complex formation, was observed upon the addition of NADPH (Figure 3.19A). When the difference between the absorbance at 458 nm and 490 nm (dAbs) was plotted over time, a kinetic profile for MI complex formation was determined (Figure 3.19B). Based on the data for the first 30 sec of reaction, the initial rate of MI complex formation was calculated to be 0.0133 dAbs/μM CYP/min. Approximately 41% of the total enzyme was converted to an MI complex. Remaining uncomplexed CYP2C9 was determined by a subsequent CO-binding study. The results showed that a significant fraction (40-60%) was able to form a ferrous CO complex after MI complex formation had ceased (data not shown). In sum, all these spectra data combined together suggested that MBI of (*S*)-warfarin 7-hydroxyaltion by noscapine was mainly due to the formation of MI complex with CYP2C9.

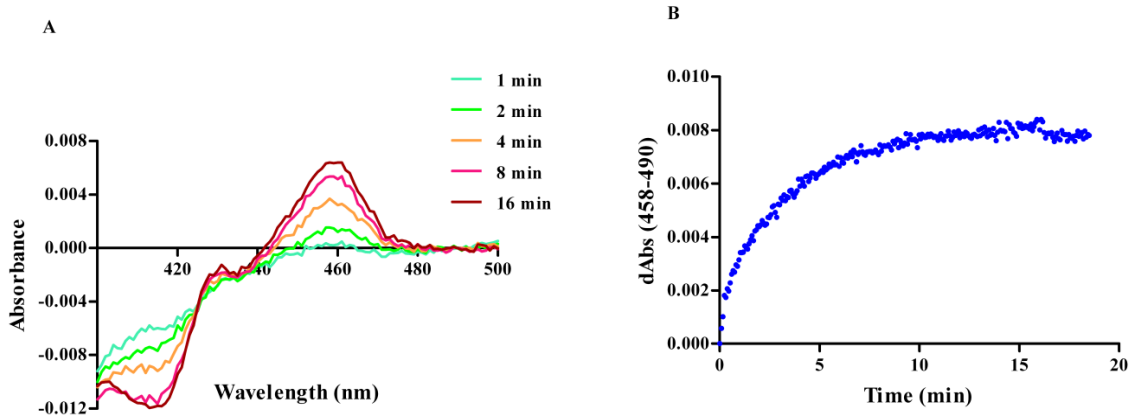

Figure 3.19 Spectral evidence for the formation of an MI complex with CYP2C9.1 and noscapine (50 μM) (A) and the time course for complex formation (B). The data shown represent the mean ± S.D. from two replicates.

3.3.3.5 Quasi-irreversibility of the Inhibition of CYP2C9 by Noscapine

The quasi-irreversibility of the inactivation of CYP2C9 by noscapine was assessed in HLM in the presence of ferricyanide. When ferricyanide was included in the preincubation, the inactivation of CYP2C9 was greatly alleviated with a similar 7-hydroxylation level of (*S*)-warfarin, compared to the control without the inhibitor and ferricyanide and that without the inhibition but ferricyanide (Figure 3.20). In contrast, the sample containing only noscapine, the level of 7-hydroxylation activity of CYP2C9 was less than 70% of the controls.

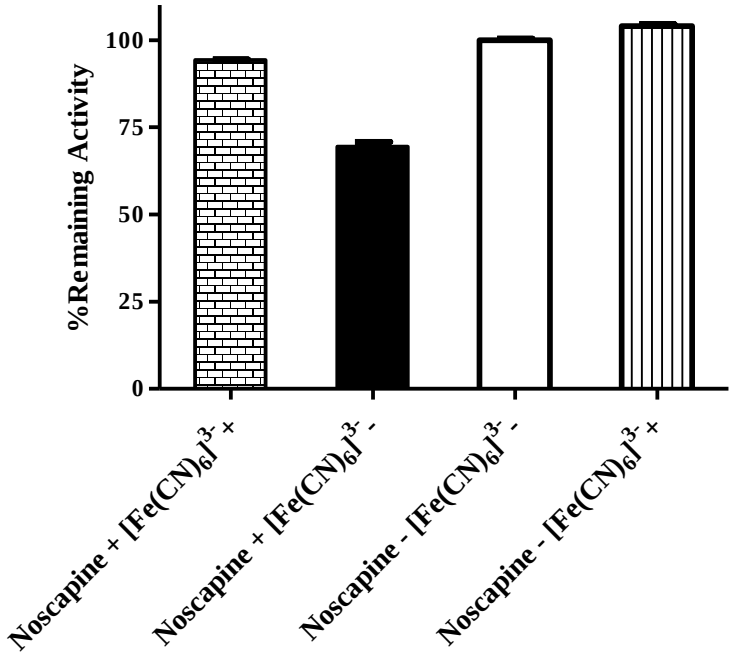

Figure 3.20 Inhibitory activity of noscapine against (*S*)-warfarin 7-hydroxylation in the presence and absence of ferricyanide. The data shown represent the mean ± S.D. from two replicates.

3.3.3.6 Prediction of *In Vivo* (*S*)-Warfarin-Noscapine Interactions

The clinical impact of CYP2C9 inhibition by noscapine was evaluated by estimating the ratio of (*S*)-warfarin AUC in the presence and absence of the inhibitor, based on the inhibitory mechanisms (i.e., competitive inhibition and MBI). The K_i and K_I values were first adjusted for non-specific binding to 0.1 mg/ml ($f_{u,m}$, 97 ± 3%) and 1.0 mg/ml ($f_{u,m}$, 22 ± 1%) HLM proteins, respectively, yielding the adjusted values ($K_{i,u}$ of 4.5 μM and $K_{I,u}$ of 1.5 μM). AUC changes upon noscapine co-administration were predicted for varying $f_{m(CYP2C9)}$ and noscapine concentrations. Values of $f_{m(CYP2C9)}$ ranging from 0 to 0.92 reflect the differential CYP2C9 enzyme activity of CYP2C9 variants (Table VII; see materials and methods for details), while noscapine concentrations ranging from 0.02 to 2.1 μM reflect C_{max} obtained from a typical oral dose of noscapine for antitussive or anticancer effects. Figure 3.21 shows 3-dimensional (and contour) plots for the estimated AUC_i/AUC ratios when noscapine inhibits CYP2C9 activity only by MBI (Figure 3.21A) or competitive inhibition mechanism (Figure 3.21B). The results indicate that in carriers of wild-type CYP2C9, a typical dose of noscapine is predicted to cause a >7-fold increase in the exposure of (*S*)-warfarin by MBI (Figure 3.21A) but a minimal increase (~3%) by the competitive inhibition mechanism (Figure 3.21B). The dose adjustment factor was then estimated for warfarin based on the combined effects of noscapine-mediated inhibition and CYP2C9 genotypes on warfarin exposure (Figure 3.21C and Table VII). The coadministration of noscapine was estimated to require up to a 7-fold decrease in warfarin dose in CYP2C9*1/*1 carriers whereas the need for dose change was smaller in the carriers of CYP2C9 variants. Together, our results indicate that MBI of CYP2C9 by noscapine may significantly increase the systemic exposure of (*S*)-warfarin, and the required warfarin dose adjustments show genotype-dependency.

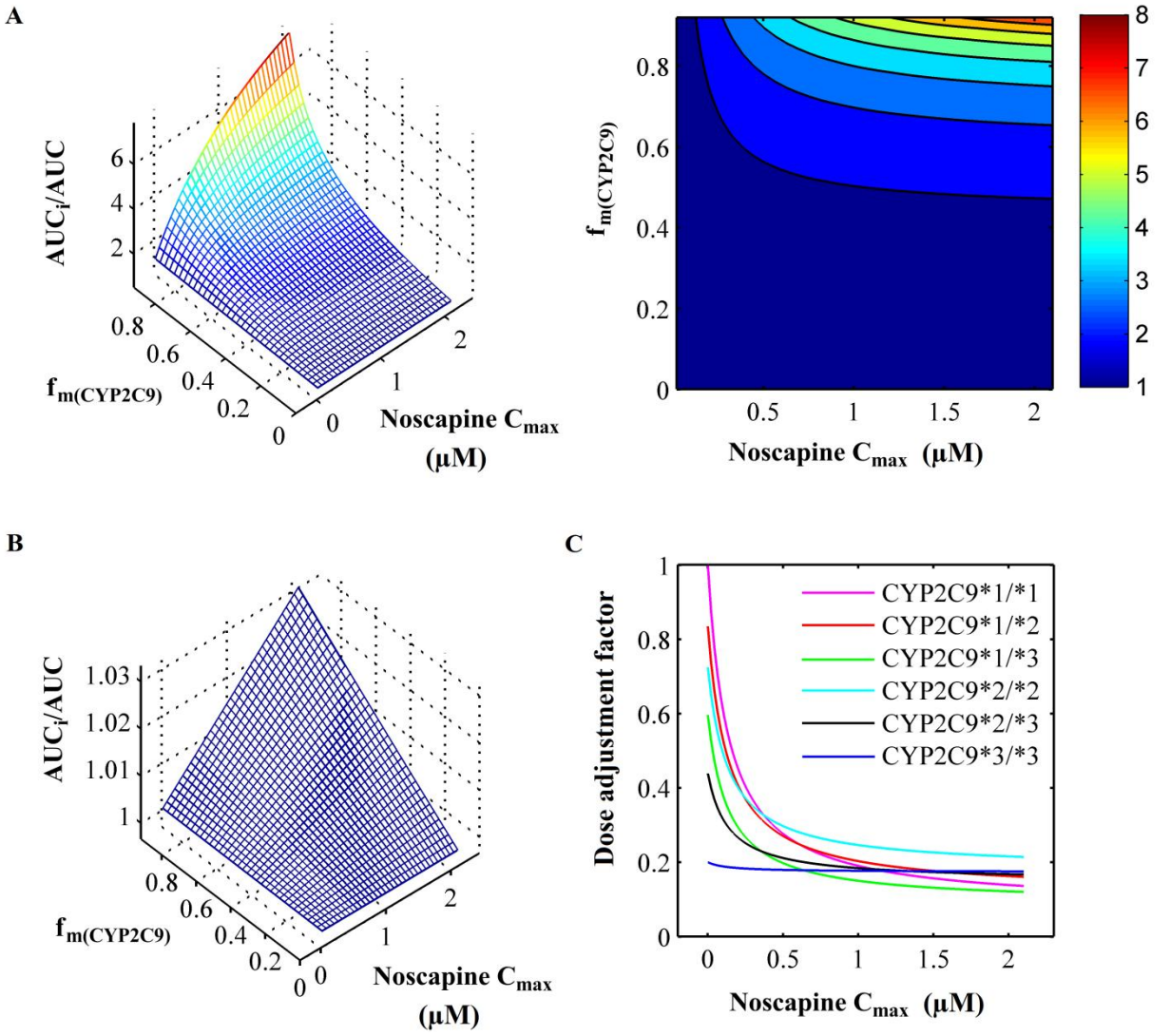

Figure 3.21 3-Dimensional and contour plots for the calculated AUC_i/AUC ratios with f_m (CYP2C9) and C_{max} of noscapine in plasma resulted from MBI (A) or competitive inhibition (B). Suggested dose adjustment factors based on the range of noscapine plasma C_{max} values and patients of different genotypes (C).

3.3.4 Discussion

Altered CYP2C9-mediated (*S*)-warfarin metabolism is one of the major causes of high inter-individual variability in warfarin response (Eriksson and Wadelius, 2012). Noscapine is both a substrate and inhibitor for CYP2C9 (Rosenborg et al., 2010; Fang et al., 2012), and is known to cause significant increases in international normalized ratio (INR) when coadministered with warfarin (Ohlsson et al., 2008; Scordo et al., 2008; Myhr, 2009). However, the direct *in vitro* evidence on the noscapine-warfarin interaction or a detailed analysis of the inhibition kinetics to predict the magnitude of *in vivo* DDI is lacking. In addition, the effect of genetic polymorphism in CYP2C9 on the noscapine-mediated inhibition remains unknown. The objective of this study was to investigate the inhibitory mechanisms of (*S*)-warfarin metabolism by noscapine and examine the effects of common genetic polymorphisms of CYP2C9 on the extent of noscapine-mediated CYP2C9 inhibition. Combined with genotype-dependent inhibition kinetic data, the magnitude of pharmacokinetic interactions and the required warfarin dosage adjustments were estimated for subjects of different genotypes.

In this study, noscapine was found to be a competitive inhibitor of CYP2C9-mediated (*S*)-warfarin 7-hydroxylation in both HLM and recombinant enzyme systems (K_i <10 μM) (Figure 3.15). Interestingly, when diclofenac 4'-hydroxyaltion was used as the probe reaction, noscapine inhibited CYP2C9 activity in a noncompetitive manner in pooled HLM (Fang et al., 2010). Similar substrate dependent difference in inhibitory mechanism was previously reported for CYP3A4 inhibitors. For example, fluconazole exhibits competitive inhibition of CYP3A4-mediated (*R*)-warfarin hydroxylation (Kunze et al., 1996), but noncompetitive inhibition of midazolam 1'-hydroxyaltion. This was attributed to the multiple binding regions for substrates or inhibitors in the voluminous active site (Gibbs et al., 1999). CYP2C9 also exhibits a capacity for multiple ligands binding (Williams et al., 2003; Wester et al., 2004). Possibly, noscapine

prevents the access of (*S*)-warfarin to the substrate-binding site in the CYP2C9 active pocket, but not that of diclofenac, resulting in the competitive inhibition of (*S*)-warfarin metabolism. This hypothesis remains to be verified through molecular modeling of CYP2C9. In the competitive inhibition of CYP2C9 activity by noscapine, the IC_{50} value for CYP2C9.3 was 1.9-fold higher than that for CYP2C9.1 (Figure 3.14). This result is in good agreement with a previous study in which fluconazole K_i value for CYP2C9.3 was found to be 2-fold higher than that for CYP2C9.1 when flurbiprofen was used as a probe substrate (Kumar et al., 2008). This genotype-dependent CYP2C9 inhibitory potency of noscapine is likely due to differences in the conformation of the active site and the orientation of inhibitor binding (Kumar et al., 2006). Taken together, noscapine inhibits CYP2C9-mediated (*S*)-warfarin metabolism via a competitive inhibition mechanism, and the inhibitory profiles exhibit substrate- and genotype-dependent variation.

Our study revealed that noscapine is also a mechanism-based inhibitor of CYP2C9, exhibiting time- and NADPH-dependent inhibition (Figure 3.16). Removal of free noscapine and its metabolites from the HLM incubation by using ultrafiltration did not reverse noscapine-mediated inhibition of (*S*)-warfarin metabolism, indicating irreversibility of the inhibition (Figure 3.18). Our spectral analysis further demonstrated a time-dependent increase in the maximum absorbance at 458 nm (Figure 3.19A), suggesting the formation of MI complex by noscapine. This is reasonable because noscapine has a methylenedioxyphenyl group incorporated into its structure (Figure 3.13A). The oxidation of this group often leads to the formation of carbene complexes with ferrous heme iron of cytochrome P450 (Franklin, 1971), which can be disrupted in the presence of ferricyanide (Figure 3.20). Since the formation of an MI complex is dependent upon catalytic rate, the susceptibility to MBI is expected to be dependent upon the relative activities of CYP variants (Polasek and Miners, 2007; Orr et al., 2012b). To verify that formation

of reactive metabolite(s) of noscapine by CYP2C9 is responsible for the MBI by noscapine, the kinetics of CYP2C9 inhibition were characterized by using CYP2C9.2 and CYP2C9.3 variants that are known to exhibit decreased enzyme activity (Liu et al., 2012). Surprisingly, our results showed that the inactivation of CYP2C9 by noscapine was >2-fold more efficient (i.e., k_{inact}/K_I) for CYP2C9.2 and CYP2C9.3 than for CYP2C9.1. This suggests that formation of reactive metabolite(s) of noscapine may be greater from CYP2C9.2 and CYP2C9.3. In fact, it was previously shown that a metabolite of noscapine is produced 1.4-fold more rapidly by CYP2C9.2 than CYP2C9.1 (Fang et al., 2012), suggesting that the CYP2C9 variants may show increased (rather than decreased) catalytic activity for certain reactions. This may be due to the structural features of CYP2C9 [i.e., a big active pocket allowing simultaneous binding of multiple ligands (Williams et al., 2003)] that potentially lead to highly substrate-dependent functionality of CYP2C9 variants (Maekawa et al., 2009). It will be of interest to examine whether the partition ratios, metabolite formation rates and noscapine depletion rates are significantly different among these enzymes.

Noscapine is a mechanism-based inhibitor of CYP2C9-mediated (*S*)-warfarin 7-hydroxylation and as expected of a P450 substrate also acts as a competitive inhibitor. However, the clinical impact of competitive inhibition on (*S*)-warfarin elimination was predicted to be minimal (i.e., at most 3%) at typical doses of noscapine while that of MBI could be significant (Figure 3.21). Our study predicted that coadministration of noscapine and warfarin could result in up to 7-fold increases in AUC of (*S*)-warfarin by MBI mechanism. Overall, the extent of the increase in (*S*)-warfarin AUC appears consistent with the result from a clinical study in which a >2-fold increase in the INR was seen in patients co-administered with noscapine (as an antitussive drug) and warfarin (Ohlsson et al., 2008). The typical dose of noscapine as a cough suppressant (50 mg) produces a C_{max} of around 0.5 μM (Haikala et al., 1986; Olsson et al., 1986). This concentration

would require up to 70% decrease in warfarin dose in both EM and IM patients but little change in PM patients, especially in carriers of CYP2C9*3/*3 (Figure 3.21 and Table VII).

Genotype	Fraction of Dose Expected to be Cleared by CYP2C9 $f_{m(CYP2C9)}$	Magnitude of the Potential (*S*)-Warfarin-Noscapine Interactions AUC$_i$/AUC	Dose Adjustment Factor [c]	
			Based Solely on Genotypes	Based on Both Genotypes and Inhibitory Effects of Noscapine
CYP2C9*1/*1	0.82-0.92 [b]	1.12-7.36	1.00	0.14-0.88
CYP2C9*1/*2	0.69-0.86	1.09-5.20	0.83	0.16-0.74
CYP2C9*1/*3	0.66-0.85	1.09-4.96	0.60	0.12-0.53
CYP2C9*2/*2	0.44-0.75	1.06-3.38	0.72	0.21-0.65
CYP2C9*2/*3	0.23-0.66	1.03-2.63	0.44	0.17-0.40
CYP2C9*3/*3	0-0.13	1.00-1.14	0.20	0.18-0.19

Table VII. ESTIMATION OF (*S*)-WARFARIN CLEARANCE FRACTION ($f_{m(CYP2C9)}$), RATIO CHANGE OF *IN VIVO* EXPOSURE TO (*S*)-WARFARIN (AUC$_i$/AUC), AND SUGGESTED DOSE ADJUSTMENT FACTOR FOR PATIENTS WITH DIFFERENT CYP2C9 GENOTYPES [a]. [a] All simulation were performed at noscapine C_{max} values range from 0.02 µmol/l to 2.1 µmol/l, and the fraction of wild-type CYP2C9 activity (FA) for each mutant were obtained directly from literature (Castellan et al., 2013). [b] Values were estimated

from mass balance data as described previously (Kunze and Trager, 1996). [c] Dose adjustment ratios were predicted at the upper most value of estimated $f_{m(CYP2C9)}$.

Our estimation is based on the previously reported plasma C_{max} after a single oral dose of noscapine ranging from 50 to 300 mg, but a higher C_{max} may be achieved clinically. In fact, the dosage of off-label use of noscapine as an anticancer agent ranges from 1,000 to 2,250 mg per day divided in 3 doses [MedInsight Research Institute, http://www.pcref.org/MedInsight%20-%20PCREF%20Noscapine%20Review.pdf]. Furthermore, noscapine is known to exhibit a nonlinear pharmacokinetic behavior in humans (Karlsson et al., 1990); a 3-fold increase in dose (from 100 mg to 300 mg) leads to a 9-fold rise in AUC. Thus, the extent of pharmacokinetic interactions between warfarin and noscapine may be greater than what was estimated in this study, indicating that careful monitoring of INR will be required when noscapine is combined with warfarin.

In conclusion, we have shown that noscapine is both a competitive inhibitor and a mechanism based inactivator of (*S*)-warfarin 7-hydroxylation by CYP2C9. Our in depth kinetic analysis of the inhibition by noscapine provided a basis to predict genotype-dependent changes in warfarin exposure upon various concentrations of noscapine. Significant changes in warfarin dosage are required due to the MBI of CYP2C9 by noscapine. These findings should shed light on better understanding and prediction of drug-drug interaction involving noscapine and CYP2C9.

References

(2008a) Handbook of anti-tuberculosis agents. Introduction. *Tuberculosis (Edinb)* **88:**85-86.

(2008b) LL-3858. *Tuberculosis (Edinb)* **88:**126.

Abdel-Rahman O, Abdel-Wahab M, Shaker M, Abdel-Wahab S, Elbassiony M, and Ellithy M (2013) Sorafenib versus capecitabine in the management of advanced hepatocellular carcinoma. *Med Oncol* **30:**655.

Ahmad S (2011) Pathogenesis, immunology, and diagnosis of latent Mycobacterium tuberculosis infection. *Clin Dev Immunol* **2011:**814943.

Ai L, Zhu L, Yang L, Ge G, Cao Y, Liu Y, Fang Z, and Zhang Y (2013) Selectivity for inhibition of nilotinib on the catalytic activity of human UDP-glucuronosyltransferases. *Xenobiotica*.

Aneja R, Dhiman N, Idnani J, Awasthi A, Arora SK, Chandra R, and Joshi HC (2007) Preclinical pharmacokinetics and bioavailability of noscapine, a tubulin-binding anticancer agent. *Cancer Chemotherapy and Pharmacology* **60:**831-839.

Arrowsmith J and Miller P (2013) Trial watch: phase II and phase III attrition rates 2011-2012. *Nat Rev Drug Discov* **12:**569.

Balliet RM, Chen G, Gallagher CJ, Dellinger RW, Sun D, and Lazarus P (2009) Characterization of UGTs active against SAHA and association between SAHA glucuronidation activity phenotype with UGT genotype. *Cancer Res* **69:**2981-2989.

Barbara JE, Kazmi F, Parkinson A, and Buckley DB (2013) Metabolism-dependent inhibition of CYP3A4 by lapatinib: evidence for formation of a metabolic intermediate complex with a nitroso/oxime metabolite formed via a nitrone intermediate. *Drug Metab Dispos* **41:**1012-1022.

Barken I, Geller J, and Rogosnitzky M (2010) Prophylactic Noscapine Therapy Inhibits Human Prostate Cancer Progression and Metastasis in a Mouse Model. *Anticancer Research* **30:**399-401.

Barry PJ and O'Connor TM (2007) Novel agents in the management of Mycobacterium tuberculosis disease. *Curr Med Chem* **14:**2000-2008.

Bissio E and Lopardo GD (2013) Incidence of hyperbilirubinemia and jaundice due to atazanavir in a cohort of Hispanic patients. *AIDS Res Hum Retroviruses* **29:**415-417.

Bressler R and Bahl JJ (2003) Principles of drug therapy for the elderly patient. *Mayo Clin Proc* **78:**1564-1577.

Brodie BB, Axelrod J, Cooper JR, Gaudette L, LaDu BN, Mitoma C, and Udenfriend S (1955) Detoxication of drugs and other foreign compounds by liver microsomes. *Science* **121:**603-604.

Brown HS, Ito K, Galetin A, and Houston JB (2005a) Prediction of in vivo drug-drug interactions from in vitro data: impact of incorporating parallel pathways of drug elimination and inhibitor absorption rate constant. *British Journal of Clinical Pharmacology* **60:**508-518.

Brown HS, Ito K, Galetin A, and Houston JB (2005b) Prediction of in vivo drug-drug interactions from in vitro data: impact of incorporating parallel pathways of drug elimination and inhibitor absorption rate constant. *Br J Clin Pharmacol* **60:**508-518.

Brunton L, Lazo J, and Parker K (2005) *Goodman & Gilman's The Pharmacological Basis of Therapeutics*.

Budha NR, Lee RE, and Meibohm B (2008) Biopharmaceutics, pharmacokinetics and pharmacodynamics of antituberculosis drugs. *Curr Med Chem* **15:**809-825.

Castellan A-C, Tod M, Gueyffier F, Audars M, Cambriels F, Kassai B, Nony P, and Genophar Working G (2013) Quantitative Prediction of the Impact of Drug Interactions and Genetic Polymorphisms on Cytochrome P450 2C9 Substrate Exposure. *Clinical pharmacokinetics* **52:**199-209.

Cerec V, Glaise D, Garnier D, Morosan S, Turlin B, Drenou B, Gripon P, Kremsdorf D, Guguen-Guillouzo C, and Corlu A (2007) Transdifferentiation of hepatocyte-like cells from the human hepatoma HepaRG cell line through bipotent progenitor. *Hepatology* **45:**957-967.

Cho SH, Warit S, Wan B, Hwang CH, Pauli GF, and Franzblau SG (2007) Low-oxygen-recovery assay for high-throughput screening of compounds against nonreplicating Mycobacterium tuberculosis. *Antimicrob Agents Chemother* **51:**1380-1385.

Chougule M, Patel AR, Sachdeva P, Jackson T, and Singh M (2011a) Anticancer activity of Noscapine, an opioid alkaloid in combination with Cisplatin in human non-small cell lung cancer. *Lung Cancer* **71:**271-282.

Chougule MB, Patel AR, Jackson T, and Singh M (2011b) Antitumor Activity of Noscapine in Combination with Doxorubicin in Triple Negative Breast Cancer. *Plos One* **6**.

Christensen K, Doblhammer G, Rau R, and Vaupel JW (2009) Ageing populations: the challenges ahead. *Lancet* **374:**1196-1208.

Cohen Y, Perronne C, Truffot-Pernot C, Grosset J, Vilde JL, and Pocidalo JJ (1992) Activities of WIN-57273, minocycline, clarithromycin, and 14-hydroxy-clarithromycin against Mycobacterium avium complex in human macrophages. *Antimicrob Agents Chemother* **36:**2104-2107.

Collins L and Franzblau SG (1997) Microplate alamar blue assay versus BACTEC 460 system for high-throughput screening of compounds against Mycobacterium tuberculosis and Mycobacterium avium. *Antimicrob Agents Chemother* **41:**1004-1009.

Corona G, Elia C, Casetta B, and Toffoli G (2010) Fast liquid chromatography-tandem mass spectrometry method for routine assessment of irinotecan metabolic phenotype. *Ther Drug Monit* **32:**638-646.

Costa DB and Huberman MS (2006) Improvement of type 2 diabetes in a lung cancer patient treated with Erlotinib. *Diabetes Care* **29:**1711.

Daly AK (2013) Optimal dosing of warfarin and other coumarin anticoagulants: the role of genetic polymorphisms. *Arch Toxicol* **87:**407-420.

Daniel WA, Syrek M, Haduch A, and Wójcikowski J (2000) Pharmacokinetics and metabolism of thioridazine during co-administration of tricyclic antidepressants. *Br J Pharmacol* **131:**287-295.

Danton AC, Montastruc F, Sommet A, Durrieu G, Bagheri H, Bondon-Guitton E, Lapeyre-Mestre M, and Montastruc JL (2013) Importance of cytochrome P450 (CYP450) in adverse drug reactions due to drug-drug interactions: a PharmacoVigilance study in France. *Eur J Clin Pharmacol* **69:**885-888.

Di L, Kerns EH, Hong Y, Kleintop TA, McConnell OJ, and Huryn DM (2003) Optimization of a higher throughput microsomal stability screening assay for profiling drug discovery candidates. *J Biomol Screen* **8:**453-462.

Diacon AH, Pym A, Grobusch M, Patientia R, Rustomjee R, Page-Shipp L, Pistorius C, Krause R, Bogoshi M, Churchyard G, Venter A, Allen J, Palomino JC, De Marez T, van Heeswijk

RP, Lounis N, Meyvisch P, Verbeeck J, Parys W, de Beule K, Andries K, and Mc Neeley DF (2009) The diarylquinoline TMC207 for multidrug-resistant tuberculosis. *N Engl J Med* **360:**2397-2405.

Donato MT, Montero S, Castell JV, Gómez-Lechón MJ, and Lahoz A (2010) Validated assay for studying activity profiles of human liver UGTs after drug exposure: inhibition and induction studies. *Anal Bioanal Chem* **396:**2251-2263.

Dooley K (Mar 3rd, 2013) Drug Interactions with ART and New TB drugs: What Do We Know? , in: *HIV/TB Research Frontiers Meeting 20th Conference on Retroviruses and Opportunistic Infections*

EMA (2011) Assessment report of Caprelsa/vandetanib (Use ECfMPfH ed.

Eriksson N and Wadelius M (2012) Prediction of warfarin dose: why, when and how? *Pharmacogenomics* **13:**429-440.

Fang Z-Z, Krausz KW, Li F, Cheng J, Tanaka N, and Gonzalez FJ (2012) Metabolic map and bioactivation of the anti-tumour drug noscapine. *British Journal of Pharmacology* **167:**1271-1286.

Fang Z-Z, Zhang Y-Y, Ge G-B, Huo H, Liang S-C, and Yang L (2010) Time-dependent inhibition (TDI) of CYP3A4 and CYP2C9 by noscapine potentially explains clinical noscapine-warfarin interaction. *British Journal of Clinical Pharmacology* **69:**193-199.

Foti RS, Rock DA, Wienkers LC, and Wahlstrom JL (2010) Selection of alternative CYP3A4 probe substrates for clinical drug interaction studies using in vitro data and in vivo simulation. *Drug Metab Dispos* **38:**981-987.

Fowler S and Zhang H (2008) In vitro evaluation of reversible and irreversible cytochrome P450 inhibition: current status on methodologies and their utility for predicting drug-drug interactions. *AAPS J* **10:**410-424.

Franklin MR (1971) The enzymic formation of methylenedioxyphenyl derivative exhibiting an isocyanide-like spectrum with reduced cytochrome P-450 in hepatic microsomes. *Xenobiotica* **1:**581-591.

Franzblau SG, DeGroote MA, Cho SH, Andries K, Nuermberger E, Orme IM, Mdluli K, Angulo-Barturen I, Dick T, Dartois V, and Lenaerts AJ (2012) Comprehensive analysis of

methods used for the evaluation of compounds against Mycobacterium tuberculosis. *Tuberculosis (Edinb)* **92:**453-488.

Fujii-Kuriyama Y, Mizukami Y, Kawajiri K, Sogawa K, and Muramatsu M (1982) Primary structure of a cytochrome P-450: coding nucleotide sequence of phenobarbital-inducible cytochrome P-450 cDNA from rat liver. *Proc Natl Acad Sci U S A* **79:**2793-2797.

Fujioka Y, Kunze KL, and Isoherranen N (2012) Risk Assessment of Mechanism-Based Inactivation in Drug-Drug Interactions. *Drug Metabolism and Disposition* **40:**1653-1657.

Fujita K, Sugiyama M, Akiyama Y, Ando Y, and Sasaki Y (2011) The small-molecule tyrosine kinase inhibitor nilotinib is a potent noncompetitive inhibitor of the SN-38 glucuronidation by human UGT1A1. *Cancer Chemother Pharmacol* **67:**237-241.

Furuta S, Kamada E, Omata T, Sugimoto T, Kawabata Y, Yonezawa K, Wu XC, and Kurimoto T (2004) Drug-drug interactions of Z-338, a novel gastroprokinetic agent, with terfenadine, comparison with cisapride, and involvement of UGT1A9 and 1A8 in the human metabolism of Z-338. *Eur J Pharmacol* **497:**223-231.

Gagez AL, Rouguieg-Malki K, Sauvage FL, Marquet P, and Picard N (2012) Simultaneous evaluation of six human glucuronidation activities in liver microsomes using liquid chromatography-tandem mass spectrometry. *Anal Biochem* **427:**52-59.

Garfinkel D (1958) Studies on pig liver microsomes I. Enzymic and pigment composition of different microsomal fractions. *Arch Biochem Biophys* **77:**493-509.

Garrett M, Poland B, Brennan M, Hee B, Pithavala YK, and Amantea MA (2013) Population pharmacokinetic analysis of axitinib in healthy volunteers. *Br J Clin Pharmacol*.

Gengenbacher M and Kaufmann SH (2012) Mycobacterium tuberculosis: success through dormancy. *FEMS Microbiol Rev* **36:**514-532.

Gibbs MA, Thummel KE, Shen DD, and Kunze KL (1999) Inhibition of cytochrome P-450 3A (CYP3A) in human intestinal and liver microsomes: Comparison of K-I values and impact of CYP3A5 expression. *Drug Metabolism and Disposition* **27:**180-187.

Gilissen RA, Barnaby RJ, and Kajbaf M (2000) Identification of UDP-glucuronosyltransferases involved in the human hepatic metabolism of GV150526, a novel glycine antagonist. *Drug Metabol Drug Interact* **16:**173-189.

Gras J (2013) Bedaquiline for the treatment of pulmonary, multidrug-resistant tuberculosis in adults. *Drugs Today (Barc)* **49:**353-361.

Grimm SW, Einolf HJ, Hall SD, He K, Lim H-K, Ling K-HJ, Lu C, Nomeir AA, Seibert E, Skordos KW, Tonn GR, Van Horn R, Wang RW, Wong YN, Yang TJ, and Obach RS (2009) The Conduct of in Vitro Studies to Address Time-Dependent Inhibition of Drug-Metabolizing Enzymes: A Perspective of the Pharmaceutical Research and Manufacturers of America. *Drug Metabolism and Disposition* **37:**1355-1370.

Guillouzo A, Corlu A, Aninat C, Glaise D, Morel F, and Guguen-Guillouzo C (2007) The human hepatoma HepaRG cells: a highly differentiated model for studies of liver metabolism and toxicity of xenobiotics. *Chem Biol Interact* **168:**66-73.

Haikala V, Sothmann A, and Marvola M (1986) Comparative bioavailability and pharmacokinetics of noscapine hydrogen embonate and noscapine hydrochloride. *European Journal of Clinical Pharmacology* **31:**367-369.

Hanioka N, Ozawa S, Jinno H, Ando M, Saito Y, and Sawada J (2001) Human liver UDP-glucuronosyltransferase isoforms involved in the glucuronidation of 7-ethyl-10-hydroxycamptothecin. *Xenobiotica* **31:**687-699.

Haniu M, Armes LG, Yasunobu KT, Shastry BA, and Gunsalus IC (1982) Amino acid sequence of the Pseudomonas putida cytochrome P-450. II. Cyanogen bromide peptides, acid cleavage peptides, and the complete sequence. *J Biol Chem* **257:**12664-12671.

Harbourt DE, Fallon JK, Ito S, Baba T, Ritter JK, Glish GL, and Smith PC (2012) Quantification of human uridine-diphosphate glucuronosyl transferase 1A isoforms in liver, intestine, and kidney using nanobore liquid chromatography-tandem mass spectrometry. *Anal Chem* **84:**98-105.

Heifets LB (1991) *Drug susceptibility in the chemotherapy of mycobacterial infections*. CRC Press, Inc., Boca Raton, Fla. .

Henderson MC, Siddens LK, Morré JT, Krueger SK, and Williams DE (2008) Metabolism of the anti-tuberculosis drug ethionamide by mouse and human FMO1, FMO2 and FMO3 and mouse and human lung microsomes. *Toxicol Appl Pharmacol* **233:**420-427.

Hirota T, Eguchi S, and Ieiri I (2013) Impact of genetic polymorphisms in CYP2C9 and CYP2C19 on the pharmacokinetics of clinically used drugs. *Drug Metab Pharmacokinet* **28:**28-37.

Hirsh J, Dalen JE, Anderson DR, Poller L, Bussey H, Ansell J, and Deykin D (2001) Oral anticoagulants: Mechanism of action, clinical effectiveness, and optimal therapeutic range. *Chest* **119:**8S-21S.

Houston JB (1981) Drug metabolite kinetics. *Pharmacol Ther* **15:**521-552.

Howlader N, Noone A, Krapcho M, Garshell J, Neyman N, Altekruse S, Kosary C, Yu M, Ruhl J, Tatalovich Z, Cho H, Mariotto A, Lewis D, Chen H, Feuer E, and Cronin K (2013) SEER Cancer Statistics Review, 1975-2010, National Cancer Institute. Bethesda, MD.

Hutzler JM, Balogh LM, Zientek M, Kumar V, and Tracy TS (2009) Mechanism-Based Inactivation of Cytochrome P450 2C9 by Tienilic Acid and (+/-)-Suprofen: A Comparison of Kinetics and Probe Substrate Selection. *Drug Metabolism and Disposition* **37:**59-65.

Hynninen VV, Olkkola KT, Leino K, Lundgren S, Neuvonen PJ, Rane A, Valtonen M, Vyyryläinen H, and Laine K (2006) Effects of the antifungals voriconazole and fluconazole on the pharmacokinetics of s-(+)- and R-(-)-Ibuprofen. *Antimicrob Agents Chemother* **50:**1967-1972.

Ito K, Brown HS, and Houston JB (2004) Database analyses for the prediction of in vivo drug-drug interactions from in vitro data. *British journal of clinical pharmacology* **57:**473-486.

Ito K, Hallifax D, Obach RS, and Houston JB (2005) Impact of parallel pathways of drug elimination and multiple cytochrome P450 involvement on drug-drug interactions: CYP2D6 paradigm. *Drug Metabolism and Disposition* **33:**837-844.

Izukawa T, Nakajima M, Fujiwara R, Yamanaka H, Fukami T, Takamiya M, Aoki Y, Ikushiro S, Sakaki T, and Yokoi T (2009) Quantitative analysis of UDP-glucuronosyltransferase (UGT) 1A and UGT2B expression levels in human livers. *Drug Metab Dispos* **37:**1759-1768.

Jacobson TA (2004) Comparative pharmacokinetic interaction profiles of pravastatin, simvastatin, and atorvastatin when coadministered with cytochrome P450 inhibitors. *Am J Cardiol* **94:**1140-1146.

Jakacki RI, Hamilton M, Gilbertson RJ, Blaney SM, Tersak J, Krailo MD, Ingle AM, Voss SD, Dancey JE, and Adamson PC (2008) Pediatric phase I and pharmacokinetic study of erlotinib followed by the combination of erlotinib and temozolomide: a Children's Oncology Group Phase I Consortium Study. *J Clin Oncol* **26:**4921-4927.

Jensen CB and Jollow DJ (1991) The role of N-hydroxyphenetidine in phenacetin-induced hemolytic anemia. *Toxicol Appl Pharmacol* **111:**1-12.

Jia L, Noker PE, Coward L, Gorman GS, Protopopova M, and Tomaszewski JE (2006) Interspecies pharmacokinetics and in vitro metabolism of SQ109. *Br J Pharmacol* **147:**476-485.

Jossé R, Aninat C, Glaise D, Dumont J, Fessard V, Morel F, Poul JM, Guguen-Guillouzo C, and Guillouzo A (2008) Long-term functional stability of human HepaRG hepatocytes and use for chronic toxicity and genotoxicity studies. *Drug Metab Dispos* **36:**1111-1118.

Kakkar T, Boxenbaum H, and Mayersohn M (1999) Estimation of Ki in a competitive enzyme-inhibition model: comparisons among three methods of data analysis. *Drug Metab Dispos* **27:**756-762.

Kaminsky LS and Zhang ZY (1997) Human P450 metabolism of warfarin. *Pharmacol Ther* **73:**67-74.

Karlsson MO and Dahlstrom B (1990) SERUM-PROTEIN BINDING OF NOSCAPINE - INFLUENCE OF A REVERSIBLE HYDROLYSIS. *Journal of Pharmacy and Pharmacology* **42:**140-143.

Karlsson MO, Dahlstrom B, Eckernas SA, Johansson M, and Alm AT (1990) PHARMACOKINETICS OF ORAL NOSCAPINE. *European Journal of Clinical Pharmacology* **39:**275-279.

Kiang TK, Ensom MH, and Chang TK (2005) UDP-glucuronosyltransferases and clinical drug-drug interactions. *Pharmacol Ther* **106:**97-132.

Klingenberg M (1958) Pigments of rat liver microsomes. *Arch Biochem Biophys* **75:**376-386.

Klotz U (2007) The role of pharmacogenetics in the metabolism of antiepileptic drugs: pharmacokinetic and therapeutic implications. *Clin Pharmacokinet* **46:**271-279.

Kumar V, Brundage RC, Oetting WS, Leppik IE, and Tracy TS (2008) Differential genotype dependent inhibition of CYP2C9 in humans. *Drug Metabolism and Disposition* **36:**1242-1248.

Kumar V, Wahlstrom JL, Rock DA, Warren CJ, Gorman LA, and Tracy TS (2006) CYP2C9 inhibition: Impact of probe selection and pharmacogenetics on in vitro inhibition profiles. *Drug Metabolism and Disposition* **34:**1966-1975.

Kunze KL and Trager WF (1996) Warfarin-fluconazole. III. A rational approach to management of a metabolically based drug interaction. *Drug Metab Dispos* **24:**429-435.

Kunze KL, Wienkers LC, Thummel KE, and Trager WF (1996) Warfarin-fluconazole .1. Inhibition of the human cytochrome P450-dependent metabolism of warfarin by fluconazole: In vitro studies. *Drug Metabolism and Disposition* **24:**414-421.

Langtry HD and Brogden RN (1997) Clarithromycin. A review of its efficacy in the treatment of respiratory tract infections in immunocompetent patients. *Drugs* **53:**973-1004.

Le Vee M, Jigorel E, Glaise D, Gripon P, Guguen-Guillouzo C, and Fardel O (2006) Functional expression of sinusoidal and canalicular hepatic drug transporters in the differentiated human hepatoma HepaRG cell line. *Eur J Pharm Sci* **28:**109-117.

Lee AYY (2009) Anticoagulation in the Treatment of Established Venous Thromboembolism in Patients With Cancer. *Journal of Clinical Oncology* **27:**4895-4901.

Lehmann CG (1835) *J Prakt Chem* **6:**113.

Lemke TLW, David A. Roche, Victoria F. Zito, S. William (2012) Drug metabolism, in: *Foye's Principles of Medicinal Chemistry*, Lippincott Williams & Wilkins.

Lephart ED (1996) A review of brain aromatase cytochrome P450. *Brain Res Brain Res Rev* **22:**1-26.

Lewis DF (2004) 57 varieties: the human cytochromes P450. *Pharmacogenomics* **5:**305-318.

Lewis DF and Ito Y (2009) Human P450s involved in drug metabolism and the use of structural modelling for understanding substrate selectivity and binding affinity. *Xenobiotica* **39:**625-635.

Liberg JPs (1829) *Ann Phys Chem* **17**.

Lin JH, Chiba M, Balani SK, Chen IW, Kwei GY, Vastag KJ, and Nishime JA (1996) Species differences in the pharmacokinetics and metabolism of indinavir, a potent human immunodeficiency virus protease inhibitor. *Drug Metab Dispos* **24:**1111-1120.

Lin JH and Lu AY (1997) Role of pharmacokinetics and metabolism in drug discovery and development. *Pharmacol Rev* **49:**403-449.

Liu Y, Jeong H, Takahashi H, Drozda K, Patel SR, Shapiro NL, Nutescu EA, and Cavallari LH (2012) Decreased Warfarin Clearance Associated With the CYP2C9 R150H (*8) Polymorphism. *Clinical Pharmacology & Therapeutics* **91:**660-665.

Liu Y, Ramirez J, House L, and Ratain MJ (2010a) Comparison of the Drug-Drug Interactions Potential of Erlotinib and Gefitinib via Inhibition of UDP-Glucuronosyltransferases. *Drug Metabolism and Disposition* **38:**32-39.

Liu Y, Ramirez J, House L, and Ratain MJ (2010b) The UGT1A1*28 polymorphism correlates with erlotinib's effect on SN-38 glucuronidation. *European Journal of Cancer* **46:**2097-2103.

Liu Y, Ramírez J, House L, and Ratain MJ (2010c) Comparison of the drug-drug interactions potential of erlotinib and gefitinib via inhibition of UDP-glucuronosyltransferases. *Drug Metab Dispos* **38:**32-39.

Liu Y, Ramírez J, House L, and Ratain MJ (2010d) The UGT1A1*28 polymorphism correlates with erlotinib's effect on SN-38 glucuronidation. *Eur J Cancer* **46:**2097-2103.

Madan J, Dhiman N, Sardana S, Aneja R, Chandra R, and Katyal A (2011) Long-circulating poly(ethylene glycol)-grafted gelatin nanoparticles customized for intracellular delivery of noscapine: preparation, in-vitro characterization, structure elucidation, pharmacokinetics, and cytotoxicity analyses. *Anti-Cancer Drugs* **22:**543-555.

Maddison J, Somogyi AA, Jensen BP, James HM, Gentgall M, and Rolan PE (2013) The pharmacokinetics and pharmacodynamics of single dose (R)- and (S)-warfarin administered separately and together: relationship to VKORC1 genotype. *British Journal of Clinical Pharmacology* **75:**208-216.

Maekawa K, Harakawa N, Sugiyama E, Tohkin M, Kim S-R, Kaniwa N, Katori N, Hasegawa R, Yasuda K, Kamide K, Miyata T, Saito Y, and Sawada J-i (2009) Substrate-Dependent Functional Alterations of Seven CYP2C9 Variants Found in Japanese Subjects. *Drug Metabolism and Disposition* **37:**1895-1903.

Mahmoudian M and Rahimi-Moghaddam P (2009) The Anti-Cancer Activity of Noscapine: A Review. *Recent Patents on Anti-Cancer Drug Discovery* **4:**92-97.

Manno M, De Matteis F, and King LJ (1988) The mechanism of the suicidal, reductive inactivation of microsomal cytochrome P-450 by carbon tetrachloride. *Biochem Pharmacol* **37:**1981-1990.

Martin P, Oliver S, Kennedy SJ, Partridge E, Hutchison M, Clarke D, and Giles P (2012) Pharmacokinetics of vandetanib: three phase I studies in healthy subjects. *Clin Ther* **34:**221-237.

Martin SJ, Garvin CG, McBurney CR, and Sahloff EG (2001) The activity of 14-hydroxy clarithromycin, alone and in combination with clarithromycin, against penicillin- and erythromycin-resistant Streptococcus pneumoniae. *J Antimicrob Chemother* **47:**581-587.

Mason HS (1957) Mechanisms of oxygen metabolism. *Science* **125:**1185-1188.

Matsumoto M, Hashizume H, Tomishige T, Kawasaki M, Tsubouchi H, Sasaki H, Shimokawa Y, and Komatsu M (2006) OPC-67683, a nitro-dihydro-imidazooxazole derivative with promising action against tuberculosis in vitro and in mice. *PLoS Med* **3:**e466.

Mayhew BS, Jones DR, and Hall SD (2000) An in vitro model for predicting in vivo inhibition of cytochrome P450 3A4 by metabolic intermediate complex formation. *Drug Metab Dispos* **28:**1031-1037.

Meng Q, Luo H, Liu Y, Li W, Zhang W, and Yao Q (2009) Synthesis and evaluation of carbamate prodrugs of SQ109 as antituberculosis agents. *Bioorg Med Chem Lett* **19:**2808-2810.

Menéndez D, Bendesky A, Rojas E, Salamanca F, and Ostrosky-Wegman P (2002) Role of P53 functionality in the genotoxicity of metronidazole and its hydroxy metabolite. *Mutat Res* **501:**57-67.

Midgley RS, Kerr DJ, Flaherty KT, Stevenson JP, Pratap SE, Koch KM, Smith DA, Versola M, Fleming RA, Ward C, O'Dwyer PJ, and Middleton MR (2007) A phase I and pharmacokinetic study of lapatinib in combination with infusional 5-fluorouracil, leucovorin and irinotecan. *Ann Oncol* **18:**2025-2029.

Miners JO and Birkett DJ (1998) Cytochrome P4502C9: an enzyme of major importance in human drug metabolism. *Br J Clin Pharmacol* **45:**525-538.

Miners JO, Mackenzie PI, and Knights KM (2010) The prediction of drug-glucuronidation parameters in humans: UDP-glucuronosyltransferase enzyme-selective substrate and inhibitor probes for reaction phenotyping and in vitro-in vivo extrapolation of drug clearance and drug-drug interaction potential. *Drug Metab Rev* **42:**196-208.

Mross K, Steinbild S, Baas F, Gmehling D, Radtke M, Voliotis D, Brendel E, Christensen O, and Unger C (2007) Results from an in vitro and a clinical/pharmacological phase I study with the combination irinotecan and sorafenib. *Eur J Cancer* **43:**55-63.

Mueller GC and Miller JA (1948) The metabolism of 4-dimethylaminoazobenzene by rat liver homogenates. *J Biol Chem* **176:**535-544.

Mueller GC and Miller JA (1949) The reductive cleavage of 4-dimethylaminoazobenzene by rat liver; the intracellular distribution of the enzyme system and its requirement for triphosphopyridine nucleotide. *J Biol Chem* **180:**1125-1136.

Mueller GC and Miller JA (1953) The metabolism of methylated aminoazo dyes. II. Oxidative demethylation by rat liver homogenates. *J Biol Chem* **202:**579-587.

Murray PR, Baron EJ, Pfaller MA, Tenover FC, and Yolken RH (1995) *Manual of clinical microbiology*. ASM Press,, Washington, D.C.

Myhr K (2009) Noscapine and warfarin--a potentially dangerous interaction. *Tidsskrift for den Norske lageforening : tidsskrift for praktisk medicin, ny rakke* **129:**540-540.

Nelson DR, Kamataki T, Waxman DJ, Guengerich FP, Estabrook RW, Feyereisen R, Gonzalez FJ, Coon MJ, Gunsalus IC, and Gotoh O (1993) The P450 superfamily: update on new sequences, gene mapping, accession numbers, early trivial names of enzymes, and nomenclature. *DNA Cell Biol* **12:**1-51.

Obach RS (1999) Prediction of human clearance of twenty-nine drugs from hepatic microsomal intrinsic clearance data: An examination of in vitro half-life approach and nonspecific binding to microsomes. *Drug Metab Dispos* **27:**1350-1359.

Obach RS, Walsky RL, and Venkatakrishnan K (2007) Mechanism-based inactivation of human cytochrome P450 enzymes and the prediction of drug-drug interactions. *Drug Metabolism and Disposition* **35:**246-255.

Obach RS, Walsky RL, Venkatakrishnan K, Gaman EA, Houston JB, and Tremaine LM (2006) The utility of in vitro cytochrome P450 inhibition data in the prediction of drug-drug interactions. *J Pharmacol Exp Ther* **316:**336-348.

Ohlsson S, Holm L, Myrberg O, Sundstrom A, and Yue Q-Y (2008) Noscapine may increase the effect of warfarin. *British Journal of Clinical Pharmacology* **65:**277-278.

Olsson B, Bolme P, Dahlstrom B, and Marcus C (1986) EXCRETION OF NOSCAPINE IN HUMAN-BREAST MILK. *European Journal of Clinical Pharmacology* **30:**213-215.

Omura K, Nakazawa T, Sato T, Iwanaga T, and Nagata O (2007) Characterization of N-glucuronidation of 4-(5-pyridin-4-yl-1H-[1,2,4]triazol-3-yl) pyridine-2-carbonitrile (FYX-051): a new xanthine oxidoreductase inhibitor. *Drug Metab Dispos* **35:**2143-2148.

OMURA T and SATO R (1964a) THE CARBON MONOXIDE-BINDING PIGMENT OF LIVER MICROSOMES. I. EVIDENCE FOR ITS HEMOPROTEIN NATURE. *J Biol Chem* **239:**2370-2378.

OMURA T and SATO R (1964b) THE CARBON MONOXIDE-BINDING PIGMENT OF LIVER MICROSOMES. II. SOLUBILIZATION, PURIFICATION, AND PROPERTIES. *J Biol Chem* **239:**2379-2385.

Orr ST, Ripp SL, Ballard TE, Henderson JL, Scott DO, Obach RS, Sun H, and Kalgutkar AS (2012a) Mechanism-based inactivation (MBI) of cytochrome P450 enzymes: structure-activity relationships and discovery strategies to mitigate drug-drug interaction risks. *J Med Chem* **55:**4896-4933.

Orr STM, Ripp SL, Ballard TE, Henderson JL, Scott DO, Obach RS, Sun H, and Kalgutkar AS (2012b) Mechanism-Based Inactivation (MBI) of Cytochrome P450 Enzymes: Structure-Activity Relationships and Discovery Strategies To Mitigate Drug-Drug Interaction Risks. *Journal of Medicinal Chemistry* **55:**4896-4933.

Pang KS and Rowland M (1977) Hepatic clearance of drugs. I. Theoretical considerations of a "well-stirred" model and a "parallel tube" model. Influence of hepatic blood flow, plasma and blood cell binding, and the hepatocellular enzymatic activity on hepatic drug clearance. *J Pharmacokinet Biopharm* **5:**625-653.

Parish T and Brown A (2008) *Mycobacteria protocols*. Humana Press, New York, USA.

Patki KC, Von Moltke LL, and Greenblatt DJ (2003) In vitro metabolism of midazolam, triazolam, nifedipine, and testosterone by human liver microsomes and recombinant cytochromes p450: role of cyp3a4 and cyp3a5. *Drug Metab Dispos* **31:**938-944.

Paul MK and Mukhopadhyay AK (2004) Tyrosine kinase - Role and significance in Cancer. *Int J Med Sci* **1:**101-115.

Peer CJ, Sissung TM, Kim A, Jain L, Woo S, Gardner ER, Kirkland CT, Troutman SM, English BC, Richardson ED, Federspiel J, Venzon D, Dahut W, Kohn E, Kummar S, Yarchoan R, Giaccone G, Widemann B, and Figg WD (2012) Sorafenib is an inhibitor of UGT1A1 but is metabolized by UGT1A9: implications of genetic variants on pharmacokinetics and hyperbilirubinemia. *Clin Cancer Res* **18:**2099-2107.

Peng B, Lloyd P, and Schran H (2005) Clinical pharmacokinetics of imatinib. *Clin Pharmacokinet* **44:**879-894.

Pernelle K, Le Guevel R, Glaise D, Stasio CG, Le Charpentier T, Bouaita B, Corlu A, and Guguen-Guillouzo C (2011) Automated detection of hepatotoxic compounds in human hepatocytes using HepaRG cells and image-based analysis of mitochondrial dysfunction with JC-1 dye. *Toxicol Appl Pharmacol* **254:**256-266.

Peters JH, Gordon GR, and Murray JF (1983) Disposition of prothionamide in rats and armadillos. *Int J Lepr Other Mycobact Dis* **51:**54-63.

Piddington DL, Kashkouli A, and Buchmeier NA (2000) Growth of Mycobacterium tuberculosis in a defined medium is very restricted by acid pH and Mg(2+) levels. *Infect Immun* **68:**4518-4522.

Po ALW and Zhang WY (1998) What lessons can be learnt from withdrawal of mibefradil from the market? *The Lancet* **351**.

Polasek TM and Miners JO (2007) In vitro approaches to investigate mechanism-based inactivation of CYP enzymes. *Expert Opinion on Drug Metabolism & Toxicology* **3:**321-329.

Poulin P (2013) Prediction of total hepatic clearance by combining metabolism, transport, and permeability data in the in vitro-in vivo extrapolation methods: emphasis on an apparent fraction unbound in liver for drugs. *J Pharm Sci* **102:**2085-2095.

Preziosi P (2007) Isoniazid: metabolic aspects and toxicological correlates. *Curr Drug Metab* **8:**839-851.

Quinney SK, Haehner BD, Rhoades MB, Lin Z, Gorski JC, and Hall SD (2008) Interaction between midazolam and clarithromycin in the elderly. *Br J Clin Pharmacol* **65:**98-109.

Quinney SK, Zhang X, Lucksiri A, Gorski JC, Li L, and Hall SD (2010) Physiologically based pharmacokinetic model of mechanism-based inhibition of CYP3A by clarithromycin. *Drug Metab Dispos* **38:**241-248.

Radominska-Pandya A, Czernik PJ, Little JM, Battaglia E, and Mackenzie PI (1999) Structural and functional studies of UDP-glucuronosyltransferases. *Drug Metab Rev* **31:**817-899.

Rahme E, Feugere G, Sirois C, Weicker S, and Ramos E (2013) Anticoagulant use in patients with cancer associated venous thromboembolism: A retrospective cohort study. *Thrombosis Research* **131:**210-217.

Rastogi N, Goh KS, Berchel M, and Bryskier A (2000) Activity of rifapentine and its metabolite 25-O-desacetylrifapentine compared with rifampicin and rifabutin against Mycobacterium tuberculosis, Mycobacterium africanum, Mycobacterium bovis and M. bovis BCG. *J Antimicrob Chemother* **46:**565-570.

Redman AR (2001) Implications of cytochrome P450 2C9 polymorphism on warfarin metabolism and dosing. *Pharmacotherapy* **21:**235-242.

Rettie AE, Korzekwa KR, Kunze KL, Lawrence RF, Eddy AC, Aoyama T, Gelboin HV, Gonzalez FJ, and Trager WF (1992) HYDROXYLATION OF WARFARIN BY HUMAN CDNA-EXPRESSED CYTOCHROME-P-450 - A ROLE FOR P-4502C9 IN THE ETIOLOGY OF (S)-WARFARIN DRUG-INTERACTIONS. *Chemical Research in Toxicology* **5:**54-59.

Ritter JK (2007) Intestinal UGTs as potential modifiers of pharmacokinetics and biological responses to drugs and xenobiotics. *Expert Opin Drug Metab Toxicol* **3:**93-107.

Ritter JK, Crawford JM, and Owens IS (1991) Cloning of two human liver bilirubin UDP-glucuronosyltransferase cDNAs with expression in COS-1 cells. *J Biol Chem* **266:**1043-1047.

Rodrigues AD, Roberts EM, Mulford DJ, Yao Y, and Ouellet D (1997) Oxidative metabolism of clarithromycin in the presence of human liver microsomes. Major role for the cytochrome P4503A (CYP3A) subfamily. *Drug Metab Dispos* **25:**623-630.

Rosenborg S, Stenberg M, Otto S, Ostervall J, Masquelier M, Yue QY, Bertilsson L, and Eliasson E (2010) Clinically Significant CYP2C Inhibition by Noscapine but Not by Glucosamine. *Clinical Pharmacology & Therapeutics* **88:**343-346.

Rozman D, Strömstedt M, Tsui LC, Scherer SW, and Waterman MR (1996) Structure and mapping of the human lanosterol 14alpha-demethylase gene (CYP51) encoding the cytochrome P450 involved in cholesterol biosynthesis; comparison of exon/intron organization with other mammalian and fungal CYP genes. *Genomics* **38:**371-381.

Rugo HS, Herbst RS, Liu G, Park JW, Kies MS, Steinfeldt HM, Pithavala YK, Reich SD, Freddo JL, and Wilding G (2005) Phase I trial of the oral antiangiogenesis agent AG-013736 in patients with advanced solid tumors: pharmacokinetic and clinical results. *J Clin Oncol* **23:**5474-5483.

Rustomjee R, Diacon AH, Allen J, Venter A, Reddy C, Patientia RF, Mthiyane TC, De Marez T, van Heeswijk R, Kerstens R, Koul A, De Beule K, Donald PR, and McNeeley DF (2008) Early bactericidal activity and pharmacokinetics of the diarylquinoline TMC207 in treatment of pulmonary tuberculosis. *Antimicrob Agents Chemother* **52:**2831-2835.

Saulter JY, Kurian JR, Trepanier LA, Tidwell RR, Bridges AS, Boykin DW, Stephens CE, Anbazhagan M, and Hall JE (2005) Unusual dehydroxylation of antimicrobial amidoxime prodrugs by cytochrome b5 and NADH cytochrome b5 reductase. *Drug Metab Dispos* **33:**1886-1893.

Schoedel KA, Pope LE, and Sellers EM (2012) Randomized open-label drug-drug interaction trial of dextromethorphan/quinidine and paroxetine in healthy volunteers. *Clin Drug Investig* **32:**157-169.

Scordo MG, Melhus H, Stjernberg E, Edvardsson AM, and Wadelius M (2008) Warfarin-noscapine interaction: A series of four case reports. *Annals of Pharmacotherapy* **42:**448-450.

Scordo MG, Pengo V, Spina E, Dahl ML, Gusella M, and Padrini R (2002) Influence of CYP2C9 and CYP2C19 genetic polymorphisms on warfarin maintenance dose and metabolic clearance. *Clinical Pharmacology & Therapeutics* **72:**702-710.

Shih TY, Pai CY, Yang P, Chang WL, Wang NC, and Hu OY (2013) A novel mechanism underlies the hepatotoxicity of pyrazinamide. *Antimicrob Agents Chemother* **57:**1685-1690.

Sia IG and Wieland ML (2011) Current concepts in the management of tuberculosis. *Mayo Clin Proc* **86:**348-361.

Silverman RB (1995) Mechanism-based enzyme inactivators. *Methods Enzymol* **249:**240-283.

Smith DA, Koch KM, Arya N, Bowen CJ, Herendeen JM, and Beelen A (2009) Effects of ketoconazole and carbamazepine on lapatinib pharmacokinetics in healthy subjects. *Br J Clin Pharmacol* **67:**421-426.

Smith I (2003) Mycobacterium tuberculosis pathogenesis and molecular determinants of virulence. *Clin Microbiol Rev* **16:**463-496.

Song Y (2011) ADMEt Evaluation of Anti-tuberculosis Compounds and New Methodologies Development in: *Department of Medicinal Chemistry and Pharmacognosy*, University of Illinois at Chicago.

Spraggs CF, Budde LR, Briley LP, Bing N, Cox CJ, King KS, Whittaker JC, Mooser VE, Preston AJ, Stein SH, and Cardon LR (2011) HLA-DQA1*02:01 is a major risk factor for lapatinib-induced hepatotoxicity in women with advanced breast cancer. *J Clin Oncol* **29:**667-673.

Sproll C, Perz RC, and Lachenmeier DW (2006) Optimized LC/MS/MS analysis of morphine and codeine in poppy seed and evaluation of their fate during food processing as a basis for risk analysis. *J Agric Food Chem* **54:**5292-5298.

Strassburg CP, Manns MP, and Tukey RH (1998a) Expression of the UDP-glucuronosyltransferase 1A locus in human colon. Identification and characterization of the novel extrahepatic UGT1A8. *J Biol Chem* **273:**8719-8726.

Strassburg CP, Nguyen N, Manns MP, and Tukey RH (1998b) Polymorphic expression of the UDP-glucuronosyltransferase UGT1A gene locus in human gastric epithelium. *Mol Pharmacol* **54:**647-654.

Strassburg CP, Oldhafer K, Manns MP, and Tukey RH (1997) Differential expression of the UGT1A locus in human liver, biliary, and gastric tissue: identification of UGT1A7 and UGT1A10 transcripts in extrahepatic tissue. *Mol Pharmacol* **52:**212-220.

Streiff MB (2009) Diagnosis and Initial Treatment of Venous Thromboembolism in Patients With Cancer. *Journal of Clinical Oncology* **27:**4889-4894.

Sun D, Chen G, Dellinger RW, Sharma AK, and Lazarus P (2010) Characterization of 17-dihydroexemestane glucuronidation: potential role of the UGT2B17 deletion in exemestane pharmacogenetics. *Pharmacogenet Genomics* **20:**575-585.

Thompson TN (2001) Optimization of metabolic stability as a goal of modern drug design. *Med Res Rev* **21:**412-449.

Tsunoda N and Yoshimura H (1981) METABOLIC-FATE OF NOSCAPINE .3. FURTHER-STUDIES ON IDENTIFICATION AND DETERMINATION OF THE METABOLITES. *Xenobiotica* **11:**23-32.

Tudela J, García Cánovas F, Varón R, García Carmona F, Gálvez J, and Lozano JA (1987) Transient-phase kinetics of enzyme inactivation induced by suicide substrates. *Biochim Biophys Acta* **912:**408-416.

Turgeon D, Carrier JS, Chouinard S, and Belanger A (2003) Glucuronidation activity of the UGT2B17 enzyme toward xenobiotics. *Drug Metab Dispos* **31:**670-676.

Uchaipichat V, Mackenzie PI, Elliot DJ, and Miners JO (2006) Selectivity of substrate (trifluoperazine) and inhibitor (amitriptyline, androsterone, canrenoic acid, hecogenin, phenylbutazone, quinidine, quinine, and sulfinpyrazone) "probes" for human udp-glucuronosyltransferases. *Drug metabolism and disposition: the biological fate of chemicals* **34:**449-456.

Uchaipichat V, Mackenzie PI, Guo XH, Gardner-Stephen D, Galetin A, Houston JB, and Miners JO (2004) Human udp-glucuronosyltransferases: isoform selectivity and kinetics of 4-methylumbelliferone and 1-naphthol glucuronidation, effects of organic solvents, and inhibition by diclofenac and probenecid. *Drug metabolism and disposition: the biological fate of chemicals* **32:**413-423.

Uchaipichat V, Suthisisang C, and Miners JO (2013) The glucuronidation of R- and S-lorazepam: human liver microsomal kinetics, UDP-glucuronosyltransferase enzyme selectivity, and inhibition by drugs. *Drug Metab Dispos* **41:**1273-1284.

Udomuksorn W, Elliot DJ, Lewis BC, Mackenzie PI, Yoovathaworn K, and Miners JO (2007) Influence of mutations associated with Gilbert and Crigler-Najjar type II syndromes on the glucuronidation kinetics of bilirubin and other UDP-glucuronosyltransferase 1A substrates. *Pharmacogenet Genomics* **17:**1017-1029.

Ure A (1841) *Pharm J Trans* **1:**24.

Urlacher VB (2012) 7.13 Oxidation: Stereoselective Oxidations with Cytochrome P450 Monooxygenases. ***Reference Module in Chemistry, Molecular Sciences and Chemical Engineering* 7**.

USFDA (2007) TYKERB (lapatinib) tablets label.

USFDA (2012a) Clinical Pharmacology and Biopharmaceutics Reviews -- Bedaquiline/Sirturo (Research CfDEa ed.

USFDA (2012b) Drug Interaction Studies — Study Design, Data Analysis, Implications for Dosing, and Labeling Recommendations

USFDA (2012c) Inlyta (axitinib) tablets Label.

van Erp NP, Gelderblom H, Karlsson MO, Li J, Zhao M, Ouwerkerk J, Nortier JW, Guchelaar HJ, Baker SD, and Sparreboom A (2007) Influence of CYP3A4 inhibition on the steady-state pharmacokinetics of imatinib. *Clin Cancer Res* **13:**7394-7400.

Venkatakrishnan K, Obach RS, and Rostami-Hodjegan A (2007) Mechanism-based inactivation of human cytochrome P450 enzymes: strategies for diagnosis and drug-drug interaction risk assessment. *Xenobiotica* **37:**1225-1256.

Wang B, Wang J, Huang SQ, Su HH, and Zhou SF (2009) Genetic polymorphism of the human cytochrome P450 2C9 gene and its clinical significance. *Curr Drug Metab* **10:**781-834.

Wang L and Weinshilboum R (2006) Thiopurine S-methyltransferase pharmacogenetics: insights, challenges and future directions. *Oncogene* **25:**1629-1638.

Weinshilboum R and Wang L (2004) Pharmacogenomics: bench to bedside. *Nat Rev Drug Discov* **3:**739-748.

Wen B and Zhou M (2009) Metabolic activation of the phenothiazine antipsychotics chlorpromazine and thioridazine to electrophilic iminoquinone species in human liver microsomes and recombinant P450s. *Chem Biol Interact* **181:**220-226.

Wester MR, Yano JK, Schoch GA, Yang C, Griffin KJ, Stout CD, and Johnson EF (2004) The structure of human cytochrome P4502C9 complexed with flurbiprofen at 2.0-angstrom resolution. *Journal of Biological Chemistry* **279:**35630-35637.

Wilkinson GR and Shand DG (1975) Commentary: a physiological approach to hepatic drug clearance. *Clin Pharmacol Ther* **18:**377-390.

Williams JA, Hyland R, Jones BC, Smith DA, Hurst S, Goosen TC, Peterkin V, Koup JR, and Ball SE (2004) Drug-drug interactions for UDP-glucuronosyltransferase substrates: a pharmacokinetic explanation for typically observed low exposure (AUCi/AUC) ratios. *Drug metabolism and disposition: the biological fate of chemicals* **32:**1201-1208.

Williams PA, Cosme J, Ward A, Angova HC, Vinkovic DM, and Jhoti H (2003) Crystal structure of human cytochrome P4502C9 with bound warfarin. *Nature* **424:**464-468.

Xie HG, Prasad HC, Kim RB, and Stein CM (2002) CYP2C9 allelic variants: ethnic distribution and functional significance. *Adv Drug Deliv Rev* **54:**1257-1270.

Xu BH, Jiang ZF, Chua D, Shao ZM, Luo RC, Wang XJ, Liu DG, Yeo W, Yu SY, Newstat B, Preston A, Martin AM, Chi HD, and Wang L (2011) Lapatinib plus capecitabine in treating HER2-positive advanced breast cancer: efficacy, safety, and biomarker results from Chinese patients. *Chin J Cancer* **30:**327-335.

Yamada T, Volkmer C, and Grisham MB (1991) The effects of sulfasalazine metabolites on hemoglobin-catalyzed lipid peroxidation. *Free Radic Biol Med* **10:**41-49.

Yamazaki H, Inoue K, Chiba K, Ozawa N, Kawai T, Suzuki Y, Goldstein JA, Guengerich FP, and Shimada T (1998) Comparative studies on the catalytic roles of cytochrome P450 2C9 and its Cys- and Leu-variants in the oxidation of warfarin, flurbiprofen, and diclofenac by human liver microsomes. *Biochem Pharmacol* **56:**243-251.

Yengi LG, Leung L, and Kao J (2007) The evolving role of drug metabolism in drug discovery and development. *Pharm Res* **24:**842-858.

Yuan H, Li N, and Lai Y (2009) Evaluation of in vitro models for screening alkaline phosphatase-mediated bioconversion of phosphate ester prodrugs. *Drug Metab Dispos* **37:**1443-1447.

Zhang ZY and Wong YN (2005) Enzyme kinetics for clinically relevant CYP inhibition. *Curr Drug Metab* **6:**241-257.

Zumla A, Nahid P, and Cole ST (2013) Advances in the development of new tuberculosis drugs and treatment regimens. *Nat Rev Drug Discov* **12:**388-404.

Zweers-Zeilmaker WM, Horbach GJ, and Witkamp RF (1997) Differential inhibitory effects of phenytoin, diclofenac, phenylbutazone and a series of sulfonamides on hepatic cytochrome P4502C activity in vitro, and correlation with some molecular descriptors in the dwarf goat (Caprus hircus aegagrus). *Xenobiotica* **27:**769-780.

VITA

Nan Zhang
PhD Candidate
Institute for Tuberculosis Research (**ITR**)
College of Pharmacy, University of Illinois at Chicago (**UIC**)
833 S. Wood St. Rm 412, Chicago, IL 60612
Email: nzhang6@uic.edu Mobile: 312-415-5823

SUMMARY

- Versatile in ADME/PK studies (microsomal/hepatocyte stability, metabolite Identification & compound soft-spot optimization, plasma protein binding, drug-drug interactions, *in vivo* animal PK studies; *in vitro-in vivo* extrapolation)
- Able to identify the potential targets and interpret mechanism of action for inhibitors based on the phenotypic activities of compounds and the resistance of cells with mutations
- Experienced in bio-analytical method development and quantification of small molecules using mass spectrometer

WORK EXPERIENCE

Internship ***May 2013 – Aug. 2013***
DMPK Department, Genentech, South San Francisco, CA

- Compared the intrinsic clearance of drugs in hepatocytes and the extrapolated hepatic clearance from regular medium and plasma incubation system, and interpreted the correlation between *in vitro* and *in vivo* data
- Explored the facilitating role of human plasma in drug uptake and clearance by utilizing oil-spin method

Technology Commercialization Graduate Assistantship ***May 2011 - March 2012***
Office of Technology Management, UIC

- Evaluated pharmaceutical inventions in terms of its novelty, potential market and commercial value
- Researched the background of biotech or pharmaceutical companies and identified the potential candidates for licensing UIC pharmaceutical technologies

EDUCATION

University of Illinois at Chicago (College of Pharmacy) ***Jan. 2014***
PhD in Medicinal Chemistry Cumulative GPA: 3.83/4.00
China Pharmaceutical University (College of Life Science and Technology) ***Jul. 2006***
BEng in Life Science and Technology Cumulative GPA: 3.90/4.00

MBA Courses

- Introduction to Marketing (MKTG 500)
- Introduction to Financial Accounting (ACTG 500)
- Introduction to Corporate Finance (FIN 500)
- Microeconomics for Business Decisions (ECON 520)

PUBLICATIONS

1. **Zhang N**, Seguin RP, Kenze KL, Zhang YY, Jeong H; ***Characterization of Inhibition Kinetics of (S)-warfarin Hydroxylation by Noscapine: Implications in Warfarin Therapy*** (Drug Metab. Dispos. accepted)
2. Brugarolas P, Movahedzadeh F, Wang Y, **Zhang N**, Bartek IL, Gao YN, Voskuil MI, Franzblau SG, He C; ***The oxidation-sensing regulator (MosR) is a new redox dependent transcription factor in Mycobacterium tuberculosis***. J Biol Chem. 2012 Nov 2; 287 (45):37703-12
3. Gill SK, Xu H, Kirchhoff PD, Cierpicki T, Turbiak AJ, Wan B, **Zhang N**, Peng KW, Franzblau SG, Garcia GA, Showalter HD;
   Structure-Based Design of Novel Benzoxazinorifamycins with Potent Binding Affinity to Wild-Type and Rifampin-Resistant Mutant Mycobacterium tuberculosis RNA Polymerases. J. Med. Chem., 2012 Mar 27; 55 (8): 3814–3826
4. **Zhang N**, Liu Y, Jeong H. ***A Potential Drug-drug Interactions Risk Caused by Lapatinib on SN-38 Glucuronidation.*** (in preparation; a manuscript draft has been written)
5. **Zhang N**, Song Y, Klein LL, Cho S, Franzblau SG. ***A Novel Rapid in vitro High-throughput Screening (HTS) Assay for Detection of the Anti-tuberculosis Activity of Liver Enzyme-derived Metabolites*.** (in preparation)

POSTER PRESENTATIONS

1. **Zhang N**, Kenny J, Mao J; ***The Impact of Human Plasma on Drug Uptake and Clearance in Human Hepatocytes.*** Presented at Genentech Intern Poster Competition, Genentech, South San Francisco, CA, Aug 7, 2013; gRED Poster #372
2. **Zhang N**, Liu Y, Jeong HY; ***Inhibition of imatinib against UDP-glucuronosyltransferase (UGT) isoforms***. Presented at Gordon Research Conference on Drug Metabolism, Holderness School, Holderness, NH, Jul 07-12, 2013; 2
3. **Zhang N**, Song Y, Klein LL, Cho SH, Franzblau SG; ***A Novel Rapid in vitro High-throughput Screening (HTS) Assay for Detection of the Anti-tuberculosis Activity of Liver Enzyme-derived Metabolites***. Presented at the 2nd Annual Society for Laboratory Automation Conference & Exhibition, Orlando, Florida, January 12-16, 2013; MP061.
4. Sun Y, Petukhova V, Giri RS, Klein LL, Song Y, **Zhang N**, Peng KW, Wan B, Wang Y, Franzblau SG; ***Identification and Structure-Activity Relationships of 2, 6-Disubstituted***

Pyrazines as Antituberculosis Agents. Presented at the 240th American Chemical Society National Meeting, Boston, Massachusetts, August 22-26, 2010; MEDI 383.

5. Sun Y, Petukhova V, Giri RS, Klein LL, Song Y, **Zhang N**, Song Y, Peng KW, Wan B, Wang Y, Franzblau SG; ***Synthesis and Biological Evaluation of 2, 6-Disubstituted Pyrazines as Antituberculosis Agents***. Presentation at the 32nd Annual National Medicinal Chemistry Symposium, Minneapolis, Minnesota, June 6-9, 2010; ABSTRACT 76.

AWARD

1. **2012 ~ 2013 W.E. van Doren Scholar (Awarded by College of Pharmacy, UIC)**

RESEARCH EXPERIENCE

Drug Metabolism & Pharmacokinetics ***Aug, 2011 ~ Present***

- Developing *in vitro* assays for detecting active liver enzyme-derived compounds against *Mycobacterium tuberculosis* by utilizing liver microsomes, S9 fractions, or HepaRG cells with clarithromycin and amidoxime analog as the assay controls
- Exploring the inhibitory effect of a series of tyrosine-kinase inhibitors on the activities of human liver UGTs and predicting the inhibitory effect *in vivo* on the metabolism of co-administered drugs
- Investigated the mechanism based inhibition of noscapine on warfarin metabolism by studying the time-dependent inhibition of noscapine on 7-hydroxylation of warfarin in human liver microsomes and recombinant CYP2C9 isoforms; predicted the AUC change of warfarin when noscapine is co-administered based on *in vitro* inhibition parameters and recommended the dosage change of warfarin for patients with different genotypes
- Performed routine human/mouse metabolic stability assays and identified metabolites of drugs or compounds generated in human/mouse liver microsomes using AB Sciex 4000 Q-Trap with the software Lightsight; investigated the non-compartment pharmacokinetic (PK) profiles of anti-tuberculosis compounds in mouse model

M. Tuberculosis Biology ***Jan, 2010 ~ Dec, 2011***

- Investigated the action of the mechanism of an anti-tuberculosis drug Clofazimine (CFZ) by identifying the antagonism between CFZ and the analogs of its target protein substrate through cellular assays and interpreting the genetic endowment of the resistant strains of *M. tuberculosis* against CFZ
- Compared the production of reactive oxygen species by CFZ and its analogs in *M. tuberculosis* whole bacterial cells and isolated bacterial membrane fractions to derive the structure-activity relationship for this series of anti-tuberculosis compounds

SCIENTIFIC SKILLS

- Project Communications: written reports, journal articles, oral presentations, posters

- Biochemistry: cell culture, bioassay/cellular assay, enzyme kinetics (reversible inhibition and time-dependent inhibition)
- Molecular Biology: PCR, electrophoresis, DNA/RNA isolation, cloning
- Microbiology: bacterial culture, media preparation, colony counting
- Analytical Chemistry: mass spectrometer (ABScieX 3200 & 4000 & 5500 QTRAP, Shimadzu single quadrupole LCMS-2020, Shimadzu IT-TOF), chromatography (HPLC, GC, TLC, preparative TLC, preparative HPLC), UV/Vis
- Organic Chemistry: organic synthesis
- Drug Metabolism and Pharmacokinetics: microsome stability, drug transport study (oil spin method), protein binding study, hepatocyte culture, amidoxime analog metabolite identification, protein binding study, animal dosing & dissection
- Computer Language Skills: R, Visual Basic

LANGUAGE

- Mandarin (native speaker)
- English (fluent)

March 31, 2014

Nan Zhang
8500 New Hampshire Ave. #410
Silver Spring, MD 20903

Email: nanzhang100@gmail.com

Dear Nan Zhang:

This is to grant you permission to include the following article in your thesis entitled "Drug Metabolism in Early Stage Drug Discovery and Drug Development" for the University of Illinois at Chicago:

> Nan Zhang, Ryan P. Seguin, Kent L. Kunze, Yan-Yan Zhang, and Hyunyoung Jeong, Characterization of Inhibition Kinetics of (*S*)-Warfarin Hydroxylation by Noscapine: Implications in Warfarin Therapy, *Drug Metab Dispos* December 2013 41:2114-2123

On the first page of each copy of this article, please add the following:

> Reprinted with permission of the American Society for Pharmacology and Experimental Therapeutics. All rights reserved.

In addition, the original copyright line published with the paper must be shown on the copies included with your thesis.

Sincerely yours,

Richard Dodenhoff
Journals Director

9650 Rockville Pike | Bethesda | MD | 20814-3995
P: (301) 634-7060 | F: (301) 634-7061 | E: info@aspet.org | www.aspet.org